CIVIL ENGINEERING STUDIES
STRUCTURAL RESEARCH SERIES NO. 514

ISSN: 0069-4274

NONLINEAR BEHAVIOR OF REINFORCED CONCRETE COOLING TOWERS

By
R. V. MILFORD
and
W. C. SCHNOBRICH

Publication of this Report
Sponsored by the
National Building Research Institute
of the
Council for Scientific and Industrial Research
Pretoria, South Africa

UNIVERSITY OF ILLINOIS
at URBANA-CHAMPAIGN
URBANA, ILLINOIS
MAY 1984

BEHAVIOR OF REINFORCED CONCRETE COOLING TOWERS

By

Rodney V. Milford

William C. Schnobrich

UNIVERSITY OF ILLINOIS
AT URBANA-CHAMPAIGN
URBANA, ILLINOIS

May 1984

ACKNOWLEDGMENT

The research reported herein was carried out by Dr. Rodney V. Milford under the direction of Dr. William C. Schnobrich, Professor of Civil Engineering. This work formed the basis of the doctoral dissertation of Rodney V. Milford.

Part of this investigation was supported by the Office of Naval Research under contract N00014-83-K-0274; NR 064-698. Computer service was provided by the Research Board of the Graduate College of the University of Illinois and by the Civil Engineering Systems Laboratory. Additional support was provided by the National Building Research Institute. These areas of support are gratefully acknowledged.

The numerical results presented in this thesis were obtained on the Burroughs B6700 computer supported by the Civil Engineering Systems Laboratory. Without the use of this resource, this project would not have been completed. Initial development of the computer program and plotting of the results were obtained with the use of the CDC Cyber 175 computing facilities, supported by the Computing Services Office.

TABLE OF CONTENTS

Page

Page

APPENDIX

LIST OF TABLES

LIST OF FIGURES

Figure Page

Figure Page

CHAPTER 1

INTRODUCTION

1.1 GENERAL

Reinforced concrete cooling towers are amongst the largest thin shell structures being constructed today. Towers exceeding 160 m (525 ft) have already been built, and towers with a height exceeding 200 m (656 ft) or more are already under consideration (Zerna and Mungan, 1982). These large size cooling towers are required for the dry cooling of high capacity power plants.

The design of cooling tower shells is invariably governed by wind loading, and often by Code of Practice requirements for an adequate factor of safety against buckling (BSI BS3445, 1975; ACI-ASCE Committee 334, 1977; IASS Working Group No. 3, 1977). However, what constitutes an adequate factor of safety against buckling, and how to calculate the buckling load has not yet been fully resolved. This can be inferred from the differences between the 1977 and draft 1982 versions of the ACI recommendations for the design of cooling towers (ACI-ASCE Committee 334, 1977 and 1982). In both versions, under the section Practice, the following guidance is given:

> "For wind load, the critical shell buckling pressure may be estimated from test results. Alternatively, a buckling analysis for wind forces should be made using the theoretical tower geometry and boundary conditions, and including the influence of dead weight. When made, the analysis should account for the influence of any anticipated reductions in stiffness caused by hairline cracking in the concrete shell."

In the commentary to the 1977 version specific reference is made to the equations of Der and Fidler (1968), and it is recommended that a factor of safety of at least two be used, when accounting for the effects of cracking and dead load. No information is given on how to include the effects of cracking and dead load. In the draft 1982 version, any specific reference to the Der and Fidler equations has been removed and replaced, in part, by a reference to review publications (Abel and Gould ,1981; Abel, et al., 1982). Unfortunately, there is little agreement in the literature as to buckling strength evaluation.

This study deals with the failure analysis of reinforced concrete cooling towers under wind loading, and investigates the effect of cracking and yielding of reinforcement on the failure load. The finite element method is employed, and suitable techniques to model material nonlinearities, cracking and geometric nonlinearities are investigated.

1.2 OBJECTIVE AND SCOPE

The objectives and scope of this investigation are summarized below:

1. Investigate the use of degenerated finite elements in reinforced concrete material applications, including large displacements. Particular attention is given to efficient and economic techniques for including material nonlinearities. Suitable corresponding geometric nonlinear formulations are investigated.
2. Develope a compatible eccentric shell stiffening element.
3. Investigate and extend cracking models for reinforced concrete panel, slab and shell systems.
4. Use the results of the above to investigate the failure of

reinforced concrete cooling towers under wind loading. The effects of geometric nonlinearities, the cracking strength of the concrete and the stabilising influence of tension stiffening of the concrete is examined and discussed.

1.3 REVIEW OF PREVIOUS RESEARCH

Research into the development of the finite element method (and in particular the degenerated shell element), reinforced concrete material modeling and cooling towers is far too numerous to even summarize here. Only a few references which are directly applicable to this investigation are noted below.

1.3.1 Degenerated finite elements

The degenerated shell finite element was originally introduced by Ahmad, et al. (1970) for the linear analysis of shells. This element is derived by constraining the 3-dimensional continuum theory to a 2-dimensional theory, simultaneously with its implementation in the finite element procedure. A review of the development of this element in both linear and nonlinear applications can be found in Hughes and Liu (1981) and Ramm (1977).

The degenerated element is simple to formulate and, in general, yields excellent results. However this element is expensive to use, in particular for nonlinear material applications. Consequently it is desirable to use techniques which yield an economic finite element formulation. Substantial savings in the computational effort required can be obtained by using explicit integration through the shell thickness, which was originally introduced for the linear analysis of thin shells by Zienkiewicz, et al.

(1971) and has been extended to the stress-resultant concept for material nonlinear applications by Parisch (1981). This approach is adopted in this investigation, and suitable corresponding geometric nonlinear formulations are presented.

The degenerated finite element has been used by Abdel Rahman (1982) and Chan (1982) for the analysis of reinforced concrete slab and shell structures. Neither reference uses a true stress-resultant constitutive approach, although little saving in computational effort would have been obtained by Abdel Rahman for slab structures.

1.3.2 Cracking models for reinforced concrete

The first finite element model of reinforced concrete to include the effect of cracking was developed by Ngo and Scordelis (1967). Cracking was modeled as a separation of the element nodes, and requires a redefenition of the topology of the structure at successive levels of cracking of the structure.

To overcome the need for automatic generation of cracks without the redefenition of the element topology, and to allow for generality in possible crack direction the 'smeared' crack was introduced by Rashid (1968). In its earliest form, the incremental constitutive matrix for singly cracked concrete retained only the modulus of concrete in a direction parallel to the crack (Rashid, 1968; Cervenka, 1970; Franklin, 1970; Mikkola and Schnobrich, 1970). To prevent numerical instabilities and to model the friction existing on a cracked surface, the shear modulus (usually together with a reduction factor) was reinstated (Hand, et al., 1972; Lin, 1973; Yuzugullu and Schnobrich, 1973).

In the smeared crack models discussed above, the direction of the initial crack is fixed once it has formed (and while it remains open). The direction of subsequent cracking depends on the stress-strain behavior assumed subsequent to the formation of the initial crack, and can be either orthogonal (Lin, 1973; Darwin and Pecknold, 1974; Kabir, 1976;) or nonorthogonal (Hand, et al., 1972; Yuzugullu and Schnobrich, 1973; Abdel Rahman, 1982) to the primary crack. However, there are inconsistencies in the treatment of subsequent cracking in the literature (ASCE, 1981).

Alternatively, it can be assumed that the crack orientation is always normal to the current direction of the maximum principal concrete stress (or strain). This model attempts to account for subsequent cracking of the concrete and changes in the average crack direction with increasing load. This approach was introduced by Cope, et al. (1977, 1980) as an approximate method for the analysis of slab structures, and by Gupta and Habibollah (1982) for panel sections by recognising that this procedure yields a lower bound to the actual failure load. The 'rotating crack model' is investigated in detail in this study.

1.3.3 Failure of wind loaded cooling towers

Research into the failure of wind loaded cooling towers was, in part, stimulated by the failures of the Ferrybridge and Ardeer cooling towers in the U.K. in 1965 and 1973 (CEGB, 1966; ICI, 1974). Since these notable failures there have been numerous publications dealing with the failure of cooling towers, and in particular buckling of cooling towers. Research into the buckling of cooling towers has been summarized by Cole, et al. (1975a) and Abel, et al. (1982), and is discussed in more detail in Chapter 5. This research deals almost exclusively with elastic buckling and bifurcation.

To date there is only one reported analytical investigation into the failure and buckling of cooling towers which includes the effect of material nonlinearities and cracking, namely that by Mang, et al. (1983). In the present investigation, the work undertaken by Mang, et al. is reexamined and the effects of cracking, tension stiffening and the tensile strength of the concrete on the failure of cooling towers is examined.

CHAPTER 2

DEGENERATED THIN SHELL ISOPARAMETRIC ELEMENTS

2.1 INTRODUCTION

The traditional approach to thin shell elements is based on classical thin shell theories (Argyris and Scharpf, 1969; Brebbia and Connor, 1969; Bergan and Clough, 1973; Thomas and Gallagher, 1975) whose governing equations are mostly complicated. In consequence, for a compatible displacement element, the displacements and some of their first and some second derivatives are required as nodal degrees of freedom. An alternative concept for developing nonlinear shell elements is to circumvent shell theories as the starting point and begin directly with the fundamental equations of nonlinear continuum mechanics. This point of view was originally adopted in the linear case by Ahmad, et al. (1970), and has subsequently been adopted by several other investigators (Ramm, et al., 1977, 1981; Hughes and Liu, 1981; Parisch, 1981; Surana, 1983). This technique has been termed the "degenerated shell element procedure" in which the 3-dimensional theory is reduced or degenerated to a shell theory simultaneously with its implementation in the finite element procedure. These elements require only C(0)-continuity and originally used the same interpolation schemes for all three displacements and two independent rotations.

While the basic concept behind the degenerated element is very simple, these elements are generally expensive and their application to material nonlinear problems in particular is therefore limited. Substantial savings in computational effort can be achieved without significant loss of accuracy

by the use of 'thin shell degenerated elements'. This approach has been adopted in this investigation. These elements are suitable for thin to moderately thick shells. Material nonlinearities enter through the use of integrated quantities, or stress resultants, by adopting a layer model. This has the advantage that when several integration points are required to represent the stresses more accurately, only the time required to compute the integrated quantities is increased. This time is negligible compared to the total computational time at the element level. Geometric nonlinearities are accounted for through nonlinear strain terms consistent with thin shell assumptions.

2.2 CHOICE OF ELEMENT

A detailed review of the development of degenerated finite elements in both linear and nonlinear applications can be found in, for example, Ramm (1977) and Hughes and Liu (1981). As noted previously, these elements require only C(0)-continuity of the displacements and independent rotations, and originally have the same interpolation scheme for all the nodal degrees of freedom- either Serendipity or Lagrangian.

Investigations have shown that, at best, the Serendipity elements are less accurate than their nearest corresponding Lagrangian elements (Hughes, et al., 1978). In plane elements, the performance of the quadratic Serendipity element declines greatly as corner angles depart from 90 degrees and when its sides become curved (Stricklin, et al. 1977; Backlund, 1978; Cook and Zhao-Hu, 1982). The element no longer passes the patch test if its sides are curved. The 9-node element is much less sensitive to shape distortion and passes the patch test under all conditions.

Excessive stiffness and shear locking of fully integrated degenerated finite elements in thin plate and shell applications are well known. This phenomenan arises due to numerical difficulties from the extreme ratio of the bending stiffness to the shear and membrane stiffnesses if the word length of the computer is too short. Shear locking in plates is avoided in most instances if reduced integration of the shear stiffness is used (Pawsey and Clough, 1971; Zinkiewicz, et al., 1971). In curved shell applications, however, it has been demonstrated that the poor performance of fully integrated elements is due to the extreme ratio of the membrane stiffness to the bending stiffness (Parisch, 1979). Either uniform or selective reduced integration of the membrane and shear stiffness matrices alleviates this problem. In material nonlinear applications, however, difficulties are introduced in choosing the best points to sample the strains when different integration rules are used to evaluate the bending and membrane contributions to the stiffness matrix.

Possibly the only defect of uniform reduced integration is that it produces rank deficiency and associated zero energy modes. Several schemes have been proposed to avoid locking and at the same time eliminate zero energy modes. This has led to the development of, amongst others, the Heterosis (Hughes, et al., 1977) and QUADH (Hughes, et al., 1977, 1981a) elements. The Heterosis element is formulated using the 9-node Lagrangian shape functions for the rotations and the 8-node Serendipity shape functions for displacements (although Abdel Rahman (1982) has successfully used the Lagrangian shape functions for the inplane displacements in plate elements). Reduced integration is applied to the shear stiffness only. The QUADH element is a four node isoparametric element in which the shear stiffness is improved firstly by applying a special form of reduced integration, and

secondly by adjusting the shear modulus according to the actual plate thickness.

The number of zero energy modes for several degenerated shell elements using reduced and selective integration is given in Table 2.1. At first sight it appears that the uniformly reduced Lagrangian elements fairs very poorly, with seven zero energy modes for the 9-node version. However all of these modes are prevented if two adjacent nodal values of the same type are constrained in at least one element. This condition is achieved in almost all practical applications, although it may be undesirable to use an element which requires special precautions.

The Heterosis element is the most attractive (its single zero energy mode is not communicable in a mesh of more than two elements), but its success has not yet been fully proven in shell applications. It also retains the undesirable characteristic of the Serendipity elements of not passing the patch test when its sides are distorted (Abdel Rahman, 1982). The QUAHD element is very economical, but its aspect ratio behavior on some problems is disappointing (Hughes and Tezduyar, 1981).

The reduced integrated 9-node Lagrangian element appears to be the best alternative and has been used as the primary element in this investigation. (The 4-, 8- and 9-node degenerated shell elements have all been implemented in FINITE (Lopez, 1977).) When zero energy modes may arise, either 3x3 integration must be used in at least one of the elements in the mesh, or a single fully integrated element with a modulus of elasticity of, say, 10^{-3} times that used for the rest of the mesh is laid on top of one element. This overlay technique has the advantage in that it does not stiffen the other modes nor increase the cost of the solution significantly. (This overlay approach does not appear to have received particular mention in the

literature). This approach has been adopted in Examples 2.5.5 and 4.5.2, and in Chapter 5.

2.3 FINITE ELEMENT DISCRETIZATION

In this section the finite element formulation is developed for the degenerated shell element. The element is developed as a thin shell element, and consistent nonlinear strain displacement relations are derived. These strain displacement relations are discussed further in Appendix A.

Vector notation and indicial notation are used as appropriate. Where indicial notation is used, the summation convention for a repeated indicial is implied. Roman subscripts range over 1,2,3 and Greek subscripts 1,2.

2.3.1 Geometry

The initial geometry of the element (Fig. 2.1) is expressed in terms of the position vector $\underline{x}^o$ of a reference surface, which for convenience is taken as the middle surface of the shell, and a position vector $\underline{v}_3$ which defines the 'normal' to the shell based at a point on the reference surface. For kinematic considerations $\underline{v}_3$ should be at least approximately normal to the middle surface.

$$\underline{x} = \underline{x}^o + \zeta \frac{t}{2} \underline{v}_3 \tag{2.1}$$

where t is the shell thickness at the point under consideration and ζ is the isoparametric coordinate in the direction of the normal. Note that all quantities in Eq. 2.1 are referred to the global (cartesian) basis $\underline{i}$. In finite element notation the initial geometry is interpolated as

$$\underline{x} = N^P(\xi,\eta)\ \underline{x}^{o^P} + \zeta N^P(\xi,\eta)\ \left(\frac{t}{2}\ \underline{v}_3\right)^P \qquad (2.2)$$

where $N^P(\xi,\eta)$ is the shape function associated with the p'th node, and summation is taken over all the nodes.

For later use it is necessary to construct a local Cartesian reference frame at each integration point with a normal strictly perpendicular to the reference surface. The frame is defined by the orthonormal basis vectors $\underline{e}_1$, $\underline{e}_2$, $\underline{e}_3$, which are calculated as follows. (See Fig. 2.1)

$$\begin{aligned}
\underline{e}_1 &= \frac{\partial \underline{x}}{\partial \xi} \Big/ \left\| \frac{\partial \underline{x}}{\partial \xi} \right\| \\
\underline{e}_3 &= \left(\underline{e}_1 \times \frac{\partial \underline{x}}{\partial \eta}\right) \Big/ \left\| \underline{e}_1 \times \frac{\partial \underline{x}}{\partial \eta} \right\| \\
\underline{e}_2 &= (\underline{e}_3 \times \underline{e}_1) \Big/ \| \underline{e}_3 \times \underline{e}_1 \|
\end{aligned} \qquad (2.3)$$

where x denotes the cross product, and $\|\,.\,\|$ denotes the Euclidian norm.

The Jacobian associated with transforming from the global to the isoparametric coordinate system is also required, and is defined as

$$\underline{J} = \left[\frac{\partial x_j}{\partial \xi_i}\right] \qquad (2.4)$$

It follows from Eq. 2.1 that

$$\underline{J} = \underline{J}^o + \zeta\ \underline{R} \qquad (2.5)$$

where $\underline{J}^o$ is the Jacobian associated with the midsurface, and $\underline{R}$ is a matrix describing the curvature of the midsurface,

$$R = \frac{t}{2}\ [\ \underline{v}_{3,\xi}\quad \underline{v}_{3,\eta}\quad \underline{0}\ ]^T \qquad (2.6)$$

At this stage the thin shell approximation is introduced, namely that the shell is sufficiently thin so that the variation in the Jacobian (and

hence the metric tensor) through the shell thickness is small. The inverse of the Jacobian can then be represented using a power expansion as

$$\underline{J}^{-1} = \underline{J}^{o\,-1} - \zeta\, \underline{J}^{o\,-1}\, \underline{R}\, \underline{J}^{o\,-1} \tag{2.7a}$$

or $$a_{ij}(\zeta) = a_{ij} + \zeta\, b_{ij} \tag{2.7b}$$

It should be noted that the usual assumption made in the literature is to neglect the variation in the Jacobian (Zienkiewicz, et al., 1971; Parisch, 1981), which is similar to Love's first approximation in classical shell theory. It will be demonstrated however that the above expansion is necessary so as to yield no strain under rigid body rotations.

2.3.2 Kinematics

The displacement representation is based on the kinematic assumption that the normal to the reference surface remains straight and inextensional during deformation. On the basis of this assumption an isoparametric element solution, in which nodal coordinates and nodal displacements are interpolated in the same order, is possible. (Strictly speaking this is a super-parametric element.)

An anagolous expression to Eq. 2.1 for the displacements of a point of the shell is given by

$$\underline{u} = \underline{u}^{o} + \zeta \frac{t}{2} \Delta\underline{u} \tag{2.8}$$

where $\underline{u}^{o}$ is the displacement of the midsurface and $\Delta\underline{u}$ is the normalized displacement of the shell relative to the midsurface. (See Fig. 2.2)

In finite element notation, Eq. 2.8 is interpolated as

$$\underline{u} = N^{P}(\xi,\eta)\ \underline{u}^{o^{P}} + \zeta N^{P}(\xi,\eta)\ \left(\frac{t}{2}\ \Delta\underline{u}\right)^{P} \tag{2.9}$$

For infinitesimal rotations (ie linear theory) the relative displacement of the shell is expressed in terms of two independent rotations (Fig. 2.3)

$$\Delta \underline{u} = \hat{\underline{v}}_{\alpha}\ \theta_{\alpha} \tag{2.10}$$

where $\hat{\underline{v}}_{\alpha}$ is the transverse vector, defined as

$$\hat{\underline{v}}_{\alpha} = (\underline{v}_{\alpha} \times \underline{v}_{3}) / \| \underline{v}_{\alpha} \times \underline{v}_{3} \| \tag{2.11}$$

where $\underline{v}_1$ and $\underline{v}_2$ are unit vectors, normal to each other and to $\underline{v}_3$, but otherwise arbitrarily defined.

For finite rotations, due to the non-vectorial nature of rotations and the desire to satisfy rigid body rotations, it is necessary to use either a trigonometric representation for the rotation of the normal (Ramm, 1977; Parisch, 1981), or by the use of the relative displacements on, say, the shell top surface together with a suitable updating algorithm (Huhges and Liu, 1981).

2.3.3 Strain displacement relations

A 'Total Lagrangian' formulation, in which stresses and strains are referred to the initial undeformed configuration, has been adopted. With reference to the Cartesian coordinate system, the Green strain tensor is given by

$$2\varepsilon_{ij} = u_{i,j} + u_{j,i} + u_{k,i}\, u_{k,j} \tag{2.12}$$

and the variation in the strain tensor is obtained as

$$2\dot{\varepsilon}_{ij} = \{ \dot{u}_{i,j} + \dot{u}_{j,i} + u_{k,i}\dot{u}_{k,j} + \dot{u}_{k,i}u_{k,j} \} + \{ \dot{u}_{k,i}\dot{u}_{k,j} \} \tag{2.13a}$$

or $$\dot{\varepsilon}_{ij} = \dot{\varepsilon}^{\ell}_{ij} + \dot{\varepsilon}^{n\ell}_{ij} \tag{2.13b}$$

In Eqs. 2.12 and 2.13 u_i is the displacement component in the i'th cartesian direction and $\dot{\varepsilon}^{\ell}_{ij}$ and $\dot{\varepsilon}^{n\ell}_{ij}$ are the linear and nonlinear parts of the incremental strain tensor, with respect to the incremental displacement. Differentiation with respect to the cartesian coordinate x_i is denoted by the subscripts ',i', while '.' denotes an incremental value (eg δu_i).

Equation 2.12 is simplified by relating derivatives (with respect to the isoparametric coordinate system) at a position (ξ,η,ζ) within the shell thickness to derivatives on the midsurface $(\xi,\eta,0)$ using Eq. 2.7. Substituting Eq. 2.8 into Eq. 2.12, and transforming derivatives from the isoparametric coordinate system to the global cartesian system using Eq. 2.7 yields

$$\begin{aligned} 2\varepsilon_{ij} = & \{ a_{ip}\bar{v}_{jp} + a_{jq}\bar{v}_{iq} + a_{ip}a_{jq}\bar{v}_{kp}\bar{v}_{kq} \} + \\ & \{ a_{ip}\bar{t}_{jp} + a_{jq}\bar{t}_{iq} + b_{ip}\bar{v}_{jp} + b_{jq}\bar{v}_{iq} \} \\ & + \text{nonlinear terms in } \zeta,\ \bar{v}_{ip} \text{ and } \bar{t}_{ip} \end{aligned}$$

or $$\varepsilon_{ij} = e_{ij} + \zeta\kappa_{ij} \tag{2.14}$$

where the over-bar '-' denotes a derivative of a cartesian component with respect to an isoparametric coordinate (eg $\partial u_i/\partial \xi_j$). $\bar{v}_{ij}$ and $\bar{t}_{ij}$ represent the components of the displacement gradient which are, respectively, independent of and dependent on ζ.

$$\bar{u}_{i,j} = \bar{v}_{ij} + \zeta\,\bar{t}_{ij} \tag{2.15}$$

Neglecting the additional nonlinear terms in Eq. 2.14 yields an expression for the extensional (e_{ij}) and curvature (κ_{ij}) strain resultants. Accounting for the nonvectorial nature of the rotations, the expression for

the extensional strain resultant yields exact strains on the midsurface. The curvature tensor can be identified as being analogous to Koiter's (1959) and Sanders' (1963) consistent linear curvature tensor for moderately small rotations, or Reissner's (1941) linear curvature tensor. These expressions yield no strain under rigid body motions. In contrast, the curvature expression suggested by Parisch (1981) does result in straining under rigid body rotations. These expressions are discussed further in Appendix A.

Retaining only the linear terms in the curvature expression is justified in problems of "medium bending" (Mushtari and Galimov, 1962). A linear curvature tensor is common in several large displacement shell theories, eg Marguerre (Green and Zerna, 1954) and Mushtari (1962). A linearization curvature tensor has also been adopted in several finite element formulations (Bergan and Clough, 1973; Thomas and Gallagher, 1975; Pica and Wood, 1980) with excellent results. It is however straight forward to include the nonlinear curvature terms (but still linear in ζ). Because this inclusion was found in this investigation to improve the convergence of the element, the nonlinear curvature terms have been retained.

The curvature tensor can be further simplified, by neglecting the variation of the Jacobian through the shell thickness ($b_{ij}=0$). This curvature expression does not satisfy rigid body rotation requirements but yields acceptable results for a linear, and hence incrementally linear, analysis.

Based on this simplification a consistent definition for the variation in the Green's strain tensor (Eq. 2.12) is obtained as

$$2\dot{\varepsilon}^{\ell}_{ij} = \dot{u}_{k,i}\overset{o}{g}_{jk} + \dot{u}_{k,j}\overset{o}{g}_{ik} \tag{2.16}$$

In Eq. 2.16 $\overset{o}{g}_{ij}$ is the deformation Jacobian associated with the midsurface.

$$g^{o}_{ij} = \delta_{ij} + \frac{\partial u_i}{\partial x_j} \Big|_{\zeta=0} \tag{2.17}$$

Equation 2.16 will be used to define the incremental tangent stiffness matrix. This equation is consistent with the thin shell assumption of neglecting the variation of the Jacobian, and hence the deformation Jacobian, through the thickness of the shell.

Equation 2.14 has been derived specifically for the case of moderate rotations, and to satisfy rigid body rotation requirements. In many cases however prebuckling rotations are small and it is acceptable to define the extensional and curvature expressions in terms of the infinitesimal rotation formulation (Eq. 2.10). This will however violate rigid body rotation requirements. It is therefore also reasonable to neglect the variation of the Jacobian through the shell thickness, which results in additional straining under rigid body rotations. A consistent definition for the total strain tensor is then obtained as

$$2\varepsilon_{ij} = \frac{1}{2}(u_{i,j} + u_{j,i}) + \frac{1}{2}(u_{k,i}g^{o}_{jk} + u_{k,j}g^{o}_{ik}) \tag{2.18}$$

Without significant loss of accuracy, a linear curvature tensor can be used, ie

$$2\kappa_{ij} = a_{ip}\bar{t}_{jp} + a_{jq}\bar{t}_{iq} \tag{2.19}$$

Equation 2.19 does not satisfy rigid body rotation requirements, but significantly does approximate Koiter's (1959) and Sanders' (1963) linear curvature tensor- as demonstrated in Example 3.5.2 of Chapter 3. (Strictly speaking Eq. 2.19 is similar to the Reissner-Love Equations as shown in Appendix A.) The incremental form of Eq. 2.19 is given by Eq. 2.16, by neglecting nonlinear curvature terms.

The relative accuracy of the different strain formulations given here are discussed in more detail in Appendix A, and demonstrated in the examples to follow. It will be demonstrated that for most typical shell applications, a nonlinear formulation based on the small rotation formulation is satisfactory.

2.3.4 Stress resultants

The separation of Eq. 2.14 into extensional and curvature terms allows for the convenient use of stress resultants. This has the advantage that numerical integration on the element level is carried out only on the mid-surface, and not at several points through the thickness of the shell for material nonlinear behavior.

The ensuing stress resultants, in local element coordinates, are defined as;

extensional
$$n_{\alpha\beta} = \frac{t}{2} \int_{-1}^{1} \sigma_{\alpha\beta} \, d\zeta \tag{2.20a}$$

flexural
$$m_{\alpha\beta} = \left(\frac{t}{2}\right)^2 \int_{-1}^{1} \zeta \, \sigma_{\alpha\beta} \, d\zeta \tag{2.20b}$$

transverse shear
$$q_{\alpha} = \frac{t}{2} \int_{-1}^{1} \sigma_{\alpha 3} \, d\zeta \tag{2.20c}$$

where $\sigma_{\alpha\beta}$ is the 2'nd Piola-Kirchoff stress tensor.

For compatibility with the material model, it is convenient to work in terms of the following stress-strain pairs: $(\frac{2}{t} n_{\alpha\beta}; e_{\alpha\beta})$ $(\frac{4}{t^2} m_{\alpha\beta}; \frac{t}{2} \kappa_{\alpha\beta})$, $(\frac{2}{t} q_{\alpha}; \gamma_{\alpha 3})$

2.3.5 Constitutive matrix

In this investigation small strains are assumed- hypoelasticity is not considered. Assuming a constitutive relation

$$\dot{\sigma}_{ij} = C_{ijk\ell}\,\dot{\varepsilon}_{k\ell} \tag{2.21}$$

the linearized stress resultant constitutive matrix, D, follows directly from the definition of the strain resultants (Eq. 2.20)

$$\begin{Bmatrix} \underline{n} \\ \underline{q} \\ \underline{m} \end{Bmatrix} = \frac{t}{2}\,\underline{D} \begin{Bmatrix} \underline{e} \\ \\ \frac{t}{2}\,\underline{\kappa} \end{Bmatrix} \tag{2.22}$$

In deriving the constitutive matrix in the element coordinates the following should be noted:

1. The plane stress hypothesis is invoked in the direction perpendicular to the middle surface (Eq. 2.3).
2. For a nonlinear material, the extensional and flexural terms are coupled.
3. A rational theory for including shear correction effects for a nonlinear material does not exist and several ad hoc procedures are used in the literature (Hughes and Liu, 1981; Owen and Figueriras, 1983). In the present formulation the simplifying assumption of a constant shear correction factor, typically 1.2, has been made.

2.3.6 Incremental equations of equilibrium

The incremental equations of equilibrium follow standard finite element procedures (Bathe, et al., 1980). The process is summarized below. Adopting a 'Total Lagrangian' formulation, the virtual work expression is given by

$$\int_V C_{ijk\ell}\,\dot{\varepsilon}_{k\ell}\,\delta\varepsilon_{ij}\,dV + \int_V \dot{\sigma}_{ij}\,\delta\dot{\varepsilon}^{n\ell}_{ij}\,dV =$$

$$= \delta W_{ext} - \int_V \sigma_{ij}\,\delta\dot{\varepsilon}^{\ell}_{ij}\,dV \tag{2.23}$$

where W_{ext} is the external virtual work.

The linearized virtual work expression (replacing $\dot{\varepsilon}_{ij}$ by $\dot{\varepsilon}^{\ell}_{ij}$) results in the incremental equilibrium equation for a single element

$$[\,\underline{K}_u + \underline{K}_g\,]\dot{\underline{d}} = \underline{R} - \underline{I} \tag{2.24}$$

where $\underline{K}_u$ is the stress independent stiffness matrix, $\underline{K}_g$ is the geometric or initial stress stiffness matrix, $\underline{R}$ is the vector of the external loads obtained from the finite element evaluation of the external work equation, $\underline{I}$ is the vector of internal nodal forces and $\dot{\underline{d}}$ is the vector of incremental nodal displacements.

Based on the thin shell assumption, the finite element matrices are evaluated by expressing the kinematic relations, Eqs. 2.13b and 2.16, in matrix form with respect to a local coordinate system as

$$\begin{aligned}\dot{\underline{\varepsilon}}^{\ell} &= \{\, \dot{e}_{11}\ \dot{e}_{22}\ \dot{\gamma}_{12}\ \dot{\gamma}_{13}\ \dot{\gamma}_{23}\,\} \\ &= \underline{\Lambda}\begin{bmatrix} B^{o} \\ \\ B' \end{bmatrix}\dot{\underline{d}}\end{aligned} \tag{2.25}$$

where $$\underline{\Lambda} = [\ \underline{I}_{5x5}\ \vert\ \zeta\ \underline{I}_{5x3}\ ] \tag{2.26}$$

and $$\begin{aligned}\dot{\underline{\varepsilon}}^{n\ell} &= \dot{\underline{u}}_{,i}\cdot\dot{\underline{u}}_{,j} \\ &= \dot{\underline{d}}^{T}\,[\underline{H}_i^{o\,T}\quad \underline{H}_i^{\prime\,T}\,]\underline{\Lambda}^{T}\underline{\Lambda}\begin{bmatrix} \underline{H}_j^{o} \\ \\ \underline{H}_j^{\prime} \end{bmatrix}\dot{\underline{d}}\end{aligned} \tag{2.27}$$

where $\underline{B}$ and $\underline{H}$ are strain displacement matrices.

It follows that:

Tangent Stiffness Matrix

$$\underline{K}_u = \int_{A^o} [\underline{B}^{o\,T} \quad \underline{B}'^{\,T}] \left\{ \int_{-1}^{1} \underline{\Lambda}^T \underline{D}\, \underline{\Lambda}\, d\zeta \right\} \begin{bmatrix} \underline{B}^o \\ \underline{B}' \end{bmatrix} dA^o \tag{2.28}$$

Geometric Stiffness Matrix

$$\underline{K}_g = \int_{A^o} [\underline{H}_i^{o\,T} \quad \underline{H}_i'^{\,T}] \left\{ \int_{-1}^{1} \sigma_{ij} \underline{\Lambda}^T \underline{\Lambda}\, d\zeta \right\} \begin{bmatrix} \underline{H}_j^o \\ \underline{H}_j' \end{bmatrix} dA^o \tag{2.29}$$

Internal Force Vector

$$\underline{I} = \int_{A^o} [\underline{B}^{o\,T} \quad \underline{B}'^{\,T}] \left\{ \int_{-1}^{1} \underline{\Lambda}^T \underline{\sigma}\, d\zeta \right\} dA^o \tag{2.30a}$$

where $$\underline{\sigma} = \{\sigma_{11} \; \sigma_{22} \; \sigma_{12} \; \sigma_{13} \; \sigma_{23}\} \tag{2.30b}$$

The terms within the brackets { } are integrated explicitly and yield, respectively, the stress-resultant constitutive matrix, a matrix of integrated stress-resultants, and a vector of stress-resultants. Area integration is carried out over the initial undeformed midsurface of the shell. In the actual implementation proceedure, the curvatures and moments associated with the transverse shear strains $\gamma_{\alpha 3}$ and stresses $\sigma_{\alpha 3}$ are not included. This results in a stress-resultant constitutive matrix of order 8x8, and strain displacement matricies $\underline{B}'$ and $\underline{H}'$ of order 3xN.

2.4 IMPLEMENTATION

The finite element discretization has been discussed in Section 2.3. In this section aspects of the implementation of this prodedure in FINITE

(Lopez, 1977) are discussed. The 4-, 8-, and 9-node elements have been implemented (BLSHELL, QSSHELL and QLSHELL) in FINITE. Both the small rotation and moderate rotation formulations have been included. These elements are compatible with the reinforced concrete material model RCSHELL described in Chapter 4. Further details are given in Appendix C.

2.4.1 Non-vectorial rotations

For geometric nonlinear applications, the nodal degrees of freedom adopted are the midsurface displacements $\underline{u}^o$ and the normalized displacement of the top surface of the shell, relative to the midsurface, $\Delta\underline{u}$. These relative displacements define a unit sphere within which the unit normal rotates. Only two relative displacements are independent, as they are constrained by the condition $\| \underline{v}_3 + \Delta\underline{u} \| = 1$.

For an infinitesimal displacement increment, the increment in the relative displacement reduces to the conventional linear form (Eq. 2.10)

$$\Delta\underline{u}^{\ell} = \hat{\underline{v}}_{\alpha}\ \theta_{\alpha} \tag{2.31}$$

The finite element matrices of Eqs. 2.28 to 2.30 utilize the definition contained in Eq. 2.31. The true increment in the relative displacement can then be obtained using the updating procedure of Hughes and Liu (1981), as shown in Fig. 2.4.

$$\begin{aligned} \underline{v}_3(t+\delta t) &= \underline{v}_3(t) + \Delta\underline{u}(\delta t) \\ &= \frac{\underline{v}_3(t) + \Delta\underline{u}^{\ell}(\delta t)}{\| \underline{v}_3(t) + \Delta\underline{u}^{\ell}(\delta t) \|} \end{aligned} \tag{2.32}$$

This approach is efficient and avoids the use of trigonometric representation for the rotations. In the present investigation, nodal

displacements are updated during the stress-strain recovery algorithm.

As noted, the variation of the Jacobian is not included in the matrices $\underline{B}$ and $\underline{H}$ of Eqs. 2.28 to 2.30, and is only included in the calculation of the total strains (and hence stresses) when using the moderate rotation option, using Eq. 2.12. The resulting stresses are then used in evaluating the internal force vector. This does result in an 'inconsistent' formulation but still retains the desired characteristic of producing zero strain under rigid body rotations. Including the first order expansion of the Jacobian in the strain displacement matricies of $\underline{B}$ and $\underline{H}$ would otherwise result in equations which are unnecessary complicated.

A disadvantage of the nodal degrees of freedom adopted (and their corresponding nodal loads) is that they are not natural to finite element users. This is demonstrated in Fig. 2.5a for specifying constraints and in Fig. 2.5b for external applied nodal moments.

2.4.2 Geometric stiffness matrix

The Geometric Stiffness matrix defined by Eq. 2.29 is seen to be composed of three stress-resultant terms. This is seen more clearly by examining the strain energy contribution to the Geometric Stiffness matrix. It follows from Eqs. 2.13b and 2.15

$$\delta\dot{U}_{K_g} = \int_v \sigma_{ij}\, \dot{v}_{ki}\, \dot{v}_{kj}\, dV + \int_v \zeta\, \sigma_{ij} (\dot{v}_{ki}\, \dot{t}_{kj} + \dot{v}_{kj}\, \dot{t}_{ki})\, dV + \\ + \int_v \zeta^2\, \sigma_{ij}\, \dot{t}_{ki}\, \dot{t}_{kj}\, dV \qquad (2.33)$$

For a nonlinear material the third term introduces an additional form of stress resultant, which is not present in linear material applications.

In Eq. 2.33 it is seen that the first term is dependent on the nonlinear portion of the extensional strain resultant $(\dot{v}_{ki}\dot{v}_{kj})$, and the

second and third terms on the nonlinear portion of the curvature strain resultant ($\dot{v}_{ki}\dot{t}_{kj}$ and $\dot{t}_{ki}\dot{t}_{kj}$). As can be inferred from the usual assumption of adopting a linear curvature tensor (see Section 2.3.3), it is acceptable to neglect the nonlinear curvature terms.

In addition, the geometric stiffness matrix is dominated by the contribution from the inplane stress resultant, and it is usual to neglect the normal shear contribution ($\sigma_{\alpha 3}$) in the first term (Pica and Wood, 1980). This contribution has also been neglected in the present formulation.

2.5 NUMERICAL EXAMPLES

In this section several examples are given to demonstrate the accuracy and applicability of this element to geometric nonlinear problems. (Material nonlinear applications are given in Chapter 4.)

All the examples considered here use the 9-node element with reduced integration. The standard Newton-Raphson solution procedure with a convergence tolerance of 1% has been used. The tolerance is defined as the ratio of the norm of the residual load to the norm of the applied load.

2.5.1 Cantilever subject to end load

This simple problem, shown in Fig. 2.6, was chosen to test the large displacement formulation, and in particular differences in using vectorial rotations and nonvectorial rotations. Note that for this structure the Jacobian does not vary through the thickness. The structure was modeled using five 9-node elements.

An analytical solution is given by Shield (1983), assuming that stretching of the beam remains negligible in comparison with the bending and

neglecting shear deformations. This structure has also been analysed by Parisch (1981).

In Fig. 2.6a a comparison is made using two variations of the small rotation formulation, together with the theoretical solution. In the first formulation the full nonlinear membrane strain displacement relation is used, together with a linear curvature tensor. The second formulation retains only the normal displacement contribution to the nonlinear extensional strain e_{11}, which results in an extensional strain resultant similar to that of Von Karman or the Donnell-Vlassov-Mushtari (Sanders, 1962) equations when applied to plates. It is seen that for this example the nonlinear strain terms retained has a significant effect on the predicted response. This dependency on the nonlinear strain terms is, however, generally not observed in statically indeterminate shell structures.

Although the overall results compare poorly with the theoretical solution, for PL^2/D less than about 1.0 satisfactory results are obtained for engineering purposes. The inadequacy of this formulation with increasing displacement is due to the incorrect representation of the rotation of the normal.

The moderate rotation formulation is compared with the theoretical solution in Fig. 2.6b. It is seen that excellent results are obtained using this formulation. This ability to be able to examine large displacements is due to the correct representation of the rotations.

2.5.2 Buckling of column

The buckling of a column under a slightly eccentric axial load is considered in Fig. 2.7. The column is modeled using five elements.

As only inplane displacements are considered, this example demonstrates the large displacement formulation under plane strain conditions. The results are compared with the analytical solution given by Timoshenko and Gere (1961), in Fig. 2.7.

2.5.3 Clamped square plate

This example has become a 'standard' in investigating geometric nonlinear thin plate formulations. The analytical thin plate solution is given by Levy (Pica and Wood, 1980) by solving Von Karman's plate equation using a double Fourier series.

The load-deflection behavior, obtained using a 2x2 mesh per quarter, is shown in Fig. 2.8. Almost identical results were obtained using both the small and moderate rotation formulations. Good agreement is obtained with the reference solution.

2.5.4 Hinged cylindrical shell

Details of this snap-through problem are given in Fig. 2.9. The structure was modeled using a 2x2 grid per quarter shell. Comparison of the vertical displacement at the apex is made with the results obtained by Bathe and Bolourchi (1980) using one cubic element and Parisch (1981) using a 4x4 mesh of QUAD4 elements (MacNeal, 1978). No discernable diference was found using the small and moderate rotation formulations. Good agreement is obtained with the results of Parisch.

2.5.5 Wind loaded cylinder

The nonlinear snap-through behavior of a wind loaded cantilever cylindrical shell under wind loading is examined. This structure has been

investigated experimentally by Kundurpi, et al. (1975), and also analytically by Brendel and Ramm (1980). Details of the cylinder are given in Fig. 2.10. The Fourier series expansion for the wind load pressure distribution as given by Kundurpi, et al. is used.

$$p = q_o \sum_n a_n \text{Cos}(n\theta) \tag{2.34}$$

where $a_o = 0.220$, $a_1 = 0.338$, $a_2 = 0.533$, $a_3 = 0.471$, $a_4 = 0.166$, $a_5 = -0.066$ and $a_6 = -0.055$, and q is the dynamic head, assumed to be constant with height. Eq. 2.34 includes an internal suction coefficient of 0.607.

One half of the shell is idealized using 4 elements in the vertical direction. In the circumferential direction 5 elements are used in the windward quadrant and 3 on the leeward quadrant. The predicted load deflection curve is shown in Fig. 2.10 and the deflected profile of the top of the cylinder at failure in Fig. 2.11. As with the previous examples the results obtained using the small and moderate rotation formulations were virtually indistinguishable. The limit load of 1.71 psi. agrees well with the experimental value of 1.90 psi., but is significantly lower than the limit load of 2.0 psi. obtained by Brendel and Ramm (1980).

2.6 SUMMARY

The degenerated finite element formulation using explicit integration has been presented in this chapter. Explicit integration has been adopted as it results in significant savings in computational effort, in particular for nonlinear material applications. The finite element formulation includes both geometric and material nonlinearities, using the Total Lagrangian formulation.

Two kinematic formulations have been presented for the large displacement analysis. The first approach uses a valid large rotation representation for the respective nodal degrees of freedom. A first order expansion of the inverse of the Jacobian is included, and the resulting strain displacement relations satisfy rigid body rotation requirements. This formulation is similar to Reissner's classical shell theory. The second formulation is a direct extension of the small displacement linear formulation to geometric nonlinear applications. The variation of the Jacobian through the shell thickness is neglected. This approach is suitable only for small rotations, as it results in straining under rigid body rotations (as does the corresponding linear formulation). This approach is similar to the Reissner-Love classical shell theory.

Several examples have been presented to examine differences in the two kinematic formulations. It has been demonstrated that for most practical applications, it is satisfactory to use a small rotation formulation to examine the prebuckling behavior of structures.

A family of degenerated shell elements, consisting of the 4-, 8- and 9-node versions, have been implemented in FINITE.

CHAPTER 3

ISOPARAMETRIC SHELL STIFFENING ELEMENT

3.1 INTRODUCTION

This chapter describes a compatible eccentric shell stiffening element for use with the degenerated shell elements described in Chapter 2. Two versions of the element are described, namely, a linear elastic version and one for material nonlinear applications. Both versions include geometric nonlinearities.

The elastic version is based on an appropriate beam theory and not a specialization of the more general thick shell element. Consequently the transverse shear and torsional behavior of any compact section is properly accounted for while still retaining the required displacement compatibility with the degenerated shell element. The material nonlinear version is essentially a specialization of the degenerated shell element to a beam, and consequently transverse shear and torsion behavior are lost.

3.2 FINITE ELEMENT DISCRETIZATION

The development of the elastic beam for small displacements is based on the derivation by Bouberg and Jirousek (1980) and Jirousek (1981).

3.2.1 Geometry

The initial geometry of the beam element is shown in Fig. 3.1 in which the superscripts 'o' refers to the reference axis (which corresponds to the mid-surface of the shell); 'e' refers to the point of contact between the

beam and the shell; 'g' refers to the centroidal axis of the beam, 's' refers to the shear center and 'g-i' defines the major principal axis of the beam. For the material nonlinear beam the shear center is assumed to coincide with the centroid, and the cross-section is limited to rectangular shapes.

The centroidal axis is related to the reference axis as

$$\begin{aligned} \underline{x}^g &= \underline{x}^o + \underline{e} + \underline{g} \\ &= \underline{x}^o + \Delta\underline{x} \end{aligned} \tag{3.1}$$

The geometry of the element is interpolated using Lagrangian shape functions in the usual manner.

A local orthogonal reference axis is constructed on the centroidal axis of the beam as shown in Fig. 3.2. The vector $\underline{a}_2^1$ defines the major principal axis of the beam as input by the user, and $\underline{a}_1$, $\underline{a}_2$ and $\underline{a}_3$ are obtained as

$$\begin{aligned} \underline{a}_1 &= \frac{\partial \underline{x}^g}{\partial \xi} \Big/ \left\| \frac{\partial \underline{x}^g}{\partial \xi} \right\| \\ \underline{a}_3 &= \frac{\underline{a}_1 \times \underline{a}_2^1}{\| \underline{a}_1 \times \underline{a}_2^1 \|} \\ \underline{a}_2 &= \frac{\underline{a}_3 \times \underline{a}_1}{\| \underline{a}_3 \times \underline{a}_1 \|} \end{aligned} \tag{3.2}$$

In general the plane defined by $\underline{g}$ and $\underline{i}$ is only approximately normal to the centroidal axis. This definition follows a similar philosophy to that for the degenerated shell element. (The definition of the reference axis differs from that used by Jirousek (1981)).

3.2.2 Kinematics

The displacement of the beam is defined in terms of the three global displacements and three global rotations associated with the shell element.

The nodal degrees of freedom do not therefore coincide with the centroidal axis of the beam, except when used as a stand-alone beam. This formulation is restricted to small rotations.

To meet the requirements of displacement compatibility along the joint axis, the displacement of the centroid of the beam is obtained by transforming the displacements of the shell to the joint axis and then to the centroid of the beam (Figs. 3.1 and 3.2).

$$\begin{aligned} \underline{u}^g &= \underline{u}^o + \underline{\omega}^o \times (\underline{e} + \underline{g}) \\ &= \underline{u}^o + \underline{A}\underline{\omega}^o \end{aligned} \tag{3.3}$$

where

$$\underline{A} = \begin{bmatrix} 0 & \Delta x_3 & -\Delta x_2 \\ -\Delta x_3 & 0 & \Delta x_1 \\ \Delta x_2 & -\Delta x_1 & 0 \end{bmatrix} \tag{3.4}$$

The rotation of the centroidal axis is identical to the rotation at the shell axis, ie.

$$\underline{\omega}^g = \underline{\omega}^o \tag{3.5}$$

3.2.3 Stress-strain relations

For a curved beam with shear deformations the constitutive equation relating the generalized stress $\underline{\sigma}$ (Fig. 3.3) to the generalized strain $\underline{\epsilon}$ can be approximated with reasonable accuracy by (Jirousek, 1981)

$$\underline{\hat{\sigma}} = \begin{Bmatrix} \hat{N} \\ \hat{Q}_2 \\ \hat{Q}_3 \\ \hat{T} \\ \hat{M}_2 \\ \hat{M}_3 \end{Bmatrix} = \begin{bmatrix} EA & & & & & \\ & GA_2 & & & & \\ & & GA_3 & & & \\ & & & GJ & & \\ & & & & EI_2 & \\ & & & & & EI_3 \end{bmatrix} \begin{Bmatrix} \hat{e}_{11} \\ \hat{\gamma}_{12} \\ \hat{\gamma}_{13} \\ \hat{\phi} \\ \hat{\kappa}_2 \\ \hat{\kappa}_3 \end{Bmatrix} \tag{3.6}$$

For small displacements the strain displacement relations are given by Jirousek (1981). In this study these relations have been extended to include geometric nonlinear behavior. The following strain displacement relations are used.

Extensional:

$$\hat{e}_{11} = \hat{u}^g_{1,\hat{x}_1} + \frac{1}{2}\,\underline{\hat{u}}^g_{,\hat{x}_1} \cdot \underline{\hat{u}}^g_{,\hat{x}_1} \tag{3.7a}$$

$$\hat{\gamma}_{12} = \hat{u}^s_{2,\hat{x}_1} - \hat{\omega}_3 + \underline{\hat{u}}^s_{,\hat{x}_1} \cdot (-\hat{\omega}_3 \quad 0 \quad \hat{\omega}_1) \tag{3.7b}$$

$$\hat{\gamma}_{13} = \hat{u}^s_{3,\hat{x}_1} + \hat{\omega}_2 + \underline{\hat{u}}^s_{,\hat{x}_1} \cdot (\hat{\omega}_2 \quad -\hat{\omega}_3 \quad 0) \tag{3.7c}$$

Curvature:

$$\hat{\phi} = \hat{\omega}_{1,\hat{x}_1} \tag{3.8a}$$

$$\hat{\kappa}_2 = \hat{\omega}_{2,\hat{x}_1} \tag{3.8b}$$

$$\hat{\kappa}_3 = -\hat{\omega}_{3,\hat{x}_1} \tag{3.8c}$$

It was demonstrated in Chapter 2 that the strain displacement relations given above are satisfactory for most applications. This formulation is, however, not capable of predicting torsional buckling which requires a nonlinear curvature (twist) relation. In stiffened shell applications,

torsional buckling is generally not possible.

In Equs. 3.7 and 3.8 $'$,$\hat{x}_1'$ stands for differentiation with respect to the local coordinate directed along the centroidal axis.

The primed displacements and rotations are associated with the local reference frame, and are related to the global components by the orthogonal transformation

$$\underline{u} = \underline{T}\,\hat{\underline{u}} \tag{3.9a}$$

and $$\underline{\omega} = \underline{T}\,\hat{\underline{\omega}} \tag{3.9b}$$

where $$\underline{T} = [\,\underline{a}_1 \;\; \underline{a}_2 \;\; \underline{a}_3\,] \tag{3.10}$$

The transformation of rotations is strictly valid only for infinitesimally small rotations.

The local inplane displacements $\hat{u}_2^s$ and $\hat{u}_3^s$ of the shear center are obtained as

$$\begin{bmatrix}\hat{u}_2\\ \hat{u}_3\end{bmatrix}^s = \begin{bmatrix}\hat{u}_2\\ \hat{u}_3\end{bmatrix}^g + \hat{\omega}_1 \begin{bmatrix}-x_2\\ -x_3\end{bmatrix}^s \tag{3.11}$$

As noted previously, for material nonlinear applications torsion and bending about the minor principal axis are not modeled. The resulting stress-strain relation is given by

$$\underline{\sigma} = \begin{Bmatrix} N_1\\ Q_3\\ M_2\end{Bmatrix} = \underline{D} \begin{Bmatrix} e_{11}\\ \gamma_{13}\\ \kappa_{12}\end{Bmatrix} \tag{3.12}$$

The constitutive matrix $\underline{D}$ follows from a similar definition to that used for the shell element.

3.2.4 Finite element formulation

The finite element formulation uses a Total Lagrangian approach, and follows the procedure discussed previously for the shell element (Section 2.3.6). This procedure is not repeated here.

3.3 LARGE ROTATION FORMULATION

The formulation outlined above is restricted to small rotations. It was demonstrated previously that for many practical applications there is no noticeable difference between a small rotation and a large rotation formulation. Furthermore, there is an additional justification in limiting the shell stiffener to a small rotation formulation. Shell stiffeners are typically used to limit the deformations of the structure, and hence it can be expected that prebuckling rotations will be small. (Note that the beam element is not compatible with the moderate rotation shell element formulation.)

A large rotation formulation similar to that presented in Chapter 2 is possible for the shell stiffener, but requires, in addition, transforming the inplane rotation of the midsurface of the shell to the centroid of the beam.

3.4 IMPLEMENTATION

Two beam elements have been implemented into FINITE (Lopez, 1977), namely a linear element BLBEAM and a quadratic element, QLBEAM. These elements include optional geometric nonlinearities, and material nonlinearities using the reinforced concrete model RCBEAM. Further details are given in Appendix C.

C(0)-continuity along the joint axis is obtained with the shell elements of Chapter 2 when the element is joined along a line of constant isoparametric shell coordinate (ie ξ constant, or η constant). In this regard it is noted that in several of the applications given by Bouberg and Jirousek (1980), C(0)-continuity is not obtained.

3.5 NUMERICAL EXAMPLES

3.5.1 Curved cantilever

The curved cantilever beam shown in Fig. 3.4 is analysed to demonstrate the small displacement linear elastic formulation. The beam is modeled using three quadratic elements. The calculated end displacement of 0.11585 in. agrees well with the calculated displacement of 0.11589 in. obtained by Jirousek (1981) and 0.11582 in. by Timoshenko (1941). The Timoshenko results are slightly stiffer since they do not consider shear deformations.

3.5.2 Snap-through of a shallow arch

The snap-through of a shallow arch subject to a concentrated midspan load is considered in Fig. 3.5. Only half of the arch has been analysed, using four quadratic elements. The solution compares well with that obtained by Bathe, et al. (1975) and by Hughes and Liu (1981).

3.5.3 Bifurcation of a circular arch

Batoz (1979) draws attention to the necessity of using a consistant shell theory when investigating bifurcation of shell and arch structures. As an example the bifurcation of a circular arch under constant dead

pressure was investigated using finite elements based on the Donnell-Mushtari-Vlassov (Sanders, 1963) and the Koiter (1959) - Sanders (1963) shell theories. As shown in Fig. 3.6 (Batoz, 1979) the DMV relations predicted a bifurcation load 22 percent higher than that obtained using the KS theory.

This problem has been analysed using eight curved beam elements and a slighty eccentric load to investigate bifurcation. In Fig. 3.6 it is seen that the present small rotation formulation, which includes a linear curvature relation, correctly approximates the Koiter-Sanders consistant strain displacement relations.

3.6 SUMMARY

Compatible eccentric shell stiffeners for the shell elements of Chapter 2 have been presented. Two versions of the element have been included, namely a Timoshenko type beam element for linear elastic applications and a modified element for nonlinear material applications. Both versions include geometric nonlinearities, using a small rotation formulation. This geometric nonlinear formulation is similar to that used in shell applications and employs a linear curvature tensor. Torsional and out of plane buckling are not accounted for.

Examples have been presented to demonstrate the application of this element to both small and large displacement applications.

A linear 2-node element and a quadratic 3-node element have been implemented in FINITE.

CHAPTER 4

CONSTITUTIVE MODELING OF REINFORCED CONCRETE

4.1 INTRODUCTION

In this Chapter the constitutive modeling of reinforced concrete under uniaxial and biaxial stress states is described. The modeling of concrete and steel properties is first briefly described, followed by a numerical algorithm for modeling the behavior of reinforced concrete shell, panel and beam type problems.

This approach is concerned with the 'average' or 'global' behavior of the concrete, and adopts the smeared crack approach together with a layered material model.

4.2 MATERIAL PROPERTIES OF CONCRETE AND STEEL

4.2.1 Stress-strain relations for plain concrete

Typical stress-strain curves for concrete under biaxial stress conditions, as is assumed to occur in slab and shell structures, are shown in Fig. 4.1 (Kupfer and Gerstle, 1975). Figure 4.2 illustrates a typical biaxial strength envelope for concrete subject to proportional biaxial loading (Kupfer and Gerstle, 1975).

Figures 4.1 and 4.2 illustrate that under biaxial compression loading, concrete exhibits an increased compressive strength, increased 'ductility' and increased stiffness. Under biaxial tension concrete exhibits a slightly increased tensile strength as compared with that under uniaxial loading.

Combinations of tension and compression result in noticeably reduced strength.

In the present study Liu's biaxial orthotropic material model (Liu, et al. 1972) is used, together with a modified form of the failure criteria proposed by Darwin and Pecknold (1974) and Rajagopal (1976). This failure envelope has been changed to yield maximum principal stresses and strains by converting, approximately, equivalent uniaxial strains to principal strains. Further details of the model are given in Appendix B.

4.2.2 Bond between concrete and reinforcement

Bond between concrete and steel reinforcement is of fundamental importance to most aspects of localized reinforced concrete behavior. Bond slip and degradation affects the stress distribution in the concrete and steel and the width and spacing of cracks (Fig. 4.3).

Based on experimental results, several mathematical formulations have been proposed for modeling the bond stress-slip behavior (ASCE, 1981; Gerstle, 1981). However in many cases bond stress-slip degradation is only of secondary importance and may not affect overall structural behavior significantly, especially for monotonic loading (Gerstle, 1981) In cases such as these it is sufficient to model bond in an averaging approach through the concept of tension stiffening, which has been adopted in this investigation.

4.2.3 Tension stiffening of cracked concrete

Cracking in reinforced concrete elements occurs at very low stresses when compared to the compressive strength of concrete. Cracking results in

a significant reduction in the stiffness of the concrete element.

The reduction in the stiffness depends on the average tensile stress in the concrete between cracks (Fig. 4.3). Under increasing load the average tensile stress carried by the concrete decreases as degradation of the bond occurs. This can be modeled in an average sence by applying a gradual unloading to the stress-strain curve of concrete in tension (Lin, 1973), or by lumping the tension stiffening into the reinforcement (Gilbert and Warner, 1978). Both of these forms of tension stiffening have been incorporated in this investigation (see Appendix B). Tension stiffening is discussed in more detail in Section 4.3.4.

4.2.4 Shear transfer in cracked concrete

The transfer of shear across cracks arises from aggregate interlock, frictional forces and dowel action. Aggregate interlock and frictional forces (interface shear transfer) are primarily affected by the crack width, while dowel action is affected by the concrete cover to the bar, presence of stirrups, bar size and tensile strength of the concrete.

Studies have shown that the overall response of the structure is not sensitive to the modeling of the shear transfer mechanism, and it is generally satisfactory to model shear transfer using either a constant or a crack width dependent shear modulus (ASCE, 1981; Gerstle 1981) A constant shear retention factor of 0.25 has been used in this investigation.

4.2.5 Steel reinforcement

Typical stress-strain curves for steel reinforcing bars loaded monotonically in tension are shown in Fig. 4.4 (Abdel Rahman, 1982). The

stress-strain curves of the steel are assumed to be identical in compression.

Steel reinforcement is modeled in this investigation as an ideal elastic-plastic material, with possible strain hardening.

4.3 NUMERICAL MODEL FOR REINFORCED CONCRETE

The numerical algorithm used in this investigation to model the behavior of cracked concrete is based on the 'rotating crack model' by Gupta and Habibollah (1982). This algorithm was derived by Gupta so as to obtain failure loads consistent with theoretical 'yield line', or limit, solutions for panel sections subjected to inplane loading. This algorithm has been extended in this investigation to include flexural behavior.

It should be noted however that this algorithm has been used in the literature much earlier, by Cope, et al. (1977, 1980), for the analysis of slab sections subject to flexural loading. This model was introduced as a simplification to the solution procedure being used, without recognition of the capabilities of the algorithm.

The model used is developed below, by considering the behavior of reinforced concrete elements subject to inplane loading.

4.3.1 Response of cracked concrete to inplane loading

The behavior of a typical reinforced panel subject to inplane loading is shown in Fig. 4.5, in which the loading is limited to biaxial tension-compression (including shear). For the purpose of this discussion it is assumed that the panel is reinforced with two orthogonal layers of reinforcement.

Prior to cracking of the concrete the panel behaves essentially linearly, but after cracking the response is strongly nonlinear. Depending on the loading arrangement as well as on the amount and orientation of the reinforcement and the concrete compressive strength, failure can result as yielding of the reinforcement, as crushing of the concrete or a combination of both.

Initially as the load is applied, cracks form approximately normal to the direction of maximum principal strain and the amount and orientation of the reinforcement has only a negligible effect on both the behavior of the panel prior to cracking and on the crack orientation. In nonisotropically reinforced panels as the loading is further increased and the reinforcement yields, these initially formed cracks become less prominent and new cracks are formed due to the ability of the cracks to transfer shear. This change in the crack direction, and the consequential change in direction of the maximum panel stiffness, was clearly observed in the experiments of Vecchio and Collins (1982).

A lower bound to the ultimate load of the panel considering failure by yielding of both layers of reinforcement (unconstrained or free shear), can be obtained from the equilibrium of a cracked element as shown in Fig. 4.6. This approach, often referred to as the "Principle of Minimum Resistance" (Gupta, 1981), yields,

$$N_{xy} = \sqrt{(N'_x - N_x)(N'_y - N_y)} \tag{4.1a}$$

and

$$\text{Tan}(\theta) = \frac{N'_x - N_x}{N_{xy}} = \frac{N_{xy}}{N'_y - N_y} \tag{4.1b}$$

in which N_x, N_y, and N_{xy} are the components of the applied inplane loading,

N'_x and N'_y are the reinforcement capacities in the x and y directions respectively and θ is the crack orientation. In this approach it is implied that the crack orientation at failure is independent of the initial crack orientation. In arriving at Eqs. 4.1, and in Fig. 4.6, it is assumed that the crack is normal to the maximum principal concrete stress and that no tension from the concrete exists across the crack. In general the orientation of the crack, or yield line, predicted by Eq. 4.1b will not coincide with the orientation of the cracks initially formed.

As noted, failure of reinforced concrete panels subject to biaxial tension-compression and/or shear loading is not limited to yielding of both layers of reinforcement, but a compressive failure can also occur. Considering failure in which the concrete crushes in compression proceded by one layer of reinforcement yielding (constrained shear), equilibrium of the cracked element in Fig. 4.6 results in

$$N_{xy} = \sqrt{(N'_x - N_x)\{N'_c - (N'_x - N_x)\}} \qquad (4.2a)$$

and

$$\mathrm{Tan}(\theta) = \frac{N'_x - N_x}{N_{xy}} = \frac{N_{xy}}{N'_c - (N'_x - N_x)} \qquad (4.2b)$$

,where N'_c is the concrete compressive force at failure, accounting for any degradation of the concrete compressive strength. In Eqs. 4.2 it is assumed that the x-direction reinforcement yields. Provided that the concrete compressive stress at failure is known, Eq. 4.2 is a lower bound to the actual failure load (Braestrup and Nielsen, 1982).

A compressive failure such as this is characteristic of heavily reinforced sections and also nonisotropically reinforced panels in which significant distortion of the concrete occurs. However the amount of

degradation of the concrete compressive strength which actually occurs is as yet unresolved. Experiments by Vecchio and Collins (1982), as well as earlier experiments by Robinson and Demorieux (1972), showed a significant degrading of the concrete strength and stiffness occurring as cracked sections are distorted. These results were obtained on specimens heavily reinforced in at least one direction, and using closely spaced reinforcement together with relatively low concrete strengths. More recent experiments to further investigate this degrading effect considering nominally reinforced sections, did not however yield significant degrading- a reduction of typically less than 10% (Schlaich and Schafer, 1983).

The suitability of Eq. 4.1 can be judged from Figs. 4.7 and 4.8 in which a comparison has been made with analytical results predicted by Vecchio and Collins (based on their experimental investigations), for panel sections loaded in pure shear. From these figures it is seen that for lightly reinforced sections, together with increasing cylinder strengths, failure of the panel occurs by yielding of both layers of reinforcement and the failure load is correctly predicted by Eq. 4.1. Conversely for heavily reinforced or highly nonisotropically reinforced sections subject to shear loading, a compression failure dominates.

Most shell structures are lightly reinforced and are constructed from at least moderately strong concrete (with a cylinder strength in excess of 30 MPa). In addition, as a result of serviceability criteria to limit crack widths (Gupta, 1981), excessive anisotropic deformations prior to failure would not be expected to occur. Noting also the uncertainty in estimating the degradation of the concrete compressive stress, it appears reasonable for most shell structures to neglect any degrading effect of the concrete.

4.3.2 Numerical modeling of cracked reinforced concrete

Equations 4.1 and 4.2 are lower bound solutions for the ultimate load for the cases considered, and were obtained by assuming that at failure the crack orientation is normal to the maximum principal concrete stress. It can be shown that for certain conditions (Braestrup and Nielsen, 1983), Eqs. 4.1 and 4.2 yield coinciding upper and lower bounds.

Hence it appears desirable that any numerical technique should approximate the changing crack direction effect observed in nonisotropically reinforced sections. However, this has not been accounted for consistently in the literature. With the exception of Cope, et al. (1977, 1980) and Gupta (1982), the crack direction is assumed fixed once it forms, and while it remains open. Retaining some shear stiffness for singly cracked concrete allows for subsequent cracking, but the direction of the second crack is limited by the shear stiffness employed for doubly cracked concrete (ASCE, 1981).

Analytical methods which do not retain some shear stiffness for doubly cracked concrete can still allow for nonorthogonal cracking (Hand, et al., 1972) although several references restrict secondary cracking to form orthogonal to the primary crack (Darwin and Pecknold, 1974; Kabir, 1976). This restriction may violate the cracking criterion within the element. Retaining some shear stiffness for doubly cracked concrete requires the formation of orthogonal cracks (Lin, 1973), unless the material axes are reorientated upon formation of the second crack to bisect the crack directions (Abdel Rahman, 1982; ASCE, 1981). Using this latter approach it is also necessary to limit the formation of subsequent cracks to above a specific divergence angle to the primary crack, say 30 degrees (Ivangi,

1981), to prevent excessive compressive stresses normal to the new material axes.

For a fixed crack direction and considering only orthogonal cracking, the failure load for the cracked element of Fig. 4.6 is given by

$$N_{xy} = \frac{1}{2}\left\{\frac{N'_x - N_x}{\mathrm{Tan}(\theta)} + (N'_y - N_y)\,\mathrm{Tan}(\theta)\right\} \tag{4.3a}$$

and

$$\mathrm{Tan}(2\theta) \propto \frac{2N_{xy}}{N_x - N_y} \tag{4.3b}$$

where θ is the (initial) crack angle.

Equation 4.3 has been obtained by assuming the concrete to be linearly elastic in compression and using a shear retention factor of 0.25. As material failure is no longer checked for arbitary directions of the maximum principal concrete stress, Eq. 4.3 will overestimate the failure load.

Gupta and Habibollah (1982) have developed an algorithm which allows for the changing crack direction effect. The relevent assumption on which this algorithm is based is that the crack direction is always normal to the direction of the major principal concrete stress. This assumption has also been made by Duchon (1972), and also by Vecchio and Collins (1982) in developing a numerical algorithm consistent with their experimental results.

Under the simplifying assumption that the directions of principal concrete stress and principal strains coincide, it follows that the rotating crack algorithm will correctly predict failure loads given by Eqs. 4.1 and 4.2. The assumption that the principal concrete stress and strain coincide was shown to be at least approximately true in the experiments of Vecchio and Collins.

This numerical solution therefore has the capability of predicting the full nonlinear response of membrane elements subjected to inplane shear and normal stresses.

4.3.3 Cracking model

The constitutive model used in this investigation is based on the incrementally linear smeared crack element model, as used by Darwin (1974), together with the material model described in Section 4.2 and Appendix B. The material model used predicts that the concrete principal stresses and strains coincide.

Progressive cracking, or changes in the crack orientation, are accounted for in the cracking model by assuming that the crack direction is always normal to the direction of the maximum principal strain. In contrast to the model used by Hand, et al. (1972), Lin, (1973), Darwin and Pecknold (1974) and Kabir (1976), the material axes are not fixed after formation of the initial crack, but its orientation is determined as the direction of the maximum principal strain at the beginning of each iteration.

For intact concrete, the concrete contribution to the incremental tangent stiffness matrix in the material coordinates is obtained as (Darwin and Pecknold, 1974)

$$\Delta\underline{\sigma} = \frac{1}{1-\nu^2}\begin{bmatrix} E & \nu\sqrt{E_1E_2} & 0 \\ \nu\sqrt{E_1E_2} & E_2 & 0 \\ 0 & 0 & \frac{1}{2}(E_1+E_2-2\nu\sqrt{E_1E_2}) \end{bmatrix} \qquad (4.4)$$

where $\Delta\sigma_i$ (i=1,2) is the stress increment in the direction of the current principal strain, $\Delta\varepsilon_i$ is the corresponding strain increment, E_i is the tangent modulus and ν is Poissons ratio.

A maximum principal stress criterion is used to determine failure in tension. The constitutive relation for cracked concrete is then obtained by setting the tangent modulus, say E , to zero in Eq. 4.4,

$$\Delta\underline{\sigma} = \begin{bmatrix} 0 & 0 & 0 \\ 0 & E_2 & 0 \\ 0 & 0 & \beta_s E_2 \end{bmatrix} \Delta\underline{\varepsilon} \tag{4.5}$$

The shear retention factor in Eq. 4.5 is introduced to account for the effective shear modulus along the cracks due to shear friction and dowel action. Note that although it is implied that there is no shear along the current crack, this does not exclude the presence of a shear stress on previously formed cracks. In fact it is this shear stress which will cause subsequent cracking and effectively produces changes in the crack orientation.

In developing a numerical algorithm, Gupta (1982) obtained the rotating crack tangent stiffness matrix as the sum of the conventional fixed crack tangent stiffness matrix (Eq. 4.5), plus a contribution which reflects possible changes in the crack direction. This can be obtained as follows,

$$\begin{aligned} \Delta\underline{\sigma} &= \underline{K}\Delta\underline{\varepsilon} + \frac{\partial\underline{\sigma}}{\partial\theta}\, d\theta \\ &= (\underline{K} + \underline{G})\, \Delta\underline{\varepsilon} \end{aligned} \tag{4.6}$$

in which $\underline{K}$ is given by Eq. 4.5, and $\underline{G}$ represents the possible changes in the crack direction.

An expression for the rotating crack tangent stiffness matrix assuming the concrete to be linearly elastic and neglecting the tensile strength of the concrete (and tension stiffening) is given by Gupta (1982), and can easily be extended to overcome these limitations using Eq. 4.6.

While Eq. 4.6 is theoretically correct (within the assumptions made), in keeping with the iterative nature of a nonlinear finite element approach any suitable incremental tangent stiffness matrix can be used. It is therefore possible to neglect the rotating crack contribution $\underline{G}$, provided that the changing crack direction is adequately accounted for in the pertinent parts of the solution procedure- in particular in selecting the material axes and transforming from the material to the global or element axes.

In this investigation it was found that neglecting the rotating crack stiffness matrix only rarely increased the number of iterations and did not introduce any numerical instabilities.

4.3.4 Tension stiffening

The inclusion of a realistic tension stiffening model is very important when analysing lightly reinforced sections subject to inplane loading, and also structures which are endangered by stability failures. An example of the significance of tension stiffening when modeling instability problems is shown in Fig. 4.9 (Eibl and Kesting, 1978). In Fig. 4.9, the factor β characterizes the length of the descending branch of the concrete stress-strain curve. (See Appendix B, Fig. B6.)

Different values of β have been used in the literature: Lin (1973) adopted a value of about 6, Gilbert and Warner (1978) used 10, and Abdel Rahman (1982) set β equal to 10 to 25. Melhorn (1981) used $\beta\varepsilon_t$ equal to 2.0 $\mu\varepsilon$ and Cope, et al. (1980) set $\beta\varepsilon_t$ to 1.5 $\mu\varepsilon$. There is however little experimental evidence from which β can be determined. It should also be noted that an upper bound to $\beta\varepsilon_t$ must be set so that the tension stiffening

does not artificially increase the total stress in the direction of any yielded reinforcement. A conservative proceedure to insure that this does not occur is to limit the upper bound of $\beta\varepsilon_t$ equal to the yield strain of the reinforcement.

Limited experimental results have been obtained from the experiments of Vecchio and Collins (1982), and these report reasonably high tension stiffening effects "even for strains one hundred times greater than the cracking strain". Admittedly these results were obtained from relatively heavily reinforced specimens, with a reinforcement percentage of 1.875% in at least one direction. In Fig. 4.10 the results obtained by Vecchio and Collins are reproduced, together with assumed unloading concrete stress-strain curves corresponding to $\beta\varepsilon_t$ equal to $2.0\mu\varepsilon$ ($\beta \simeq 20$). From Fig. 4.10 it appears that β=20 is sufficiently conservative. Consequently that value has been used as the default value in this investigation.

An alternative approach has been used by Mang and Floegl (1981, 1982), which is based on bond slip. Using a shear-slip relationship together with an experimental expression for the bond stress, the additional work done by the bond force can be found. This method attempts to take into account the angle between the crack and the intersecting reinforcing bar, the crack propagation through the thickness and secondary cracking between primary cracks. However, this proposed model requires that the crack spacing has to be specified a priori. This model is referred to again in Chapter 5.

4.3.5 Comparison with experiments

The response of panel sections to inplane shear and normal stresses has been extensively investigated by Vecchio and Collins (1982). Their

experiments covered a wide range of orthogonal reinforcement percentages, but most of the specimens were heavily reinforced in at least one direction. Twelve nonisotropically reinforced specimens, with 1.875% reinforcement in the strong direction, were tested in pure shear. Most of these specimens failed in compression, or experienced edge related failures. Five isotropically reinforced specimens, with 1.875% reinforcement in both directions and a yield strength exceeding 420 MPa, were tested under combined stress states. As can be expected, all of these specimens failed in compression.

A comparison has been made with selected experimental results to evaluate the suitability of the rotating crack model. This comparison is directed mainly at failures of panel sections in unconstrained shear. Details of the material properties and the loading arrangements for the panels selected are given in Tables 4.1 and 4.2 respectively. Of the nonisotropically reinforced panels, only panel PV11 failed by yielding of both orthogonal layers of reinforcement. Panels PV18 and PV19 failed in bond and shear respectively, but yielding of the second layer of reinforcement was imminent, and therefore these specimens have also been included. Panels PV16, PV17 and PV25 have also been included, but the results for these panels are the same using both the rotating and fixed crack models.

The comparison of the experimental response and the numerical results are shown in Figs. 4.11 to 4.16 while further details are given in Table 4.3. In general good agreement is obtained using the rotating crack model. It should be noted that part of the discrepancy, in both the failure mode and the failure laod, between the rotating crack model and the experimental results of panels PV18 and PV19 is due to a degradation of the concrete

strength. This degradation of the concrete compressive strength is not accounted for in the present model. It is interesting to note from Figs. 4.14 and 4.15 that the fixed crack model significantly overestimates the ultimate load of anisotropically reinforced specimens in which the direction of the principal load is at an angle greater than about 45 degrees to the principal reinforcement direction.

4.3.6 Extension to model flexural behavior

The algorithm presented previously can be extended to model flexural behavior, or combined inplane-flexural behavior, by combining the solution algorithm together with the layered material model approach (Hand, et al., 1972). In this approach the concrete is divided up into a number of 'layers' through the thickness and each layer is assumed to be in a state of plane stress. The rotating crack concept is then applied to each cracked layer individually. It will be demonstrated below that this model does give yield line orientations and failure loads consistent with experimental results and yield line theory.

The rotating crack model, together with the more conventional fixed crack model, have also been compared to the statically determinate specimens tested by Cardenas and Sozen (1968). Two groups of specimens with varying orientations of reinforcement have been investigated, namely specimens subject to uniaxial bending (M2/M1 = 0) and biaxial bending (M2/M1 = -0.14).

Details of the specimens investigated are given in Table 4.4 and Figs. 4.17 to 4.19. The predicted response of these specimens are shown in Figs. 4.20 to 4.27 and summarized in Table 4.5. It is seen from these figures that the rotating crack model is satisfactory in modeling the behavior of

these specimens, not only with regard to the yield moment and ultimate moment but also in predicting the yield line orientation (and hence the curvature distribution) at failure. The deficiency of the fixed crack model in predicting the behavior of anisotropically reinforced specimens with respect to the principal load, as seen in Section 4.3.4, can also be seen in Figs. 4.25 and 4.26.

4.4 IMPLEMENTATION

The layered constitutive material model discussed above has been implemented in FINITE (Lopez, 1977). Two models have been written, namely a general shell element material model RCSHELL and a simplified beam material model RCBEAM. These models are compatible with the degenerated shell and beam elements discussed in Chapters 2 and 3.

The stress resultant constitutive matrix is obtained by integrating Eq. 4.4 through the shell thickness, and adding the normal shear components. It is assumed in this material model that the normal shear does not affect the biaxial behavior of the concrete. The normal shear is based on the initial modulus of the concrete, and does not depend on the cracking of the element. This approach is similar to that implied in most shell elements which do not account for shear deformations.

4.5 NUMERICAL EXAMPLES

Three examples are given below to demonstrate the application of the material model described above in finite element applications.

4.5.1 Delft beam

The first example considered is that of a symmetrically loaded simply supported beam (Walraven, 1982). Details of the beam and material properties are given in Fig. 4.28. The beam is analysed using five quadratic beam elements together with the beam element material model.

A comparison between the measured and predicted response is given in Fig. 4.29. For this simple example excellent agreement has been obtained.

4.5.2 Duddeck's slabs

In this example three corner supported slabs tested by Duddeck, et al. (1978) are studied. The first slab is isotropically reinforced while the latter two have differing degrees of orthotropy of reinforcement. The slabs have well defined support conditions with only the transverse deflection at the supports restrained.

Details of these slabs have been taken from Abdel Rahman (1982). The material properties are given in Table 4.6 and structural details in Fig. 4.30. One quarter of the slab has been analysed using nine quadratic shell elements, which were evaluated using reduced integration. To prevent spurious energy modes (involving the vertical displacement) an additional fully integrated element with a modulus of elasticity of 1.0 has been superimposed over the central element.

Only the rotating crack model has been used to investigate these slabs. Load-central deflection curves are given in Figs. 4.31 to 4.33 for Slabs S1, S2 and S3 respectively. Also presented are the results obtained by Abdel Rahman for β=25. The experimental and predicted failure loads are summarized in Table 4.7. Also included in Table 4.7 are failure loads based

on a yield line solution (neglecting the compression reinforcement, Abdel Rahman (1983)). Satisfactory agreement has been obtained with the experimental results. It should be noted that the results obtained by Abdel Rahman were obtained using a fixed crack model and by limiting subsequent cracking to occur above a divergence angle of 30 degrees to the primary cracks. Crack patterns for the three slabs and status of yield conditions in the reinforcement at the integration points are given in Figs. 4.34 to 4.36.

4.5.3 Bouma's cylindrical shell

A series of eleven one-eighth scale model cylindrical shells with edge beams have been tested by Bouma, et al. (1961). The cylindrical shells were constructed of reinforced mortar. Each shell has a rigid end diaphragm which is simply supported on the four corners. One of these shells, Shell A2, is investigated here. This example has also been investigated by Arenson (1979) and Abdel Rahman (1982).

Dimensions of the shell are given in Fig. 4.37 and the reinforcement details in Fig. 4.38. The material properties used are given in Table 4.8, and have been taken from Arenson (1979).

The full scale shell was designed for dead load plus 25% to account for live load. The loading on the model is therefore 2.45 kN/m^2 on the shell roof and 0.49 kN/m on the edge beams. This load is increased proportionally in the test.

Details of the finite element mesh used are given in Fig. 4.39. One quarter of the shell is modeled using eight quadratic shell elements and four quadratic beam elements. As discussed in Chapter 3, the beam elements do not account for torsion or bending about the minor principal axes.

In Fig. 4.40 the central deflection of the edge beam is plotted against the total load applied to the shell. Two analyses have been undertaken, namely including and neglecting geometric nonlinearities. The failure load of 44.0 kN obtained for the small displacement analysis is close to the ultimate load of 40 kN calculated according to a simple beam-type analysis reported by Bouma. Good agreement with the experimental ultimate load of 50 kN is obtained by including geometric nonlinearities, but the present load-displacement curve appears to be too stiff. The results obtained by Arenson are also included in Fig. 4.40.

The predicted crack pattern for the shell near failure is shown in Fig. 4.41. The shell failed by yielding of the reinforcement in the beams and yielding of the transverse reinforcement at the top of the shell, near the center line of the shell.

4.6 SUMMARY

The modeling of cracked reinforced concrete using the 'rotating crack' algorithm has been discussed. In this algorithm progressive cracking, or changes in the crack orientation, are accounted for by assuming that the crack orientation is always normal to the current maximum principal strain direction. It has been demonstrated that this algorithm yields failure loads consistent with yield line solutions.

This algorithm has been implemented together with a nonlinear biaxial orthotropic material model. The stress-strain behavior of the concrete is described using Liu's material model (1972) and a modified form of the failure envelope used by Darwin (1974) and Rajagopal (1976). The material model is described in detail in Appendix B. Full bond is assumed between the concrete and reinforcement, and tension stiffening is included.

This model is primarily restricted to static loading applications, but limited unloading capabilities have been included to model unloading which can occur in structural instability applications.

CHAPTER 5

FAILURE OF REINFORCED CONCRETE COOLING TOWERS UNDER WIND LOADING

5.1 INTRODUCTION

The safety of cooling towers under wind loading has been the subject of extensive research over the past twenty years or so. Much of this research is as a consequence of the failure of the Ferrybridge Towers in 1965 in the U.K. (CEGB, 1976), and the failure of the Ardeer tower in Scotland in 1973 (ICI, 1974). The collapse of these towers has since been explained as resulting from, amongst other contributing factors, an under-estimation of the design wind load and due to gross imperfections respectively. In addition to these failures a cooling tower collapsed in Northern France in 1979, and more recently a 114 m high (375 ft) cooling tower collapsed at Fiddler's Ferry Power Station in the U.K. in January 1984 (ENR, 1984). The only other report of damage to cooling towers due to wind loading concerns the damage which was sustained by the Port Gibson tower in Mississippi USA during a tornado.

To date the safety of cooling towers under wind loading has not been satisfactorily resolved, in particular with regard to the buckling safety and the effect of cracking on the strenght or stability of the tower. These effects are likely to become even more important as the height of these towers approaches 200 m (565 ft).

This Chapter investigates the effect of cracking on the failure and stability of reinforced concrete cooling towers. These results are then examined in the light of present day practice, and in particular against

methods of design for strength and buckling which are based on an assumed elastic behavior of the tower.

5.2 REVIEW OF PREVIOUS RESEARCH

5.2.1 Experimental results

A series of wind tunnel experiments were carried out by Der and Fidler (1968) to investigate buckling of cooling towers under wind loading. To date these tests remain the basis for judging the buckling safety of cooling towers used in most codes of practice (BSI BS3445, 1975; ACI-ASCE Committee 334, 1977; IASS Working Group No. 3, 1977), and also form the standard against which many investigators have evaluated their analytical techniques for cooling tower buckling.

The Der and Fidler tests consisted of investigating PVC and copper model towers. The resulting elastic snap-through load was obtained as

$$q_c = C\ E\ (t/R)^{2.3} \qquad (5.1)$$

where q_c is the dynamic head at which buckling occurs, C is an imperical coefficient, E is the modulus of elasticity of the shell, t is the thickness of the shell at the throat and R is the radius of the shell parallel circle at the throat.

The mean value of C recorded in the experiments for 15 intact models was 0.068, with the lower bound of 0.052 being adopted in most codes of practice.

A recent re-evaluation of these tests (Abel, et al., 1982) has, however, indicated possible inaccuracies in the origional experiment, and a corrected mean C-value for the PVC models of 0.072 has been put forward.

While this has resulted in closer agreement with analytical predictions, a re-evaluation of test data some 20 years later is clearly undesirable. The results of tests presently being conducted at Bochum University (Zerna and Mungan, 1982) and at the Electricity de France (Sageau, 1984) are therefore eagerly awaited.

Equation 5.1 clearly makes no provision for variations in the wall thickness, height to radius ratio, location of the throat, boundary conditions, self-weight of the tower, wind distribution, etc. Furthermore this formula is limited to elastic buckling and does not account for material nonlinearities and cracking. Wind tunnel tests to simulate cracking are discussed in Section 5.2.4.

Although not directly concerned with cooling towers, the wind tunnel tests on open ended cylindrical shells reported by Kundurpi, et al. (1975) need to also be mentioned. This experiment investigated several different height to wall thickness ratios and aspect ratios. The elastic snap-through load obtained can be expressed approximately as

$$q_c = \begin{cases} 0.262\ E\ (t/R)^{2.5} & \text{for } H/R = 2 \\ 0.060\ E\ (t/R)^{2.33} & H/R = 3 \\ 0.019\ E\ (t/R)^{2.20} & H/R = 4 \end{cases} \qquad (5.2)$$

The dependency of the empirical coefficient C on the aspect ratio of the shell (H/R) is clear from Eq. 5.2. Similar results would be expected to apply to toroidal sections, but this has not been investigated experimentally.

An extensive and carefully controlled set of experiments has been carried out by Mungan (1976, 1979) to investigate buckling of cylindrical and toroidal shells under combined axial and pressure loads. This

investigation also included stiffened shells. These tests were conducted on epoxy resin models and loaded under water. These experiments led to the development of the 'Buckling Stress State' approach (BSS), in which the buckling safety of the shell is assessed in terms of a critical combination of meridional and circumferential stresses occurring at any point within the shell. If the buckling stress state is exceeded, local buckling is assumed to occur which generally results in failure. The BSS method has been adopted in the Recommendations by the IASS Working Group No. 3 (1977) for the design of cooling towers.

The philosophy behind this approach, in which it is assumed that once the buckling stress state for a particular shell is known, then the buckling safety can be evaluated independently of the loading condition is disputed in several references, in particular by Abel, et al. (1982). The main criticism of this method is that the BSS interaction formulae is based on model studies with much different characterestics from those in an actual tower, particularly boundary conditions and loading. Another criticism, not referred to by Abel, et al. is that the BSS approach was developed by investigating axisymmetric bifurcation of shells whereas failure of cooling towers under wind loading is a very nonlinear snap-through phenomenan. Zintilis and Croll (1983) also note that in the experiments leading to the BSS approach, the critical combination of stresses were recorded at the throat of the model tower, and that this is not an optimal choice of location.

Additional experimental investigations include microconcrete model tests reported by Rowe (1981) and by Swartz, et al. (1982), and additional bifurcation tests on plastic models by Veronda and Weingarten (1973).

5.2.2 Bifurcation studies

Linear bifurcation studies have frequently been used as a basis for approximating the nonlinear snap-through phenomenan. Various approaches have been used, including Equivalent Axisymmetric Loading (Langhaar, et al., 1970), Equivalent Axisymmetric Stresses (Cole, et al, 1975b) and Nonaxisymmetric Bifurcation (Mang, et al., 1981).

In support of a linear bifurcation approach is the consistency in the differences between bifurcation and experimental results for the wind loaded cylinder tests of Kundurpi, et al. (1975). Good agreement has also been obtained with the revised Der and Fidler tests using bifurcation results based on the equivalent axisymmetric loading approach (Abel, et al. 1982).

Analytical studies have shown the linear bifurcation loads to be lower than the corresponding analytical nonlinear buckling load (Mang, et al. 1983). (but significantly higher than the origional Der and Fidler experimental results). Linear bifurcation loads based on the actual assumed load distribution are also significantly lower than equivalent axisymmetric bifurcation loads (Mang, et al., 1983).

5.2.3 Geometric nonlinear analyses

Geometric nonlinear analyses have been carried out for elastic towers by Chan and Firman (1970), Yen and Shieh (1973) and Mang, et al. (1977, 1983). Both Chan and Yen contain errors (Cole, et al., 1975a) but the former have been approximately corrected by Ewing (1971) who together with the results of Mang, et al. predict nonlinear snap-through loads far in excess of those obtained by Der and Fidler- the nonlinear snap-through load predicted by Mang, et al. (1977) is higher than the uncorrected Der and Fidler experimental results by a factor of 2.6.

It is interesting to note that geometric nonlinear results for cylindrical shells show good agreement with experiment (Brendel and Ramm (1980) and Fig. 2.10).

5.2.4 Cracking and material nonlinearities

The conventional approach to the design of reinforced concrete cooling towers to satisfy a minimum strength requirement is based on an elastic analyses of the structure. Reinforcement is then proportioned so as to resist the factored component of the principal membrane forces in the same direction (ACI-ASCE Committee 334, 1977). Alternatively the reinforcement can be proportioned using a more refined method, which is based on the ultimate strength of an isolated section subject to the membrane forces (Gupta, 1981).

In the absence of geometric nonlinear effects the approach used by Gupta (1981) will provide a lower bound to the actual ultimate load of the tower, but will not yield any information regarding the magnitude of displacements at failure, or even above the cracking load. A finite element analysis to investigate the post-cracking behavior of cooling towers is given in Mang, et al. (1983), and is also the subject of investigation of Section 5.3.

Concern has also been expressed about the effect of cracking on the stability of cooling towers. To investigate any decrease in the buckling capacity due to cracking, Der and Fidler tested a model with 26 vertical slits in the upper rim to simulate cracking. They found that the 'cracks' caused a 21% reduction in the buckling load. Hayman and Chilver (1971) carried out model tests to supplement the Der and Fidler studies by cutting the models from top to bottom to represent loss of local circumferential

flexural rigidity, and then applied tape to both sides of the shell to maintain both meridional stiffness and displacement continuity. Their results indicated that five to seven full-height 'cracks' reduced the buckling load by about 55%. Cole, et al. (1975b) investigated the effects of cracking by using orthotropic properties for the top axisymmetric finite element to represent complete loss of circumferential stiffness. This resulted in a reduction of the predicted bifurcation load as compared to that using an isotropic model by a factor of about 3.4. This latter investigation is subject to some question, as it does not account for partial closing of cracks in compression (Stallbohm, et al., 1976). This argument can also be applied to the wind tunnel tests by Hayman and Chilver (1971).

In the reinforced concrete finite element analysis undertaken,by Mang, et al. (1983), geometric nonlinearities were also included to investigate buckling. This reference found no evidence of 'buckling' before a complete material failure had occurred. It was found that geometric nonlinear effects decreased the ultimate load by about 20%. This is investigated further in Section 5.3

5.2.5 Foundation flexibility

The influence of foundation flexibility on the bifurcation of cooling towers under axisymmetric loading has been investigated analytically by Langhaar, et al. (1970) and Cole, et al. (1975a). Cole characterizes the foundation flexibility by a nondimensional meridional spring stiffness obtained by assuming that the meridional membrane stress resultant is linearly proportional to the meridional displacement. Both Langhaar and Cole found that a decrease in the meridional spring stiffness from 10^{10}

(simply supported base) to 1.0 resulted in a decrease in the buckling load by a factor of about 1.3, while a decrease in the axial spring stiffness from 10^{10} to 0.1 reduced the buckling load by a factor of approximately 2.1 to 2.4. Cole estimates that for large cooling towers currently operating and being built in the USA, the meridional support stiffness is about 1.0. Mang, et al.(1983) reports the results of an investigation (Mehl, 1982) which concludes that "the influence of the flexibility of the supports on the buckling pressure of (the Port Gibson Tower) is relatively small."

However, the results obtained by Langhaar and by Cole were obtained for the bifurcation of cooling towers under axisymmetric loading, and these results are not necessarily representative of snap-through loading.

The effect of foundation flexibility on the stress distribution within the cooling tower has been investigated by Dumitrescu, et al. (1983).

5.3 NUMERICAL INVESTIGATION

The tower adopted for this investigated is that of a tall cooling tower with the geometry of the Port Gibson Tower, Mississippi. This tower has been chosen as it has been the subject of other investigations (Mang, et al., 1983; Hayashi and Gould, 1982, 1983), and is typical of a large cooling tower in use today.

The behavior of the tower is investigated under dead load and increasing wind load, considering material nonlinearities and combined geometric and material nonlinearities.

5.3.1 Description of the tower

The geometry of the shell of the tower and the wall profile is given in Fig. 5.1. The tower stands 150.5 m (494 ft) tall and has a mininum wall

thickness of 203 mm (8 in). The radius of the tower at the throat is 36.3 m (119 ft) and at the base 59.7 m (196 ft). The shell is thickened locally at the top and base to form ringbeams.

Above the throat of the tower the geometry of the meridian curve is that of a hyperbola, while below the throat the meridian is an elliptical segment. The geometry of the shell is given by the second order curve

$$a\bar{z}^2 + bR\bar{z} + cR^2 + d\bar{z} + eR + f = 0 \qquad (5.3)$$

where $\bar{z} = z - 120.0$ m, ie the elevation of the tower measured from the throat. The coefficients in Eq. 5.3 are given in Table 5.1.

5.3.2 Material properties

The material properties of the concrete and reinforcement are given in Table 5.2 and Fig. 5.2. These properties are the same as those adopted by Mang, et al. (1983), except for the tensile strength of the concrete and the reinforcement quantities. A tensile strength for the concrete of 3.0 MPa, which is slightly less than that used by Mang et al., has been adopted for the initial investigation of the cooling tower. Where noted, a tensile strength of 1.5 MPa has also been used. The reinforcement quatities have been taken from Hayashi and Gould (1983) in which the reinforcement has been designed in accordance with the ACI-ASCE recommendations (1977) together with the procedure given by Gupta (1981). In the upper one third of the tower the meridional reinforcement is controlled by the 0.35% minimum requirement, while the circumferential reinforcement is controlled throughout by the 0.35% minimum. The reinforcement used in this investigation (and by Hayashi) is slightly less than that used by Mang.

5.3.3 Finite element discretization

The finite element mesh used is shown in Fig. 5.3. The shell has been idealized using 90 quadratic Lagrangian shell elements (QLSHELL). Material nonlinearities have been included using the material model RCSHELL. The geometric nonlinear investigation is based on the small rotation formulation of Chapter 2, which has been shown to be adequate for snap-through buckling.

No mesh convergence study was performed for this investigation. A linear analysis was first undertaken, and the results compared with those obtained by Hayashi and Gould (1982). Close agreement was obtained with the present mesh. A convergence study should include the effects of both material and geometric nonlinearities, but the cost of such a study is prohibitive and was not attempted.

The simplifying assumption of a hinged base and a rigid foundation has been made. The influence of foundation flexibility is beyond the scope of this investigation.

5.3.4 Loading

The tower has been analyzed for combined dead and wind loading. The wind loading used is a codified psuedo-static approach in which it is assumed that the tower behaves quasi-statically to a particular (design) gust load. The vertical and circumferential wind load distribution used is taken from Mang, et al. (1983), which is similar to that used in the current ACI-ASCE recommendations for exposure C open terrain.

$$p(z,\theta) = q_o H(z)\, G(\theta) \tag{5.4}$$

where $H(z)$ is the vertical distribution of the design wind pressure profile

$$H(z) = (z/10)^{2/7} \tag{5.5}$$

and z is in meters.

$G(\theta)$ is the circumferential pressure distribution, including internal suction

$$G(\theta) = \sum_{n} A_n \cos(n\theta) \tag{5.6}$$

The Fourier coefficients, A_n, are given in Table 5.3

q_o is the design dynamic head at the reference 10m elevation. A reference windspeed of 40.2 m/s (90 mph) (Note that Mang has used a corresponding reference wind speed of 42.7 m/s (95 mph).)

The meridional forces due to dead, reference wind load and combined dead plus wind load acting along the windward meridion are shown in Fig. 5.4. Also included in Fig. 5.4 is the yield strength of the meridional reinforcement $A_s f_s$ and the cracking strength of the tower $N_{ct}+N_s$ in the meridional direction.

All the results presented in this investigation are expressed in terms of a normalized load factor, , obtained from the reference wind load distribution as

$$\lambda = \frac{p\ (v)}{p\ (40.2m/s)} \tag{5.7}$$

5.3.5 Numerical results

A parameter study consisting of four investigations has been carried out for this tower, namely

TOWER I: Material and geometric nonlinearities included, tension

stiffening factor β equal to 20. (See Fig. 5.5.)

2. TOWER II: Material nonlinearities included but geometrically linear, tension stiffening factor equal to 20.
3. TOWER III: Material and geometric nonlinearities included, but tension stiffening factor reduced to 5. (See Fig. 5.5.)
4. TOWER IV: Material and geometric nonlinearities included, tension strength of concrete reduced by half to 1.50 MPa and tension stiffening factor β reduced to 10.

Tower I has been adopted as the reference tower for this investigation.

The load displacement behavior for a point on the tower, at an elevation z = 101 m (331 ft) on the windward meridian, is shown in Fig. 5.6. An ultimate load factor of approximately 2.10 is obtained for Tower I, 2.25 for Tower II, 1.725 for Tower III and 1.35 for Tower IV. The load factor at which cracking occurs is approximately 1.45 for the first three towers, and 1.0 for Tower IV.

To keep these numbers in perspective, it should be noted that this tower has been designed according to the ACI provisions (ACI-ASCE Committee 334, 1977; Hayashi and Gould 1982) as

$$0.9\ A_s f_s = 0.9\ D + 1.30\ W$$

or

$$A_s f_s = 1.0\ D + 1.44\ W \qquad (5.8a)$$

ie

$$= 1.44 \qquad (5.8b)$$

For the reinforcement actually used, an ultimate load factor based on a linear analysis of 1.52 is obtained. A load factor of 1.38 is obtained for cracking of the concrete by neglecting the contribution from the reinforcement and 1.46 by including the effect of reinforcement.

Examination of the load displacement behavior of Towers I and II in Fig. 5.6 shows that geometric nonlinear effects decrease the ultimate load

by about 7%, but this reduction is accompanied by significantly increased displacements at the same load level. In both cases failure is initiated by first yield of the reinforcement, and this is followed by a rapidly increasing zone of yielding at little increase in load. No attempt was made to follow the propagation of yielding through the tower.

The nonlinearity in the load displacement behavior is illustrated in Fig. 5.7, in which the deflected profile for the windward meridian for Tower I is shown for increasing load level. The radial displacement at the level of the throat for the reference tower near failure (λ=2.075) is shown in Fig. 5.8, and the corresponding deflected profile for several meridians (where θ = 0 corresponds to the windward meridion) is shown in Fig. 5.9.

The crack pattern for the tower at failure is shown in Fig. 5.10. This crack pattern clearly identifies the main load carrying mechanism within the tower. Changes in the principal strain direction, and hence changes in the average crack direction, were generally small but in some areas rotations of up to 20 degrees were observed.

A comparison is made with the results obtained by Mang, et al. (1983) in Fig. 5.11, where the displacement of the windward meridion at an elevation of 82 m (269 ft) is plotted against the load factor. The load factor by Mang, et al. has been corrected by a factor $(95/90)^2$ to account for the different reference wind speed used. The results for Mang, et al. include geometric nonlinearities and tension stiffening.

The difference in the results for Tower I and that obtained by Mang, et al. is attributed directly to the tension stiffening used. As noted in Chapter 4, modeling of instability problems is very sensitive to the amount of tension stiffening used- see Fig. 4.9. The tension stiffening used for

Tower I is relatively high, but as has been shown in Fig. 4.10 it is still considerably less than that observed in the Vecchio-Collins experiments.

The tension stiffening used by Mang is based on a bond slip model developed by Mang and Floegl (1981,1983). There is little experience by which this model can be judged, but it appears to effectively yield very low tension stiffening values.

In order to evaluate the role of tension stiffening further, Tower III was undertaken. For this tower, tension stiffening which was felt to be unrealistically low was specifically chosen. The tension stiffening used is shown in Fig. 5.5.

The load displacement behavior of Tower III has been included in Figs. 5.6 and 5.11. It is seen that decreasing the tension stiffening used significantly reduces the ultimate load when geometric nonlinearities are included. Similar results to those obtained by Mang, et al. (1983) are now obtained, as shown in Fig. 5.11.

The difference in the behavior between Tower I and Tower II can be explained with the aid of Fig. 5.12. In this figure the numerical model for the uniaxial force-strain relation in the meridional direction at an elevation of 59.2 m (188 ft) for Towers I and III. This elevation corresponds to the 'critical section' at which cracking first occurs. From Fig. 5.12b it is seen that subsequent to cracking the total force at the critical section is released, whereas for Tower I, numerically, the cracked section does not release the meridional force immediately after cracking.

This is clearly seen by examining the variation in the meridional force and meridional strain for integration points on the circumference, at the level of the critical section. These results are shown in Figs. 5.13 to 5.16 for Towers I and III. The somewhat erratic behavior in Fig. 5.15 is

due to the fact that the meridional forces are not necessarily recorded immediately prior to cracking. However, the general trend in Fig. 5.15 indicates a rapid redistribution of stresses as cracking occurs, whereas Fig. 5.13 indicates a gradual redistribution of stresses.

It is also interesting to note that first yielding of the reinforcement for Towers I and II occurs at the same point at which cracking is initiated (z=57.18 m). However, for Tower III, although cracking first occurs at the same elevation, first yielding of the reinforcement occurred at an elevation of 86.2 m (283 ft). This is due to the ultimate capacity of the reinforcement being substantially less than the cracking strength of the section at this elevation (see Fig. 5.5), and due to the rapid redistribution of the meridional force from the concrete to the reinforcement as a result of the low tension stiffening used.

The inability of Tower III to compensate for the redistribution of the meridional force by a shift in the neutral axis can be seen in Fig. 5.17. In this figure, the distribution of the meridional force and strain along the circumference at which yielding first occurs, is shown for increasing load. A small change in the neutral axis position is observed for λ = 1.725, but this is clearly not sufficient to prevent failure by excessive displacements resulting from straining of the windward meridian.

The influence of the tension strength on the failure load of the cooling tower is also shown in Fig. 5.6. For Tower IV a tensile strength of 1.5 MPa has been used. In fact, a tensile strength of 1.5 MPa is more appropriate in situations such as this, where the stress distribution is approximately uniform across the thickness of the section, and accounting for the possible effects of creep and shrinkage of the concrete. The tensile strength of approximately 3.0 MPa used by Mang, et al. (1983) (and

adopted for Towers I, II and III) is more appropriate of the modulus of rupture of concrete which is applicable in situations were a high stress gradient exists, such as flexural applications. For Tower IV it is seen that the required load factor of 1.52 is not achieved. First yielding of the reinforcement occurs at an elevation of 105.2 m, at which the reinforcement capacity is less than the tensile capactiy of the concrete, and at a maximum displacement exceeding 540 mm.

5.3.6 Discussion of results

Before discussing the results obtained in this investigation, it is worth summarizing additional failure loads for this tower, based on various sources. These results are tabulated in Table 5.4.

The Der and Fidler equation given in the 1977 ACI-ASCE Recommendations (1977) gives a factor of safety against elastic buckling of 4.46, while the IASS Buckling Stress State approach (1977) gives a factor of safety of 3.08 (see Fig. 5.16). Note that the ACI-ASCE requires a factor of safety of 2.0, whereas the IASS requires a factor of safety of 5.0.

Elastic bifurcation results based on equivalent axisymmetric stress conditions yield a factor of safety of 14.39 and equivalent axisymmetric pressure yield a factor of safety of 15.41 (Mang, et al., 1983). An elastic nonlinear snap-through analysis undertaken by Mang, et al. (1977) yielded a factor of safety of approximately 24.

Undoubtedly, further research will be done in the area of elastic buckling of cooling towers so as to explain the discrepency between the experimental and analytical results. However, as can be seen from Table 5.4, failure loads based on assumed elastic behavior are much higher than can be expected to occur before cracking of the concrete dominates the

solution. The same view is held by Mang, et al. (1983). It is expected that these conclusions would also hold for very large cooling towers (say, 200 m in height).

The post cracking behavior of the cooling tower was found in this investigation to be very dependent on the assumptions made which influence the load carried by the concrete in tension. Using a relatively high tension stiffening model, the results obtained in this investigation differ significantly from those obtained by Mang, et al. These results indicate a usable reserve of strength above the cracking load of the tower. The failure mode observed for Tower I can be regarded as a 'ductile' failure as compared to the rapid 'brittle' failure observed for Tower III. Using a low tension stiffening model, similar results to Mang, et al. have been obtained. The extreme sensitivity of these results on the analytical description of tension stiffening contradicts the normally held opinion that tension stiffening can change the shape of the load deflection curve but not its limiting or ultimate load. The present observations are however dependent on the structural form, and the loading.

Mang, et al. (1983) notes that at present it seems premature to make generalizations about the ultimate load based on the available numerical evidence. This is not entirely clarified by this investigation but it has been shown that it may be premature to make generalizations about the actual mode of failure. The results shown in Fig. 5.6 illustrate the range of results obtained in the present investigation. While there is some doubt as to the validity of the failure mechanism observed by Mang and for Tower III, it is nevertheless clear that the behavior of the concrete in tension plays a dominant role in the failure of reinforced concrete cooling tower shells.

The results presented here indicate that the ultimate load of cooling towers is not solely a function of the reinforcement quantities used as

implied in Codes of Practice and Recommendations (ACI-ASCE Committee 334, 1977) The failure load obtained in this study varied from 2.10 to 1.35 depending on the assumptions made regarding the tension strength and tension stiffening. The role of the reinforcement appears to be more concerned with crack control (spacing and width) and therefore, effectively, on the tension stiffening effect. Due consideration should therefore be given to the spacing of reinforcement and bar diameters. At present these effects cannot be realistically accounted for using analytical models as there is insufficient experimental information available.

For the present investigation, for Towers I and III it is seen that the load factor based on an elastic analysis is a conservative estimate of the ultimate strength of the tower. There is therefore some tentative evidence that a linear analysis will yield an acceptable factor of safety against failure, although caution must be expressed in generalizing this to other towers. In particular it has been shown that the ultimate load of the cooling tower is dependent on the tension strength of the concrete, and for the particular tower investigated the uncracked tower yielded the required ultimate load factor (for f_t =3 MPa). Towers for which this is not achieved would be expected to behave differently, as demonstrated by Tower IV of this investigation. A linear elastic analysis will not, however, account for the possible large deflections above the cracking load.

Towers III and IV failed by yielding of the reinforcement in the vicinity of the throat. The ultimate load of Towers III and IV would however have been increased, and the 'ductility' of the structure improved, if the reinforcement capacity in the vicinity of the throat of the tower had exceeded the intact strength of the concrete. Hayashi and Gould (1983) note

that this would be good practice, and the results of this investigation support this view.

Due to the uncertainty in the post-cracking behavior of the tower, it is apparent that the cracking load must also be investigated, possibly to satisfy a lower factor of safety than that required at ultimate. A reasonable approach is to ensure that under working loads, cracking does not occur in the cooling tower shell. This requirement would be satisfied for the present tower- see Fig. 5.6. In this regard it is noted that requirements "to insure that neither cracking nor deflections are excessive under conditions of unfactored loading" (ACI-ASCE Committee 334, 1977) are meaningless, as the extent of cracking observed in either Tower I or Tower III cannot be predicted by a linear elastic analysis.

5.4 SUMMARY

The failure of an isolated cooling tower under wind loading has been examined. It has been confirmed that cracking and the subsequent redistribution of stresses plays a very important role in the post cracking behavior and failure of the tower. The results obtained in this investigation indicate that the ultimate load based on a linear elastic analysis is a conservative estimate of the actual failure load, but this conclusion is dependent on the tension strength of the concrete. Before these results can be generalized, additional investigations involving towers of differing height and wall thickness are required.

At present, as there is uncertainty in the actual post cracking behavior of cooling towers, is seems necessary that the cracking strength of the tower must be investigated in the design process.

CHAPTER 6

SUMMAY AND CONCLUSIONS

6.1 SUMMARY

The application of the degenerated Lagrangian shell elements in reinforced concrete panel, slab and shell applications is presented. The shell element is derived as a thin shell element using a stress-resultant constitutive matrix, which results in significant savings in material nonlinearities applications. A compatible eccentric shell stiffening element is also presented.

Suitable geometric nonlinear formulations are investigated and presented for the shell and beam element. Two kinematic formulations are investigated, the first approach uses a valid large rotation representation for the respective nodal degrees of freedom, and satisfies rigid body rotation requirements for arbitary large rotations. The second kinematic formulation is based on the conventional infinitesimal rotational degrees of freedom. This latter formulation results in straining under rigid body rotations.

Intact concrete is modeled using Liu's biaxial orthotropic material model (Liu, et al., 1972), together with a modified form of the biaxial failure envelope used by Darwin (1974) and Rajagopal (1976). Cracking of concrete in tension is modeled using a maximum principal stress criterion.

The constitutive matrix for cracked concrete is modeled using the rotating crack model (Gupta and Habibollah, 1982), in which the direction of the crack is not fixed after the formation of the crack, but rather it is assumed that the crack direction is normal to the current direction of the

maximum principal strain. The cracks defined by this model are not cracks in the strict sense, but rather notational cracks defineing the average crack direction. Comparisons between this model and a conventional fixed crack model are presented.

Numerical examples are presented in which the present finite element formulation and material model are compared with analytical solutions and experimental results for beam, slab and shell structures.

The failure of reinforced concrete cooling tower shells under wind loading is then investigated. The wind loading is treated as quasi-static loading as used in Codes of Practice and Recommendations. The cooling tower investigated is typical of a large cooling tower in use to day, and has been designed in accordance with he current ACI-ASCE Recommendations (1977). The effects of cracking of the concrete, tension stiffening and the tensile strength of the concrete on the failure load of the tower is investigated.

6.2 CONCLUSIONS

The examples investigated to examine the differences between a valid large rotation and an infinitesimal rotation formulation showed no noticeable difference between the two formulations. An exception to this is the large displacement analysis of some statically determinate beam type problems. As the nodal degrees of freedom used in the infinitesimal rotation formulation are more convenient to use, this approach has been adopted for the remainder of the investigation for slab and shell type structures.

It has been demonstrated that the rotating crack algorithm yields significantly better results than the conventional fixed crack model. This improvement in the predicted stiffness and failure load of panel, slab and

shell structures is not only restricted to specimens in which significant distortion of the principal strain axis occurs with increasing load, but also specimens in which only small changes in the average crack orientation occur. The numerical results have demonstrated that this model correctly predicts failure loads and yield line orientations for panel and slab sections.

The investigation into the failure of wind loaded cooling tower has shown that cracking and the subsequent redistribution of stresses plays a very important role in the post-cracking behavior and failure of the tower. The behavior of the tower has been shown to be dependent on the assumptions made regarding the tension strength of the concrete and the tension stiffening. At present there is insufficient data available on tension stiffening effects to enable one to make definite conclusions about the post-cracking behavior of cooling towers.

Based on the present investigation, there is tentative evidence to suggest that the ultimate load based on a linear analysis is a conservative estimate of the actual failure load. A linear analysis will not, however, account for possible large displacements above the cracking load. Due to the uncertainty in the post-cracking behavior of the tower, it is strongly suggested that the cracking load of cooling towers be investigated in actual designs.

6.3 RECOMMENDATIONS FOR FURTHER RESEARCH

Some possible extensions to the present investigation and further research needs arising out of this study are included below.

1. Experimental investigations to measure tension stiffening effects in lightly reinforced panel sections are required. Load cases

investigated should include those in which the reinforcement is orientated in the principal load directions.

2. This study should be extended to investigate towers of differing size and shape, as well as stiffened cooling towers, so that design criteria can be formulated.
3. The behavior of cooling towers under asymmetric loading due to the group effect of cooling towers should be investigated.
4. The influence of initial imperfections on the stability and failure of cooling towers should be investigated. Of particular importance is the effect of gross imperfections.
5. The rotating crack algorithm should be extended to cyclic loading applications.
6. The implications of the use of a constant shear correction factor and the neglect of the nonlinearities associated with the transverse shear stress may warrent further investigation.

TABLES

Table 2.1 Zero Energy Modes for Degenerated Shell Elements in Excess of Rigid-Body Modes.

ELEMENT	INTEGRATION RULE	
	REDUCED	SELECTIVE
S4/L4	7	5
S8	4	3
S12	0	0
L9	7	1
L16	7	not available
QUADH	-	0
HETEROSIS	-	1

Table 4.1 Material Properties for Vecchio-Collins Specimens.

SPECIMEN	REINFORCEMENT				CONCRETE		
	ρ_x (%)	ρ_y (%)	f_{sx} (MPa)	f_{sy} (MPa)	f'_c (MPa)	f_t (MPa)	ε_o
PV11	1.785	1.306	235	235	15.6	1.5	0.00260
PV16	0.740	0.740	255	255	21.7	1.0	0.00200
PV17	0.740	0.740	255	255	18.6	2.0	0.00200
PV18	1.785	0.315	431	412	19.5	1.8	0.00220
PV19	1.785	0.713	458	299	19.0	2.0	0.00215
PV25	1.785	1.785	466	466	19.2	1.3	0.00180

E_s=21000 MPa; $E_c=2f'_c/\varepsilon_o$

Table 4.2 Loading Details for Vecchio-Collins Specimens.

SPECIMEN	LOADING PATTERN
PV11	pure shear
PV16	pure shear
PV17	uniaxial compression
PV18	pure shear
PV19	pure shear
PV25	shear & biaxial compression ($\sigma_n = -0.67\tau$)

Table 4.3 Experimental and Numerical Results for Vecchio-Collins Specimens.

SPECIMEN	EXPERIMENTAL			ROTATING CRACK MODEL		FIXED CRACK MODEL	
	FAILURE MODE	V_u (MPa)	θ[1] (deg)	FAILURE MODE	V_u (MPa)	θ[2] (deg)	V_u (MPa)	θ[3] (deg)
PV11	Yielding	3.56	50	Yielding	3.59	49	3.64	45
PV16	Yielding	2.14	45	Yielding	1.90	45	1.90	45
PV17	Compression	19.4	-	Compression	21.0	-	21.0	-
PV18	Bond	3.04	60	Yielding	3.18	68	4.55	46
PV19	Shear	3.95	57	Yielding	4.30	62	5.20	46
PV25	Shear	9.12	-	Compression	9.60	-	9.60	-

Notes: 1) Average orientation of maximum principal concrete stress and strain.
2) Yield line orientation.
3) Orientation of maximum principal strain.

Table 4.4 Material Properties for Cardenas-Sozen Specimens.

SLAB	t (in)	f'_c (psi)	ρ_1 (%)	ρ_2 (%)	ρ_2/ρ_1	α_1 (deg)	f_s (ksi)
B7	4.14	5150	0.790	0.862	1.10	-45	50.0
B9	4.23	3820	0.774	0.422	0.55	45	50.0
B11	4.12	4800	0.794	0.433	0.55	-22.5	50.0
B12	4.12	5170	0.794	0.433	0.55	67.5	47.6
B27A	4.04	5230	0.810	0.884	1.10	-66	49.9
B31	4.00	5600	0.818	0.223	0.27	-66	44.8
B32	4.10	5500	0.798	0.218	0.27	46.5	55.7
B33	4.07	4930	0.804	0.219	0.27	-21	45.7

E_c = 3000 ksi; $f_t = 5.5\sqrt{f'_c}$ ksi; E_s = 30000 ksi

Table 4.5 Experimental and Numerical Results for Cardenas-Sozen Specimens.

SLAB	EXPERIMENTAL			ROTATING CRACK MODEL		FIXED CRACK MODEL	
	M_y [1] (k-in/in)	M_u [2] (k-in/in)	θ_u [3] (deg)	M_y (k-in/in)	θ_u (deg)	M_y (k-in/in)	θ_ε [4] (deg)
B7	5.60	5.85	0	5.78	0	5.78	0
B9	3.90	4.45	-17	3.98	-17	4.34	-3
B11	4.50	5.35	19	4.77	14	4.41	3
B12	2.80	3.82	-10	3.26	-11	3.35	3
B27A	5.08	5.50	0	4.90	1	4.90	-4
B31	1.65	2.05	13	1.62	13	1.62	-1
B32	2.76	3.10	-25	2.82	-24	3.36	-3
B33	4.18	4.60	26	4.14	26	4.66	5

Notes: 1) Yield moment.
2) Ultimate moment.
3) Yield line orientation.
4) Direction of maximum principal strain at bottom of slab.

Table 4.6 Material Properties for Duddeck's Slabs.

SLAB	f'_c (MPa)	f_t (MPa)	ε_o με	E_c (MPa)	f_s (MPa)	E_s (MPa)	TOP ρ_x (%)	TOP ρ_y (%)	BOTTOM ρ_x (%)	BOTTOM ρ_y (%)
S1	43	2	2.7	16.4×10^3	670	201×10^3	.297	.297	.611	.611
S2	43	2	2.7	16.4×10^3	670	201×10^3	.388	.205	.800	.420
S3	43	2	2.7	16.4×10^3	670	201×10^3	.435	.158	.895	.326

Table 4.7 Experimental and Numerical Results for Duddeck's Slabs.

SLAB	EXPERIMENTAL (kN)	YIELD LINE SOLUTION (kN)	PRESENT (kN)
S1	61.66	56.0	60.0
S2	43.46	39.0	46.0
S3	34.25	31.0	35.5

Table 4.8 Material Properties for Bouma's Cylindrical Shell.

Concrete			
	E_c	30000	MPa
	f'_c	30	MPa
	f_t	4.5	MPa
	ν	0.2	
Reinforcement			
	E_s	210000	MPa
	E_{sp}	2000	MPa
Shell:	f_s	295	MPa
Beam:	f_s	280	MPa

Table 5.1 Coefficients Defining the Geometry of the Meridian Curve.

Coefficient	z-120>0 Hyperbola	z-120<0 Ellipse
a [1]	-0.01506	-0.28035
b [1]	0	0
c [1]	1.0	1.0
d [m]	0	0
e [m]	-68.46	76.88
f [m^2]	1167.17	-4112.73

Table 5.2 Material Properties for Cooling Tower.

Concrete				
E	28268	MPa	4160	ksi
f'_c	27.6	MPa	4000	psi
f_t	3.0	MPa	435	psi
ν	0.2		0.2	
γ	24.25	kN/m^3	47.4	lb sec^2/ft^4
Reinforcement				
E_s	200600	MPa	29000	ksi
E_{sp}	10300	MPa	1500	ksi
f_s	413.7	MPa	60	ksi

Table 5.3 Fourier Coefficients for Wind Load Distribution.

n	A_n	n	A_n
0	0.38330	7	-0.04474
1	-0.27918	8	-0.00833
2	-0.61978	9	-0.00972
3	-0.50927	10	-0.01356
4	-0.09167	11	-0.00597
5	0.11794	12	-0.01667
6	0.03333		

Table 5.4 Failure Loads for Cooling Tower.

SOURCE	BASIS	LOAD FACTOR
Present	Cracking	1.45
	Ultimate load- linear analysis	1.52
	Material nonlinear, geometric linear	2.25
	Material & geometric nonlinear	
	i) high tension stiffening	2.10
	ii) low tension stiffening	1.75
	iii) low tension strength	1.35
Der & Fidler	Elastic snap-through	4.46
IASS	Buckling stress state	3.08
Mang et al	Cracking	1.43 [1.34]
	Ultimate load- linear analysis	1.71 [1.53]
	Material nonlinear, geometric linear	1.95 [1.74]
	Material & geometric nonlinear	1.69 [1.49]
	Elastic behavior	
	i) Linear bifurcation	5.38
	ii) Elastic snap-through	-24
	iii) Equivalent axisymmetric pressure	15.31
	iv) Equivalent axisymmetric stress	14.39

Notes: Quantities in brackets refer to load factors based on the reference wind speed of 95 mph used in Ref. 76.

FIGURES

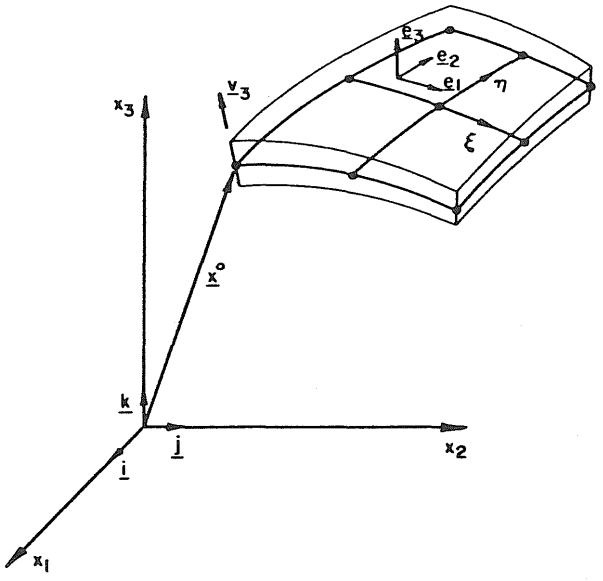

Figure 2.1 Initial Geometry of Degenerated Shell Element.

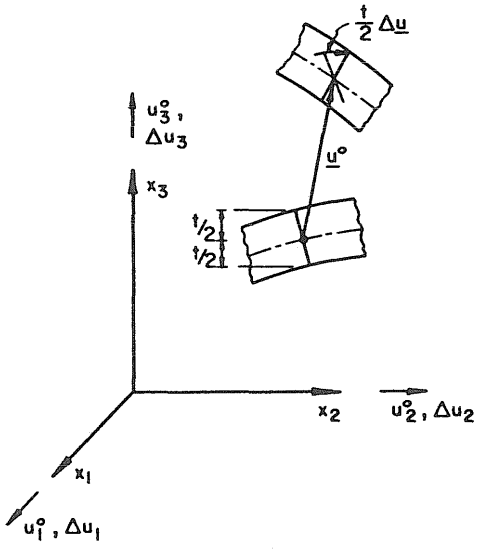

Figure 2.2 Nodal Degrees of Freedom for Moderate Rotations.

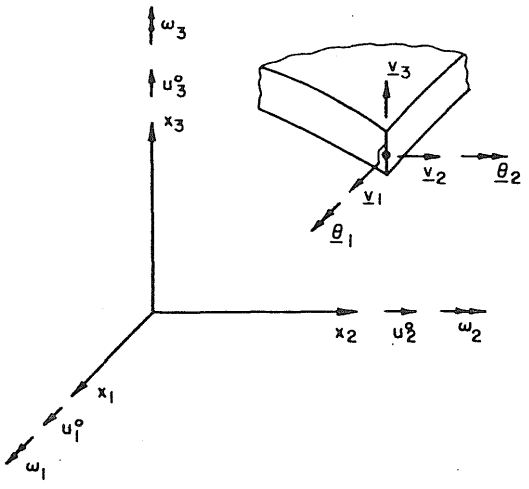

Figure 2.3 Nodal Degrees of Freedom for Small Rotations.

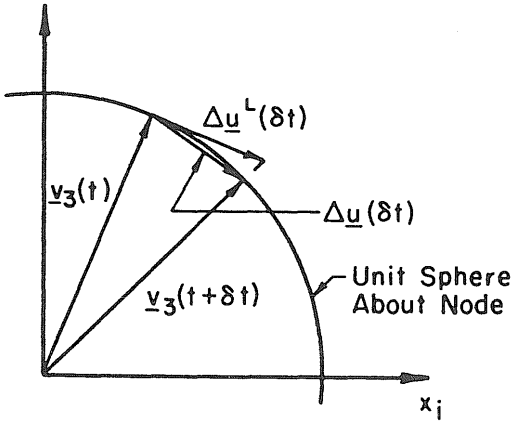

Figure 2.4 Updating of Nodal Degrees of Freedom.

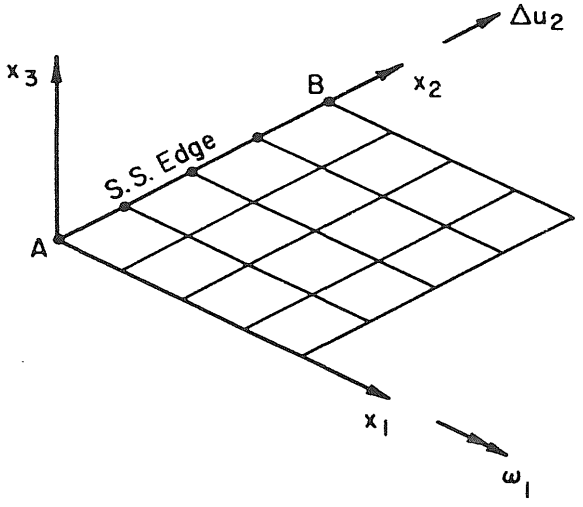

Along Edge A-B
$\omega_1 = 0$ or $\Delta u_2 = 0$

(a)

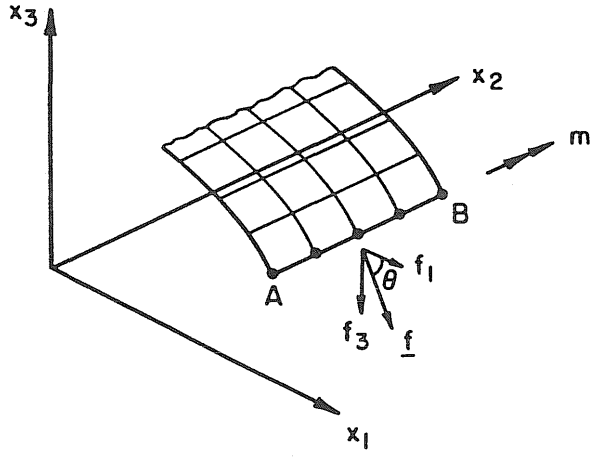

Along Edge A-B
$\underline{m} = m\ (0\ 1\ 0)$ or
$\underline{f} = m\ (\cos\theta\ 0\ -\sin\theta)$

(b)

Figure 2.5 Nodal Rotation Constraints and Applied Moments.

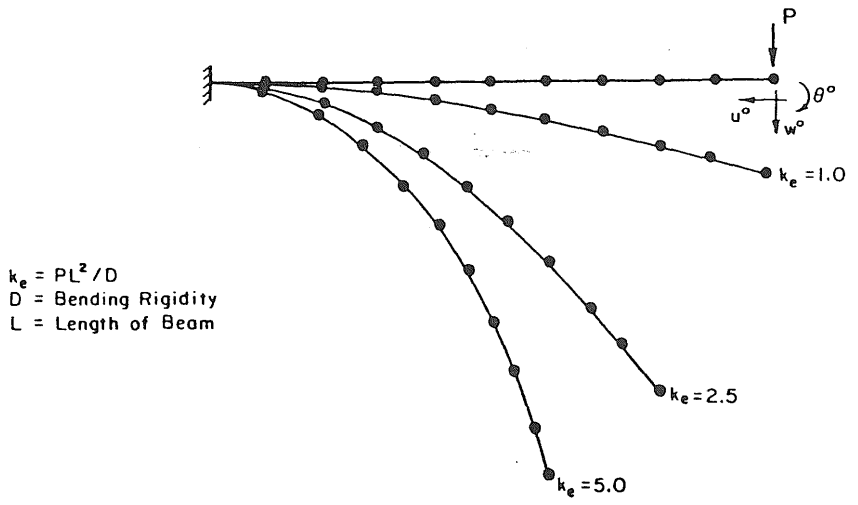

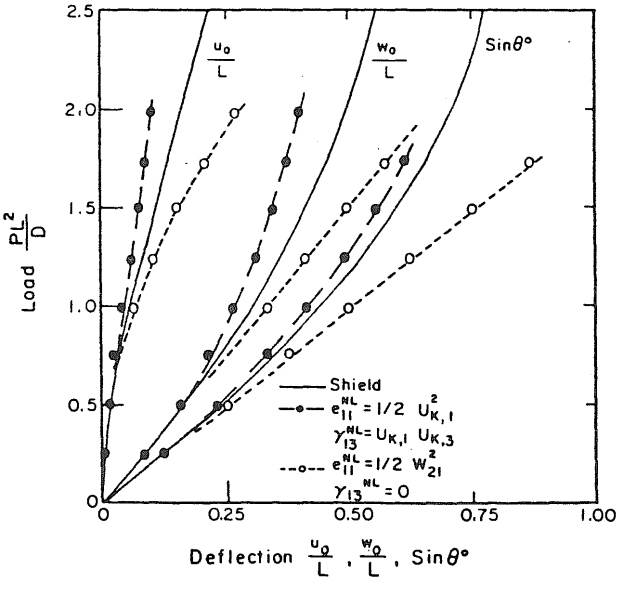

(a)

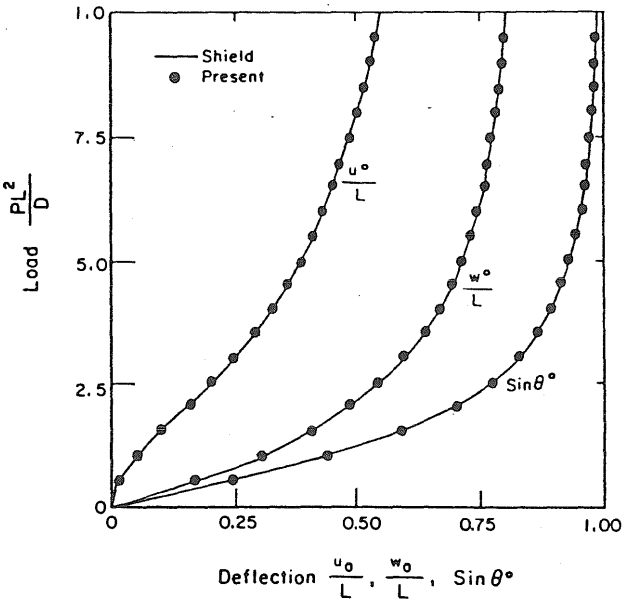

(b)

Figure 2.6 Large Deflection of Cantilever.

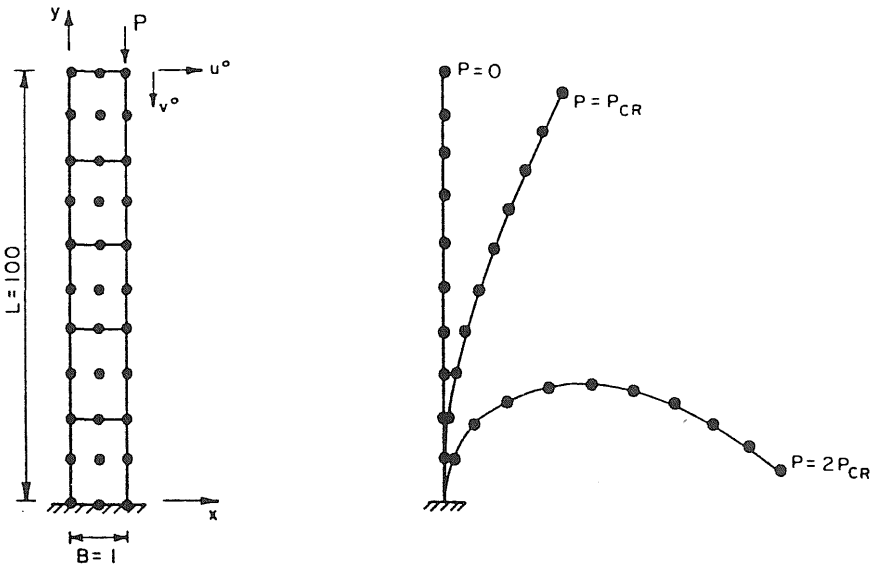

Thickness = 1
E = 12
ν = 0

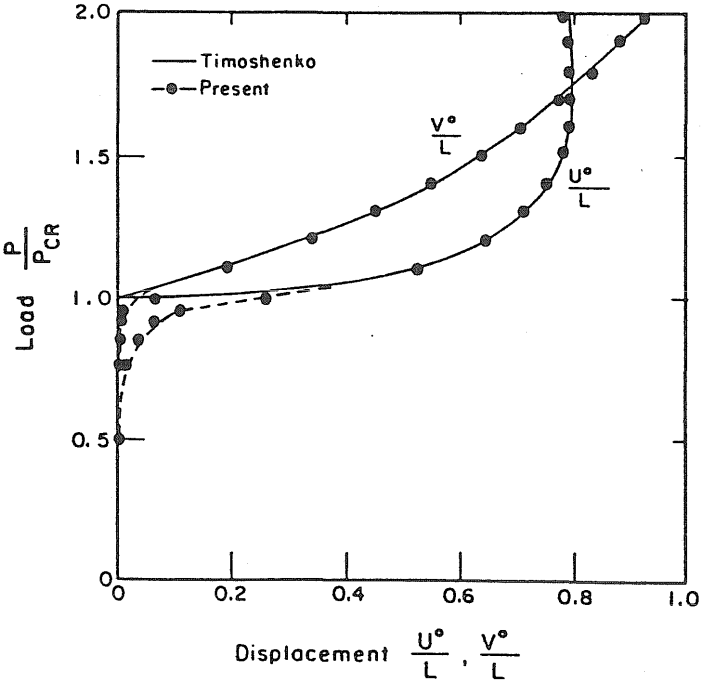

Figure 2.7 Buckling of Column.

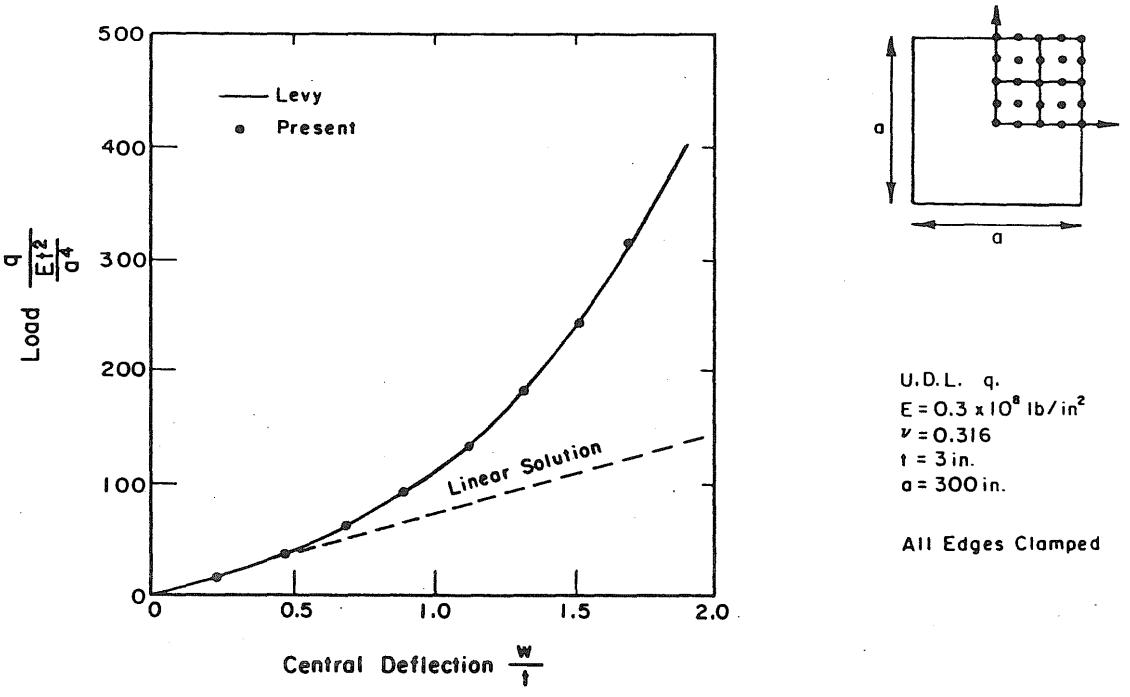

Figure 2.8 Large Deflection of Clamped Square Plate.

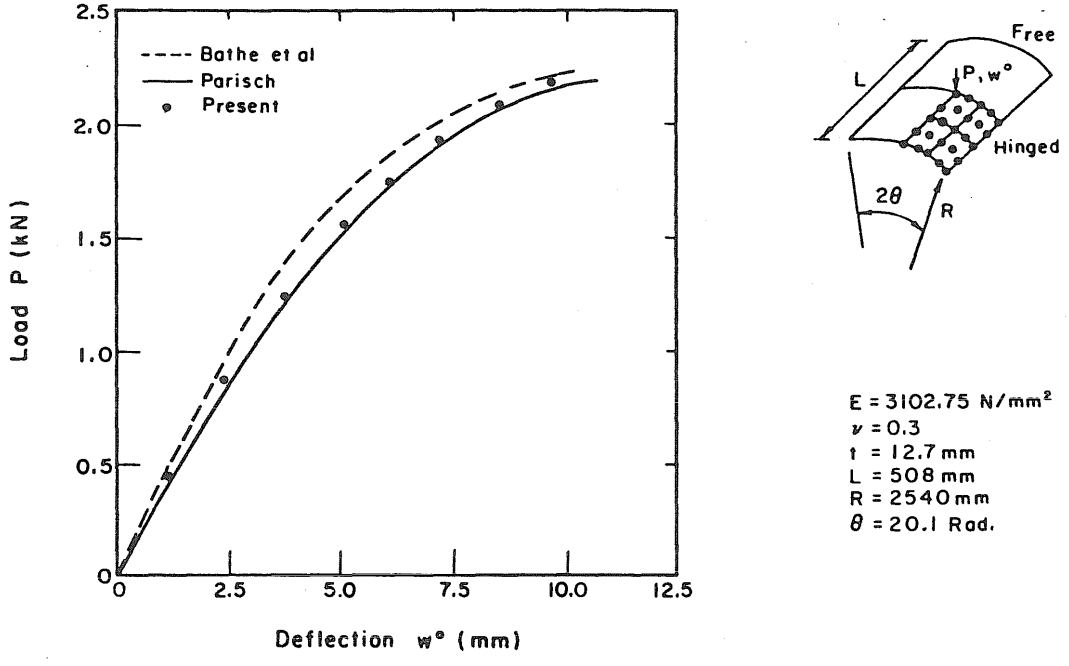

Figure 2.9 Large Deflection of Hinged Cylindrical Shell.

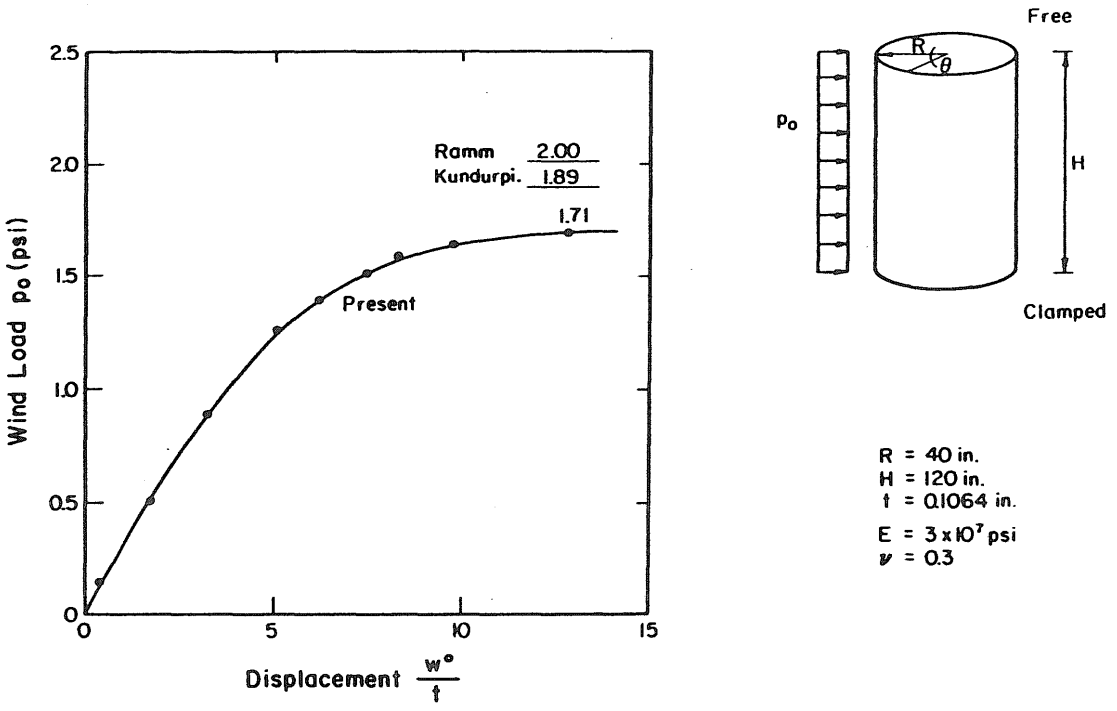

Figure 2.10 Load Displacement Curves for Wind Loaded Cylinder.

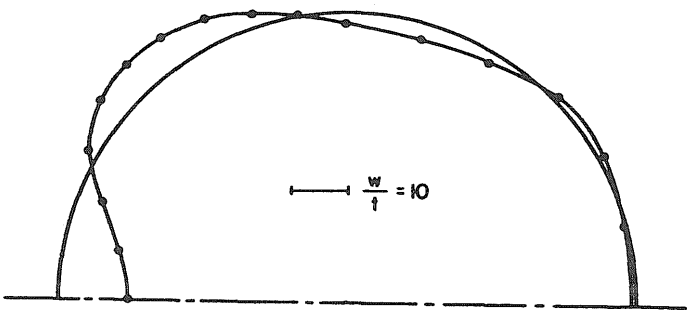

Figure 2.11 Deflected Profile of Wind Loaded Cylinder.

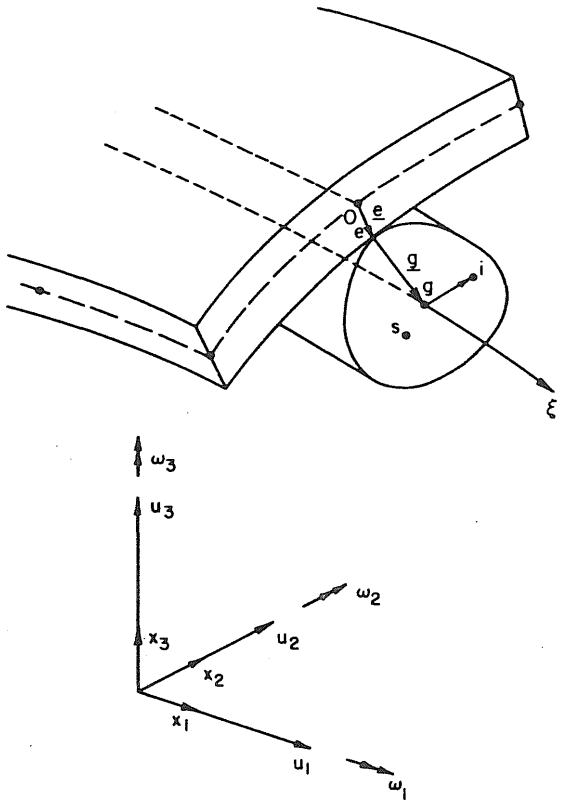

Figure 3.1 Initial Geometry and Kinematics of Beam Element.

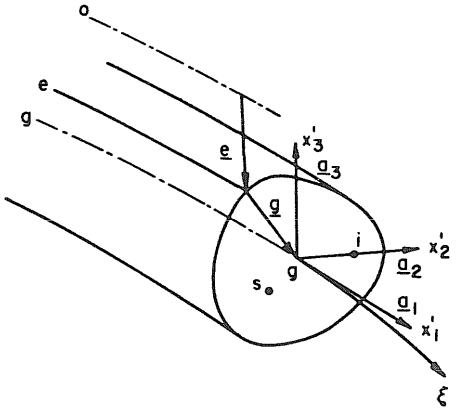

Figure 3.2 Local Reference Frame for Beam Element.

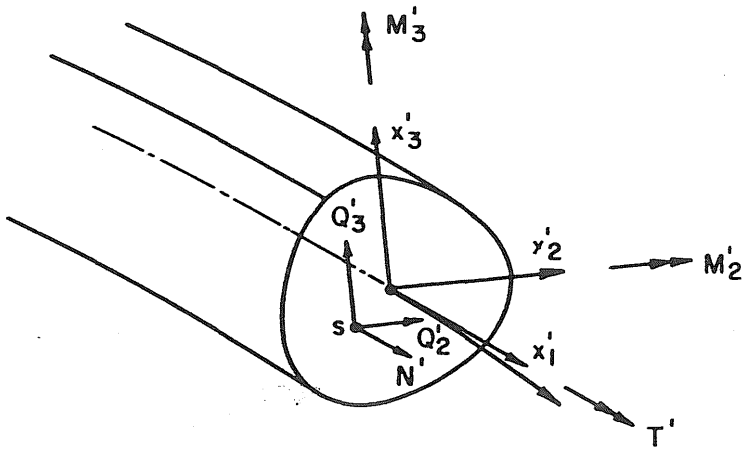

Figure 3.3 Generalized Stress Resultants for Beam Element.

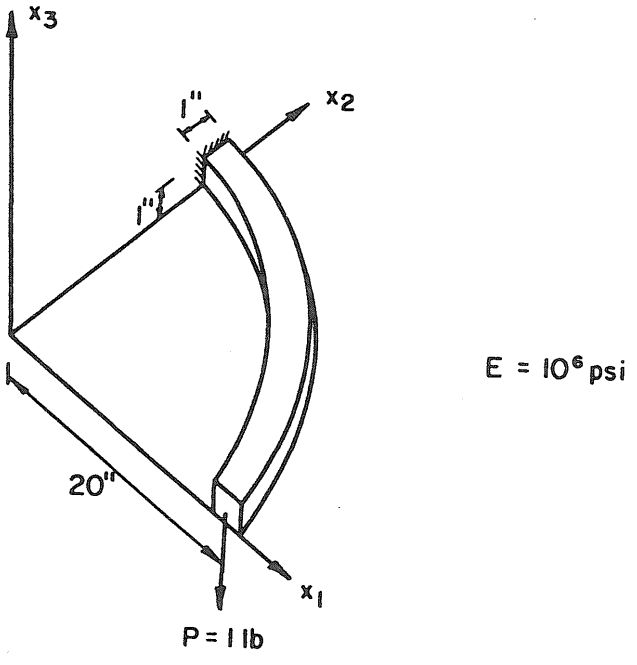

Figure 3.4 Curved Cantilever Beam.

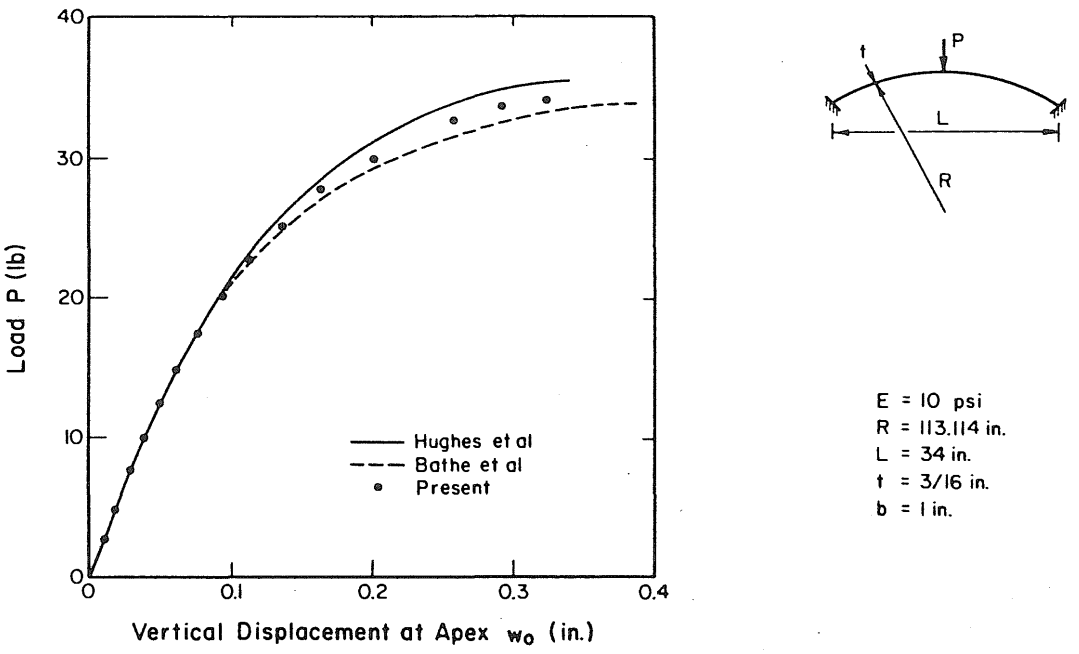

Figure 3.5 Large Displacement of Shallow Arch.

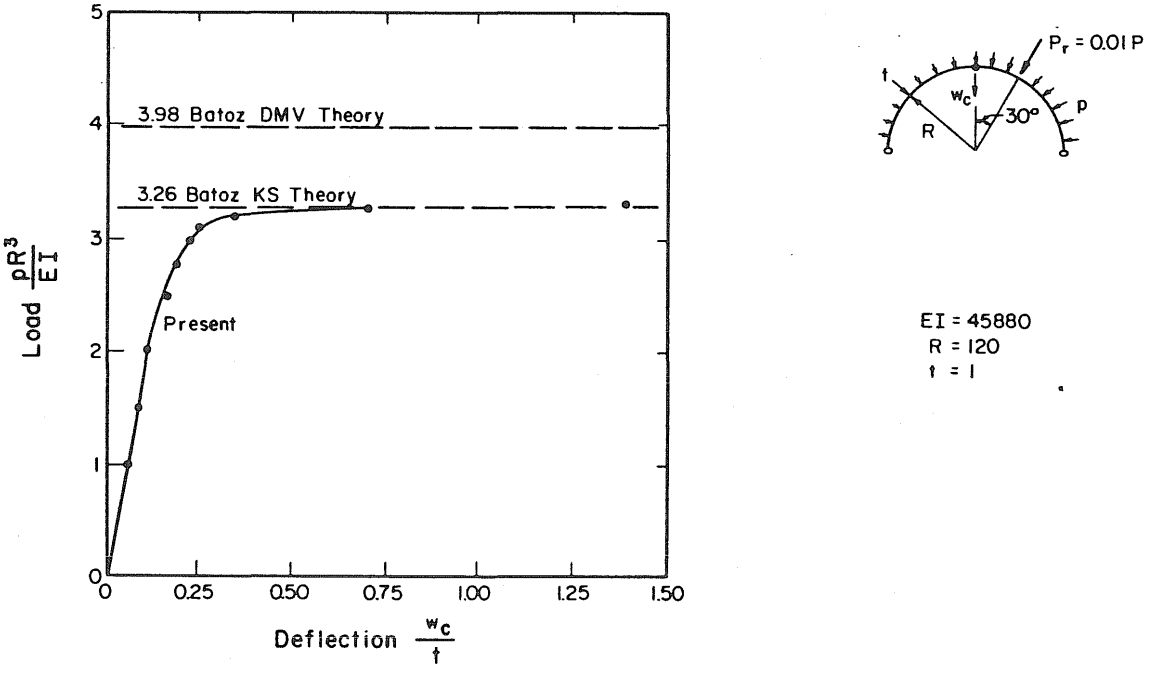

Figure 3.6 Bifurcation of Circular Arch.

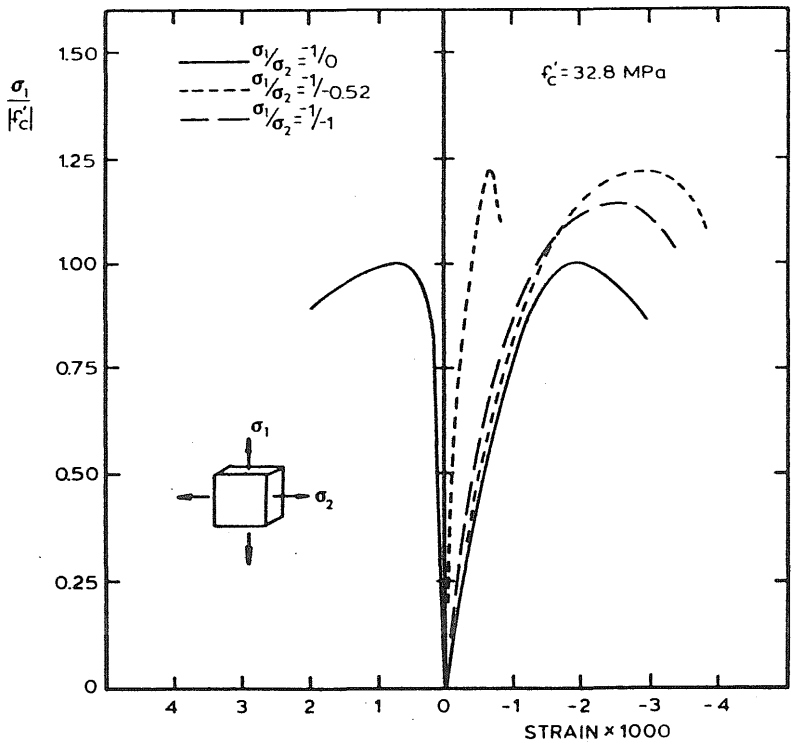

Figure 4.1 Biaxial Stress Strain Curves for Concrete.

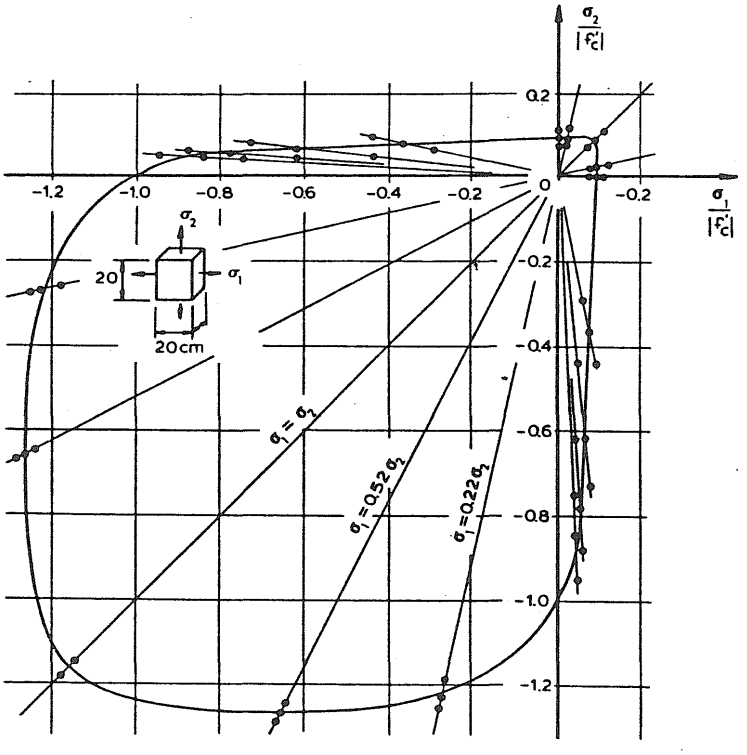

Figure 4.2 Biaxial Failure Envelope for Concrete.

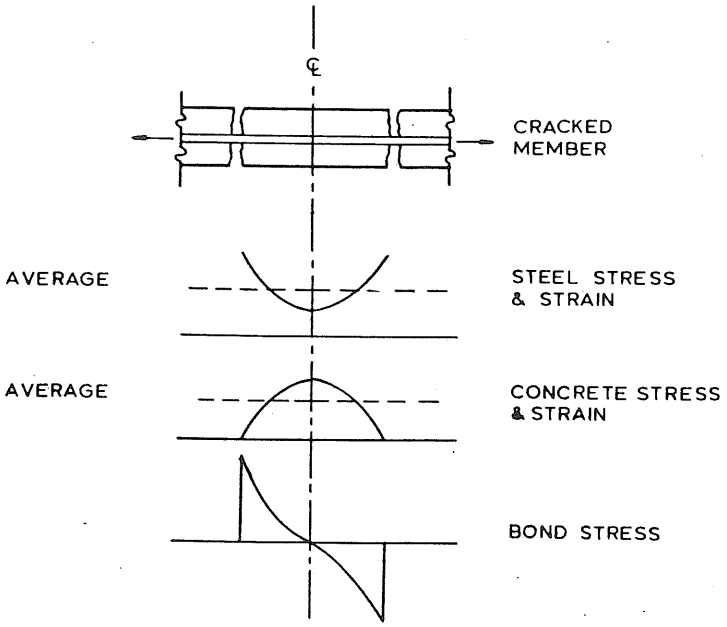

Figure 4.3 Stress Distribution in Cracked Concrete.

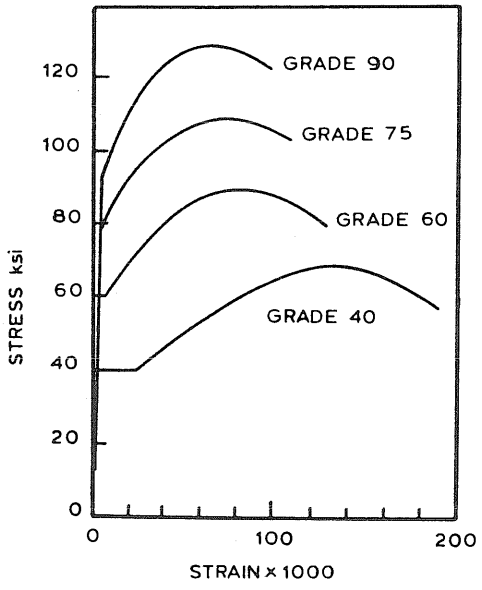

Figure 4.4 Stress-Strain Curves for Reinforcement.

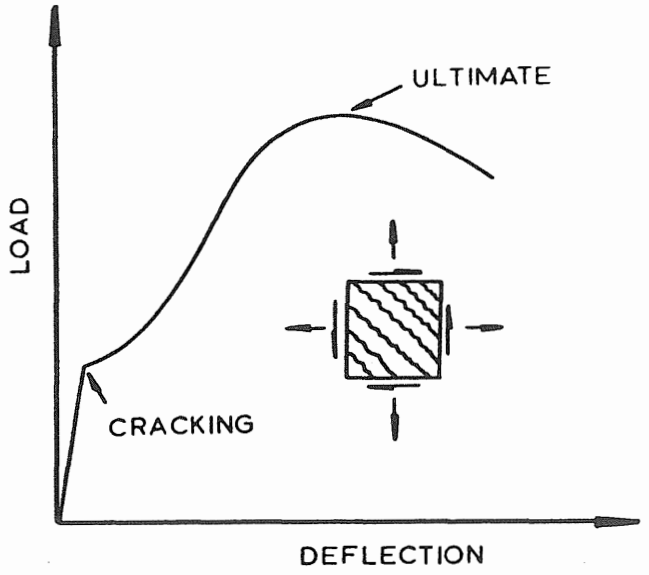

Figure 4.5 Load Displacement Curves for Panel Subjected to Inplane Loading.

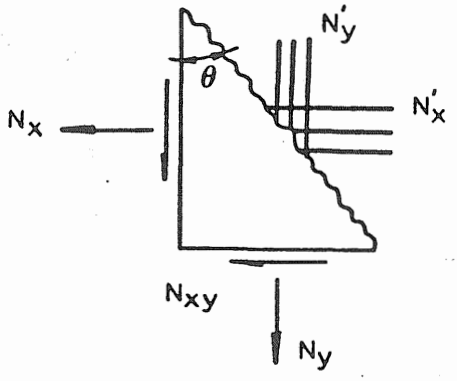

Figure 4.6 Stresses Acting on Cracked Element.

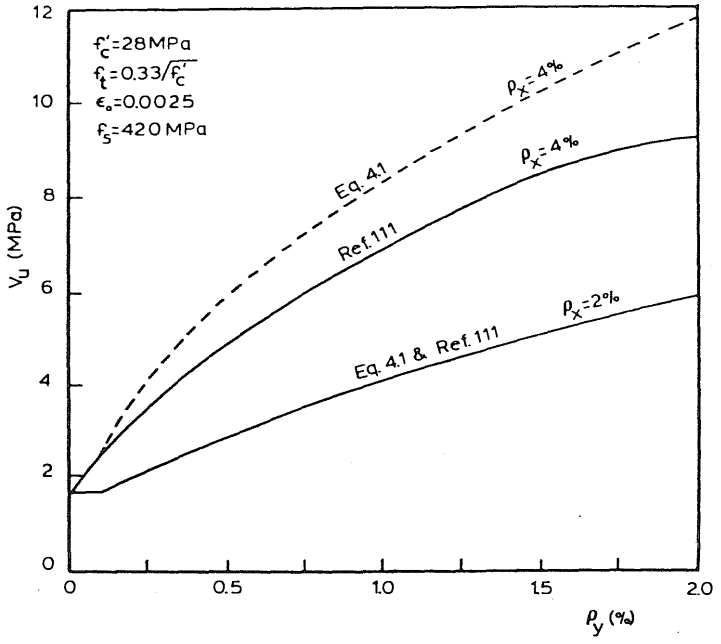

Figure 4.7 Influence of Reinforcement Ratio on Shear Strength of Panel Sections.

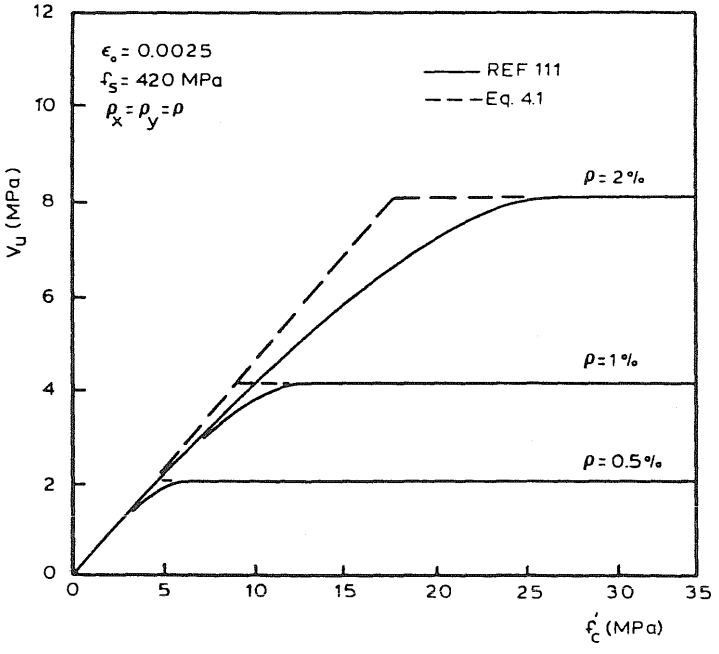

Figure 4.8 Influence of Concrete Compressive Strength on Shear of Panel Sections.

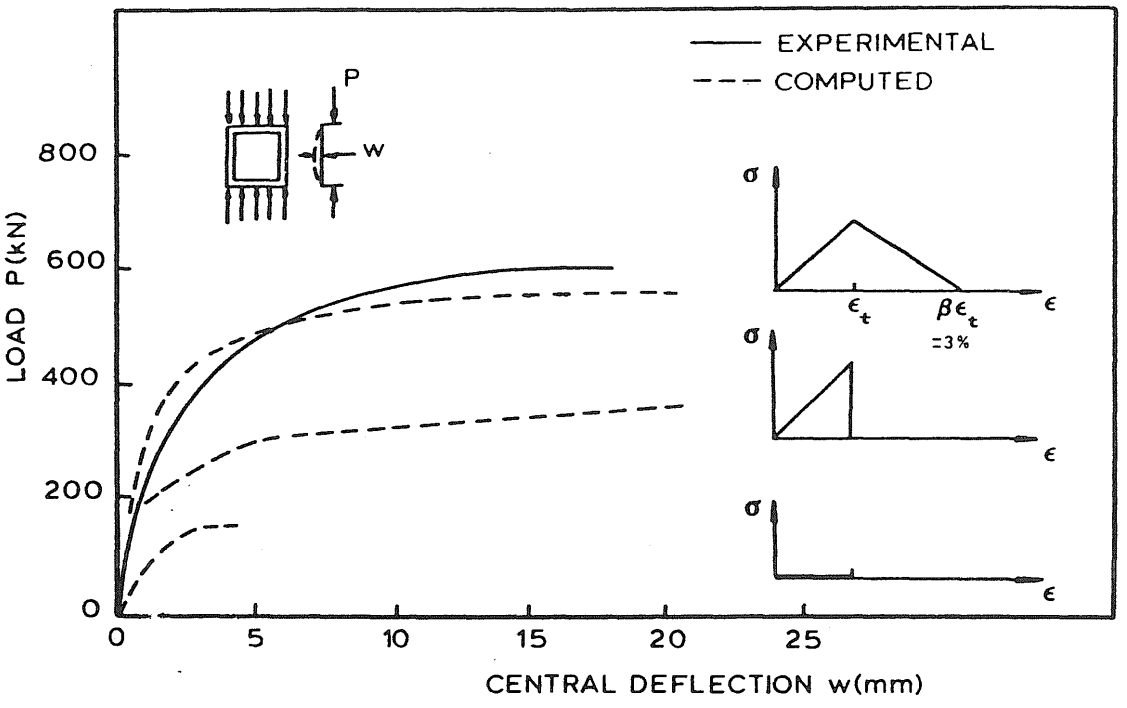

Figure 4.9 Effect of Tension Stiffening on Calculated Response.

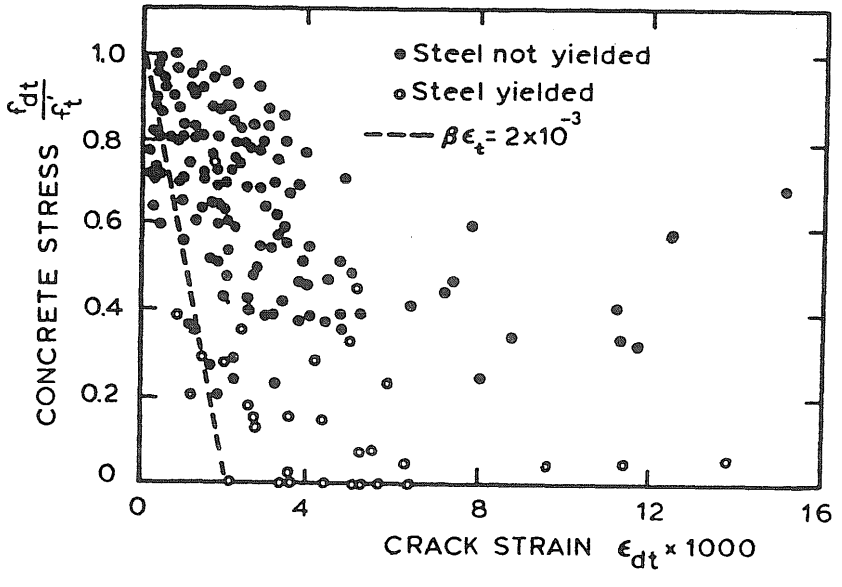

Figure 4.10 Measured Tension Stiffening for Panel Sections.

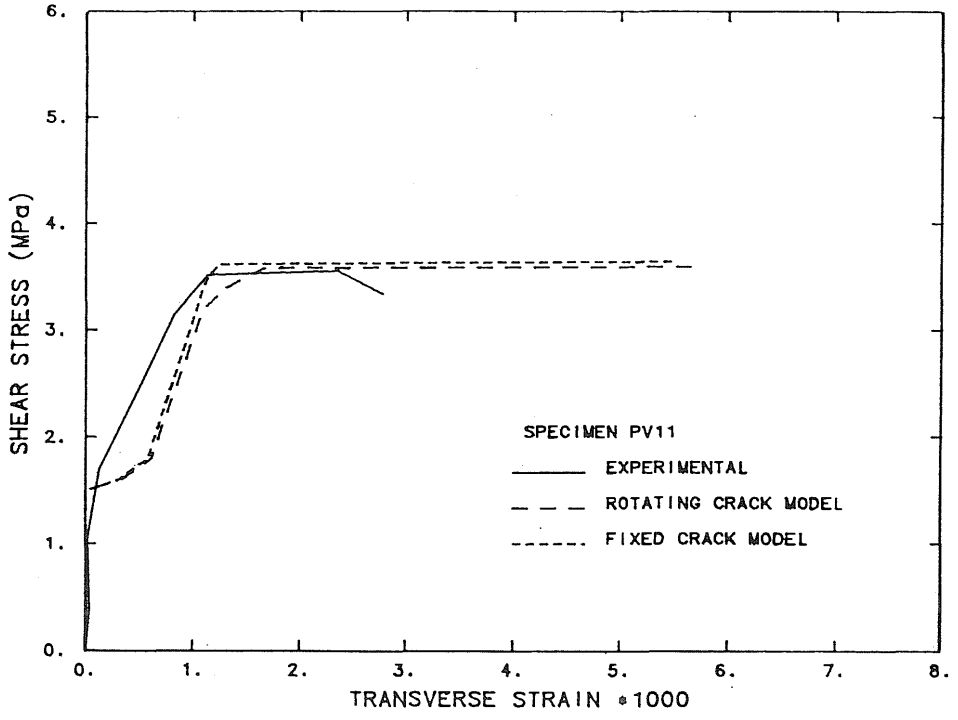

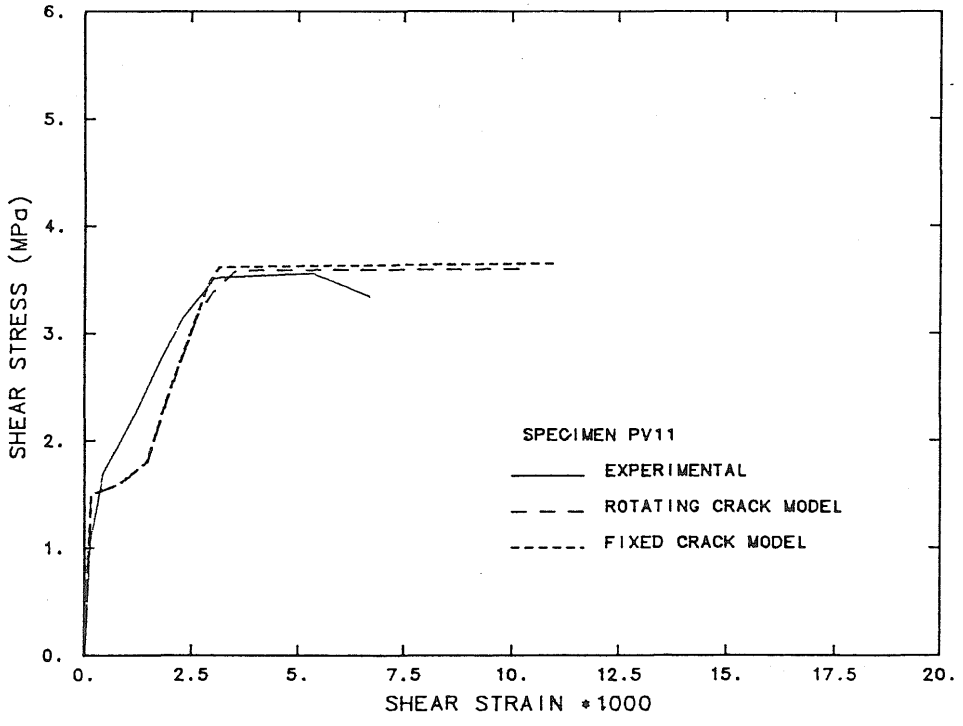

Figure 4.11 Load-Strain Curves for Specimen PV11.

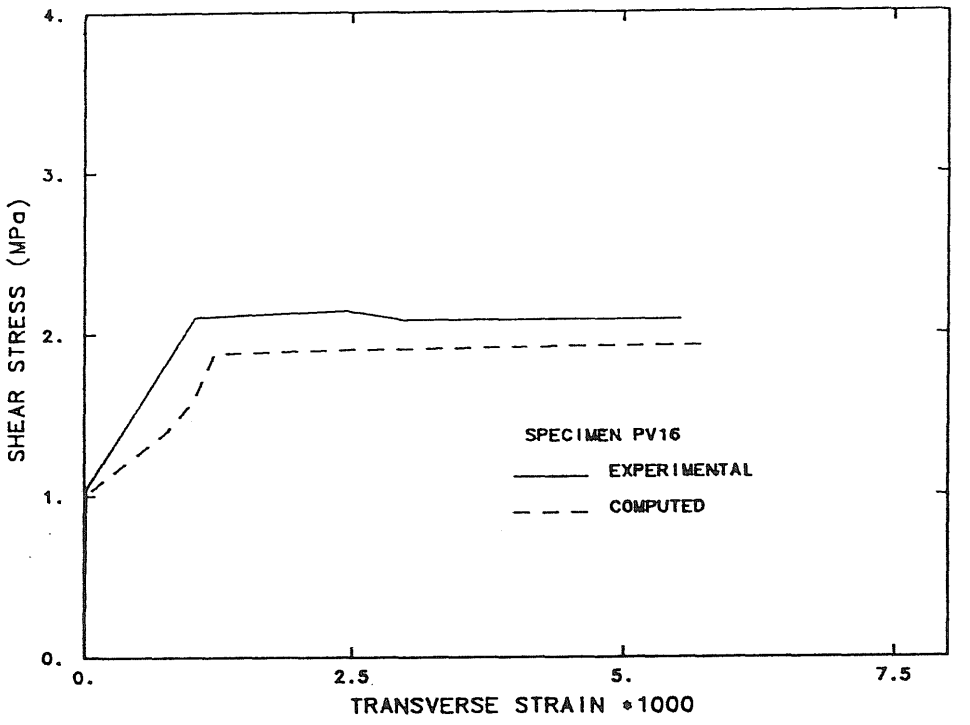

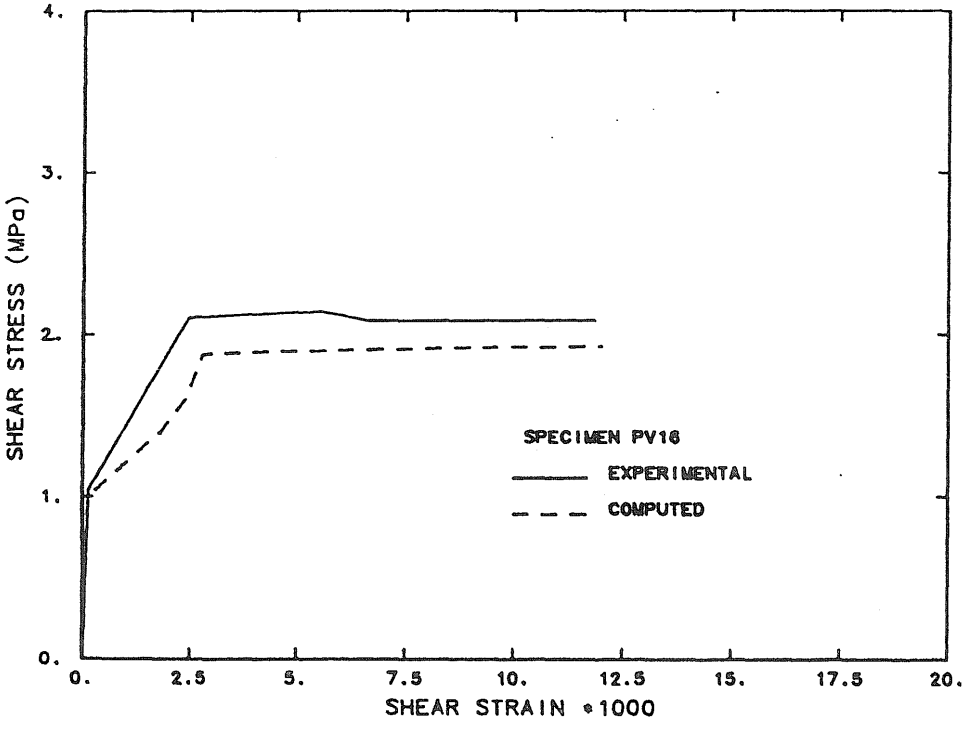

Figure 4.12 Load-Strain Curves for Specimen PV16.

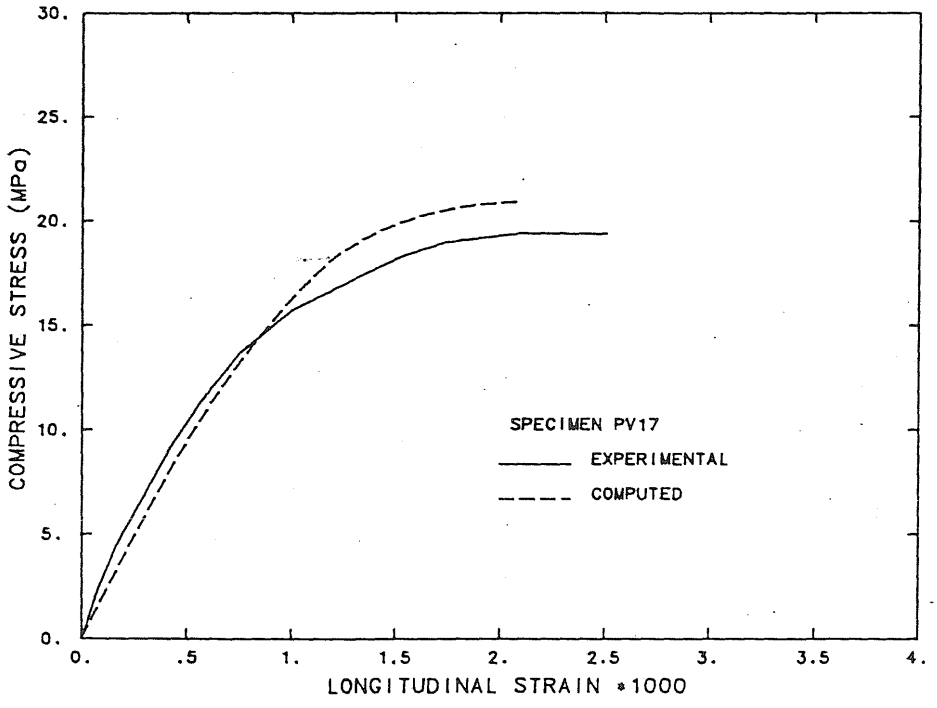

Figure 4.13 Load-Strain Curves for Specimen PV17.

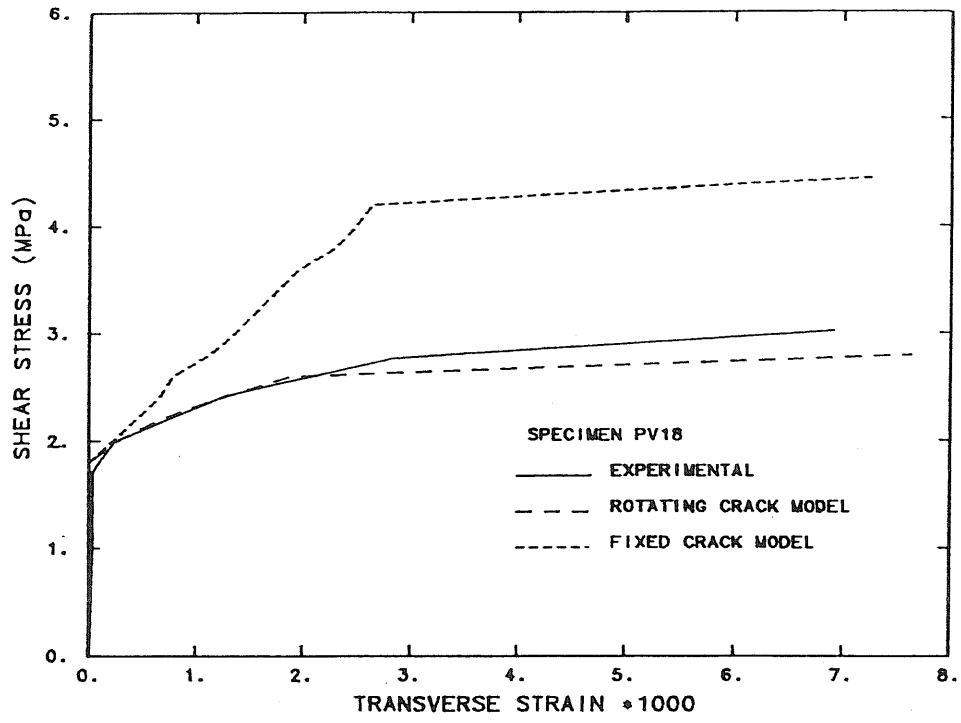

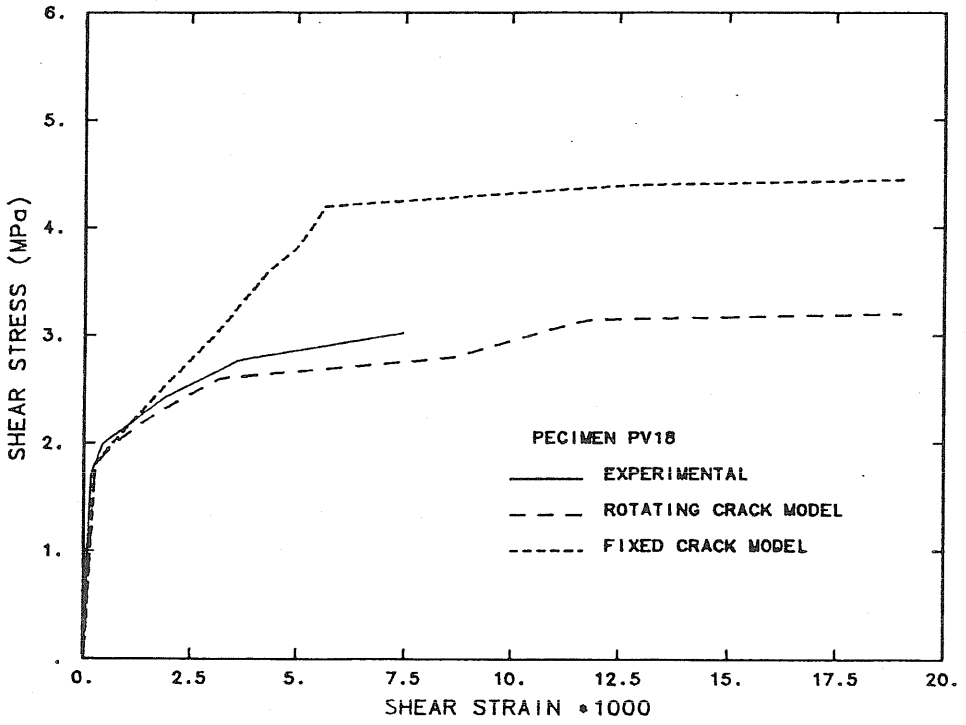

Figure 4.14 Load-Strain Curves for Specimen PV18.

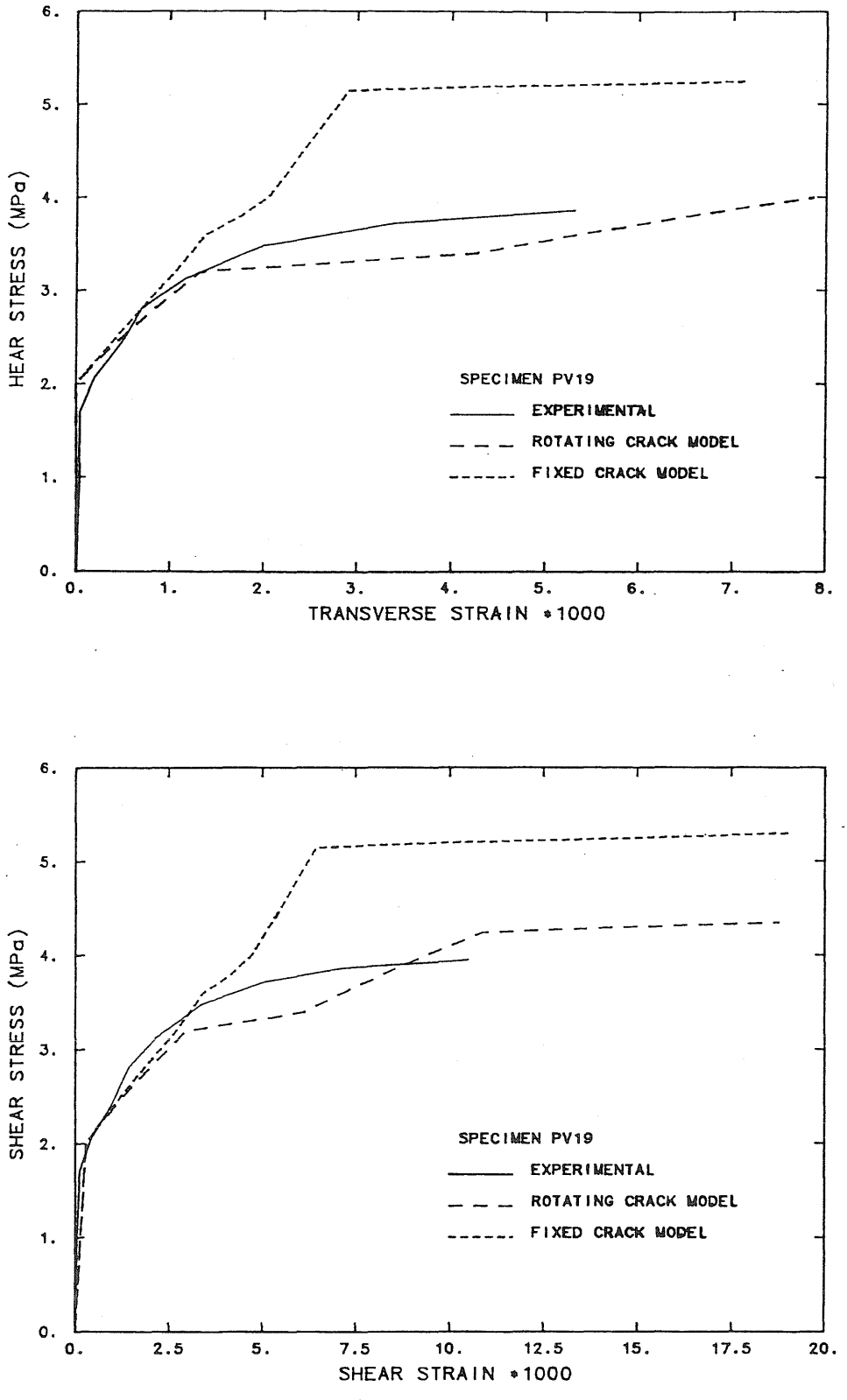

Figure 4.15 Load-Strain Curves for Specimen PV19.

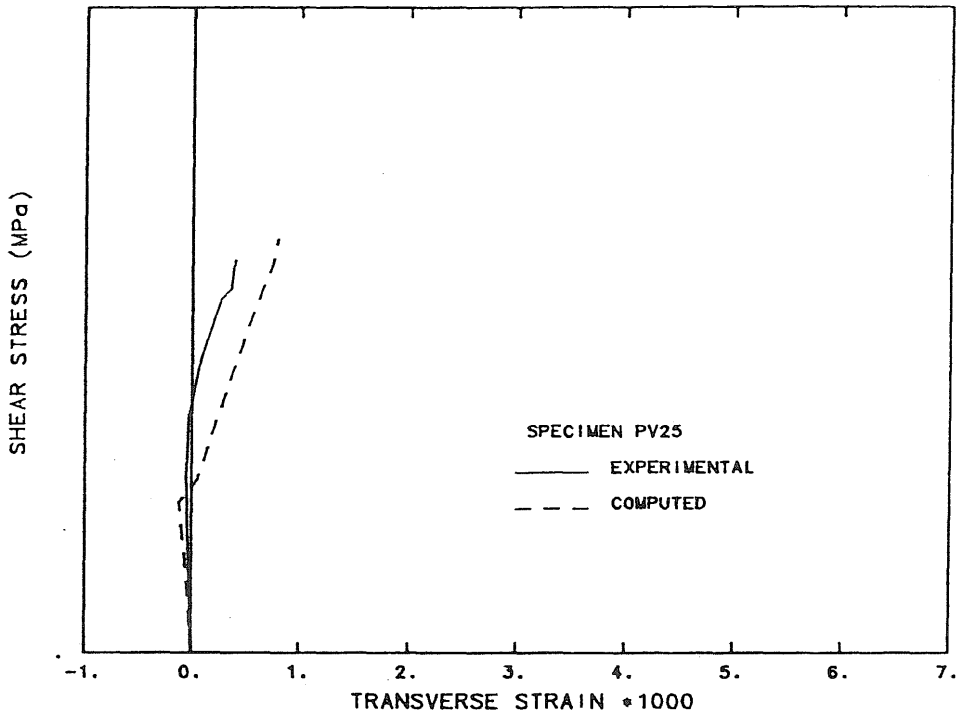

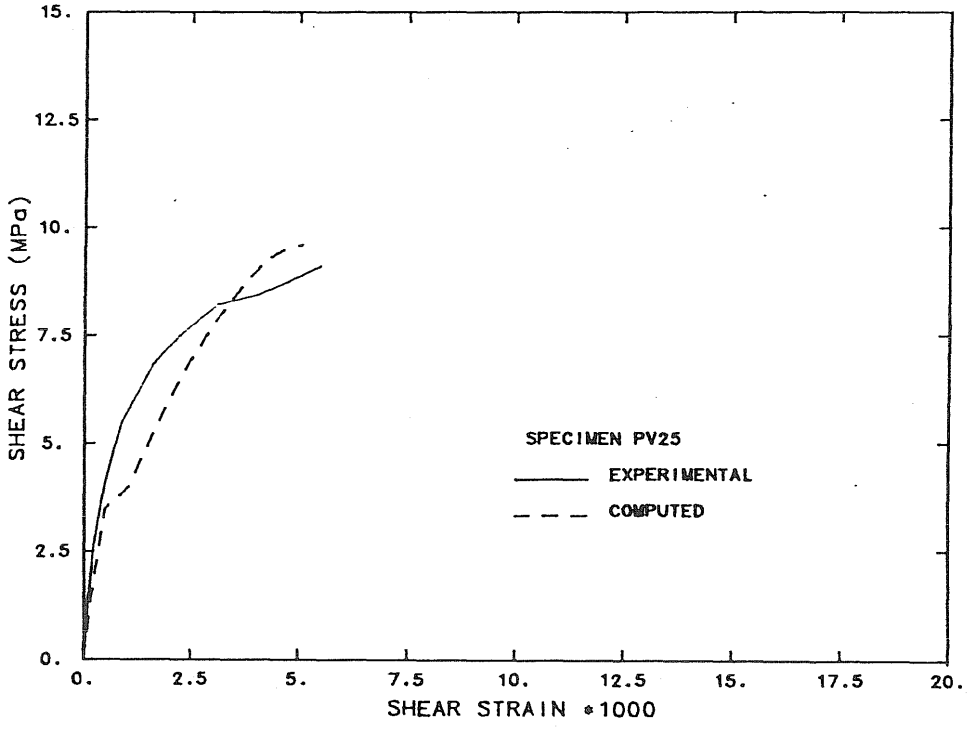

Figure 4.16 Load-Strain Curves for Specimen PV25.

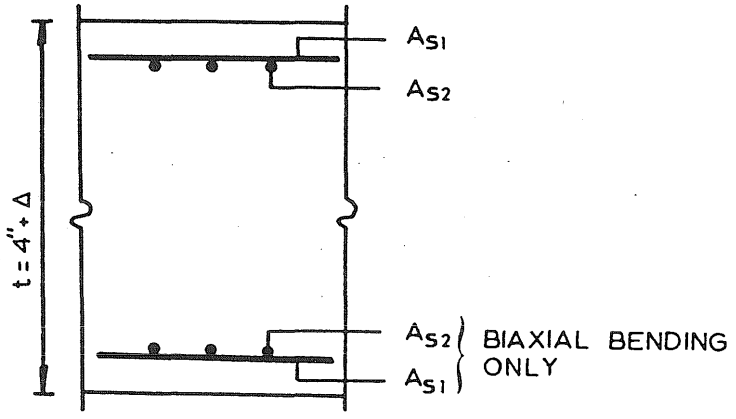

1/4" Diameter Bars.

Cover to Top Reinforcement 3/8"

Cover to Bottom Reinforcement 3/8" + Δ

Figure 4.17 Details for Cardenas-Sozen Specimens.

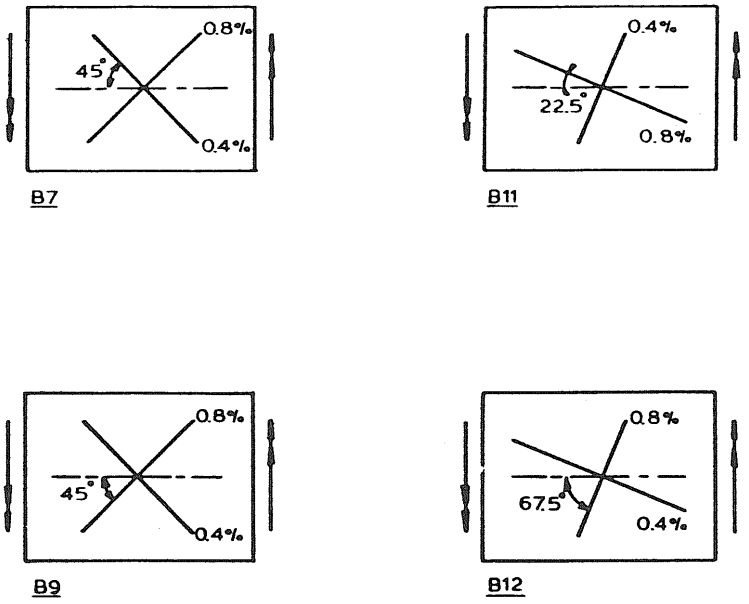

Note: Reinforcement quantities shown are nominal values.

Figure 4.18 Reinforcement Details for Specimens Subjected to Uniaxial Bending.

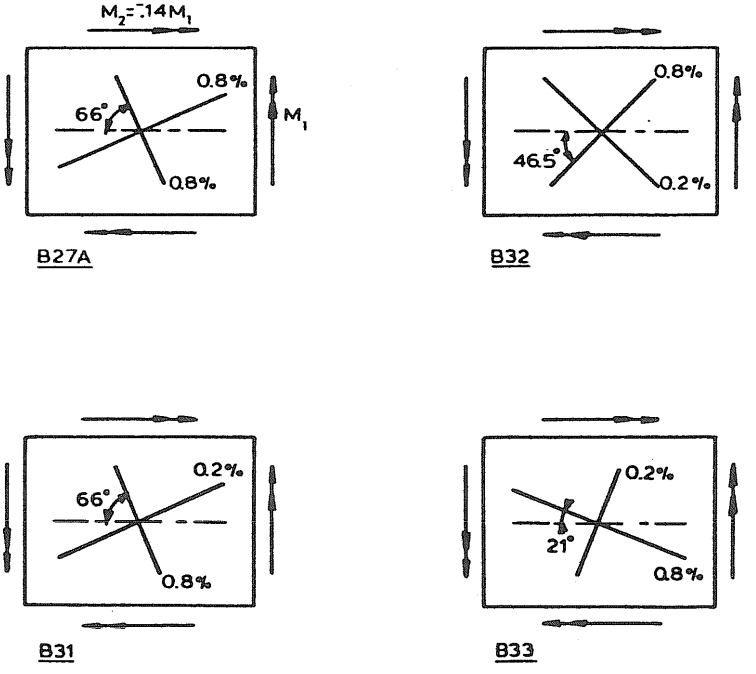

Note: Reinforcement quantities shown are nominal values.

Figure 4.19 Reinforcement Details for Specimens Subjected to Biaxial Bending.

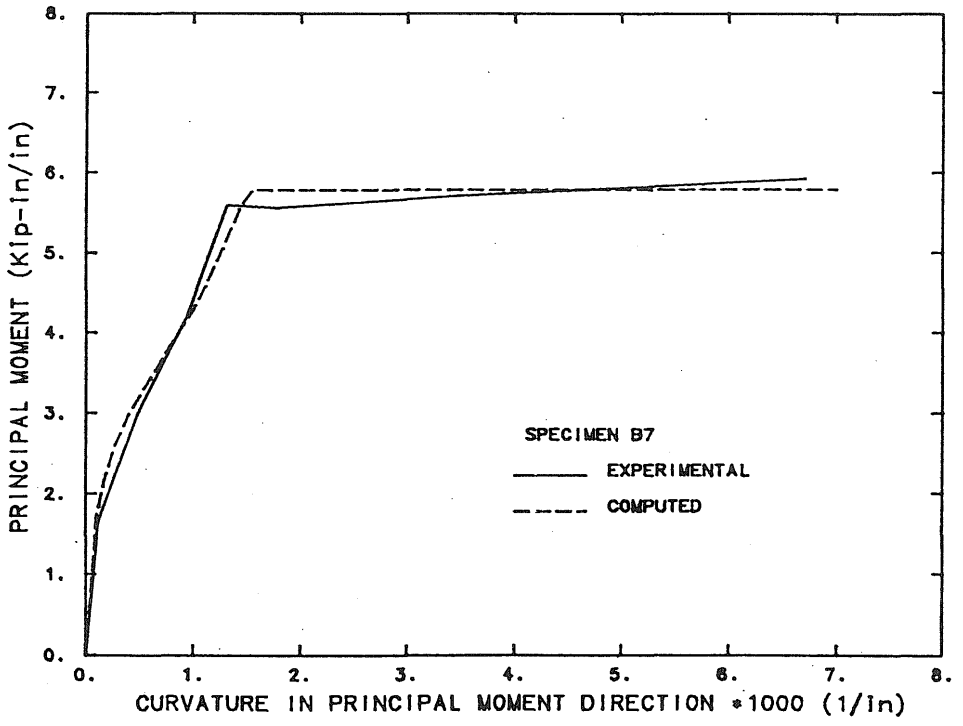

Figure 4.20 Moment-Curvature Curves for Specimen B7.

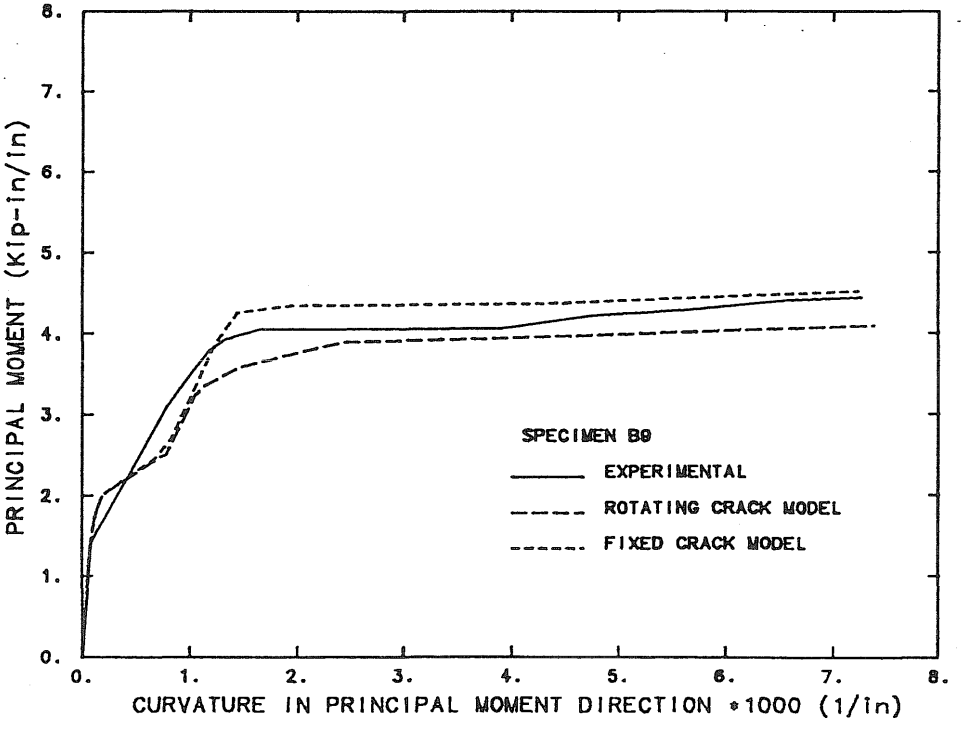

Figure 4.21 Moment-Curvature Curves for Specimen B9.

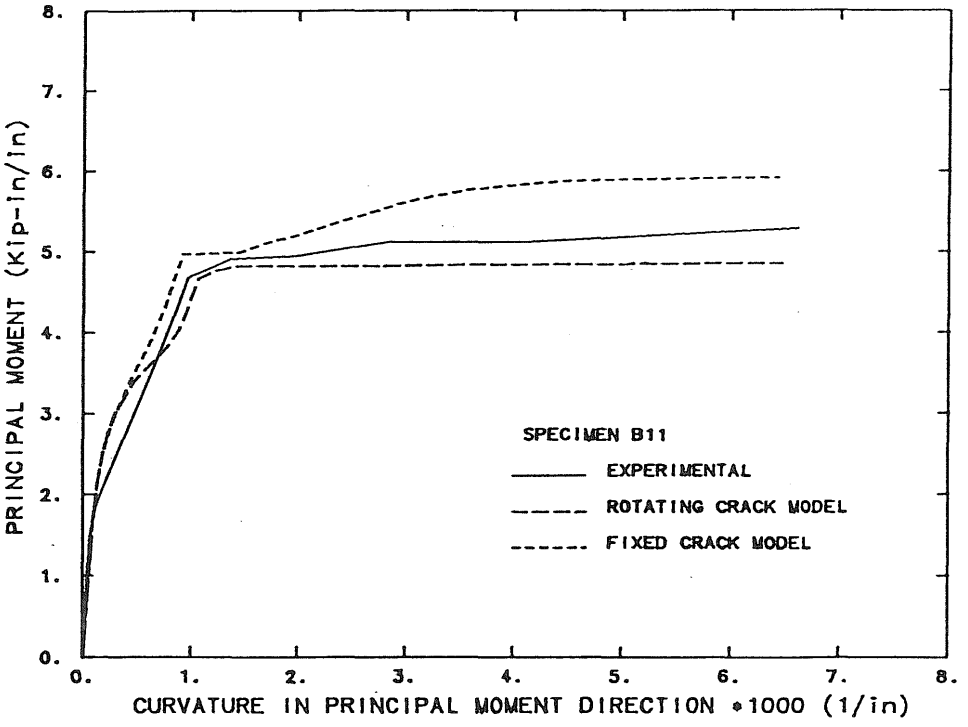

Figure 4.22 Moment-Curvature Curves for Specimen B11.

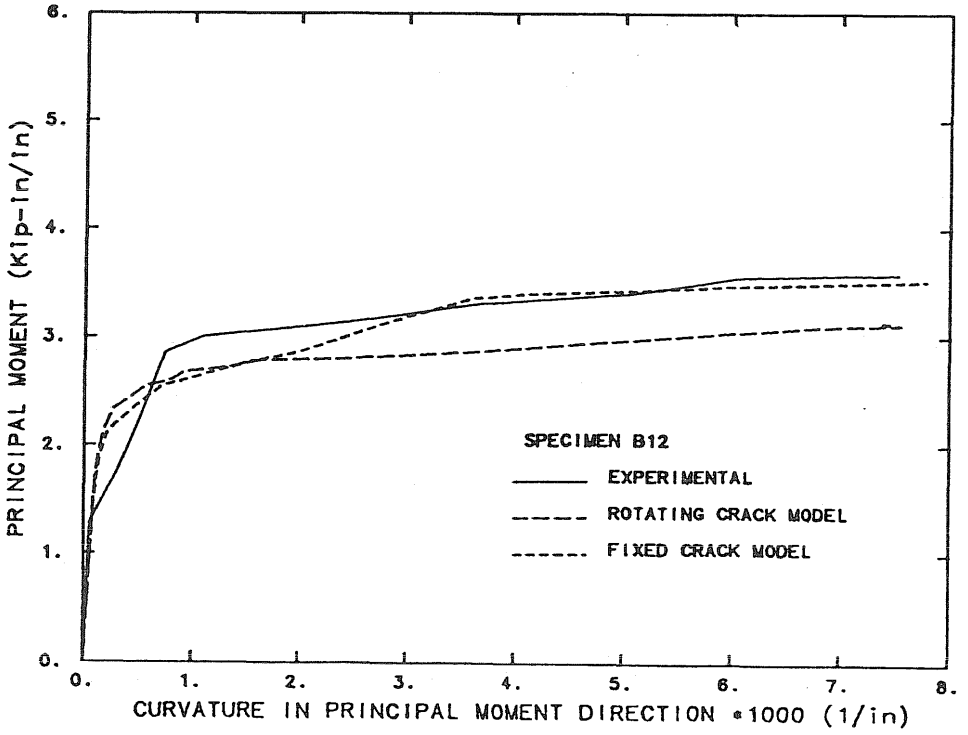

Figure 4.23 Moment-Curvature Curves for Specimen B12.

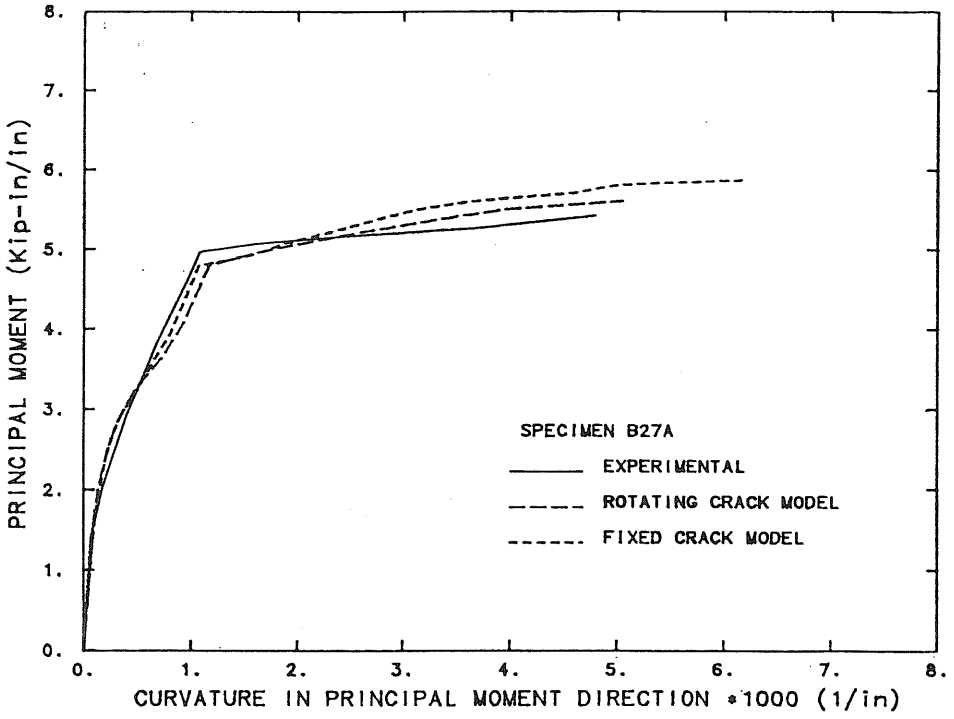

Figure 4.24 Moment-Curvature Curves for Specimen B27A.

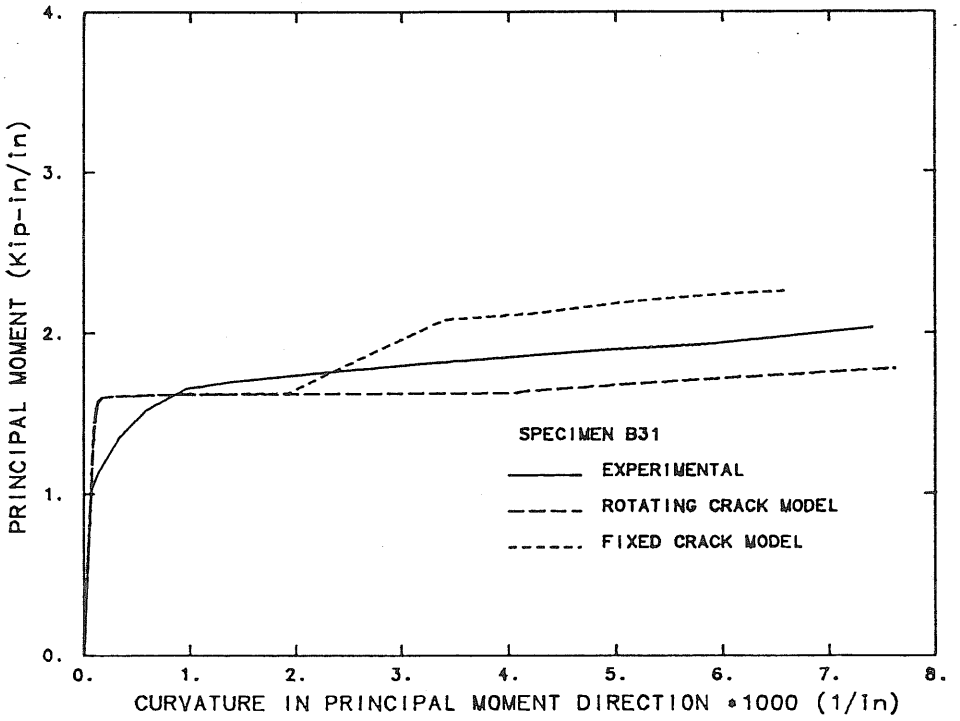

Figure 4.25 Moment-Curvature Curves for Specimen B31.

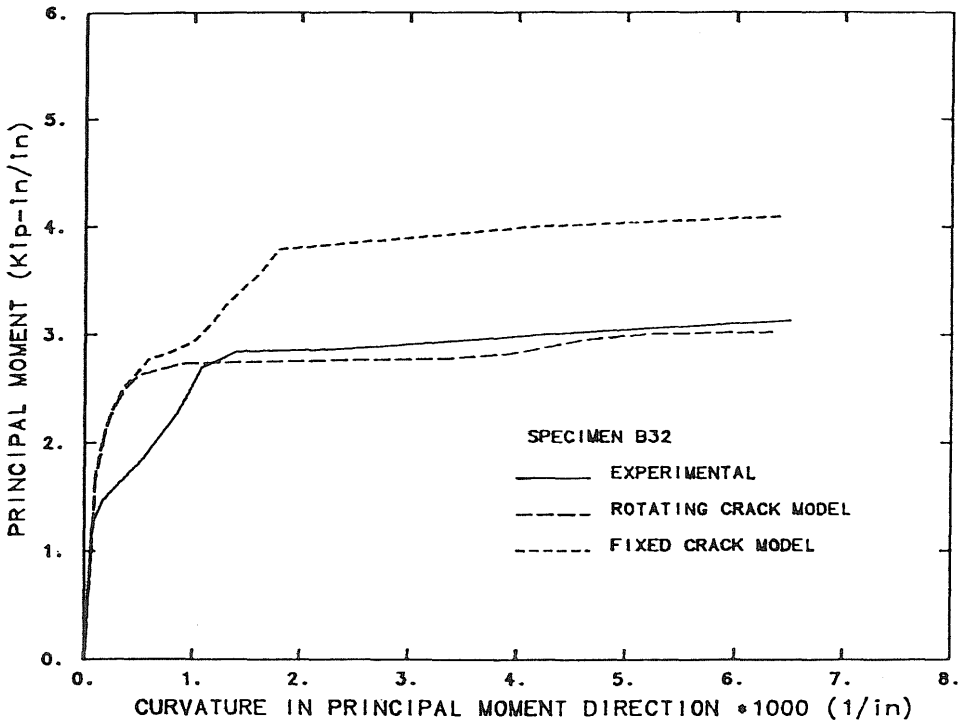

Figure 4.26 Moment-Curvature Curves for Specimen B32.

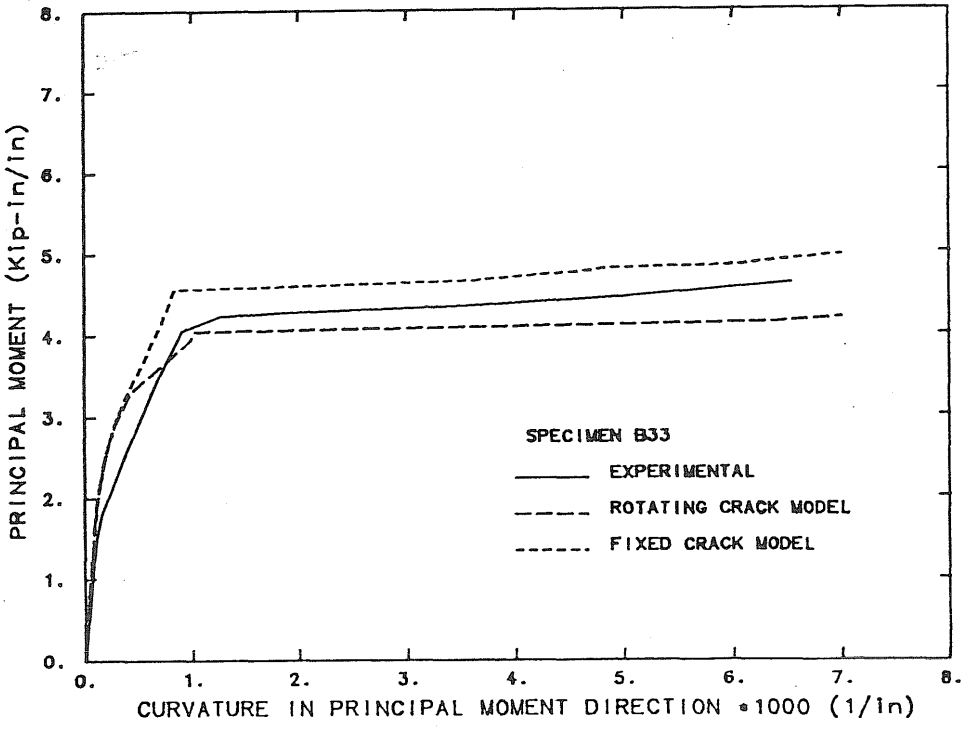

Figure 4.27 Moment-Curvature Curves for Specimen B33.

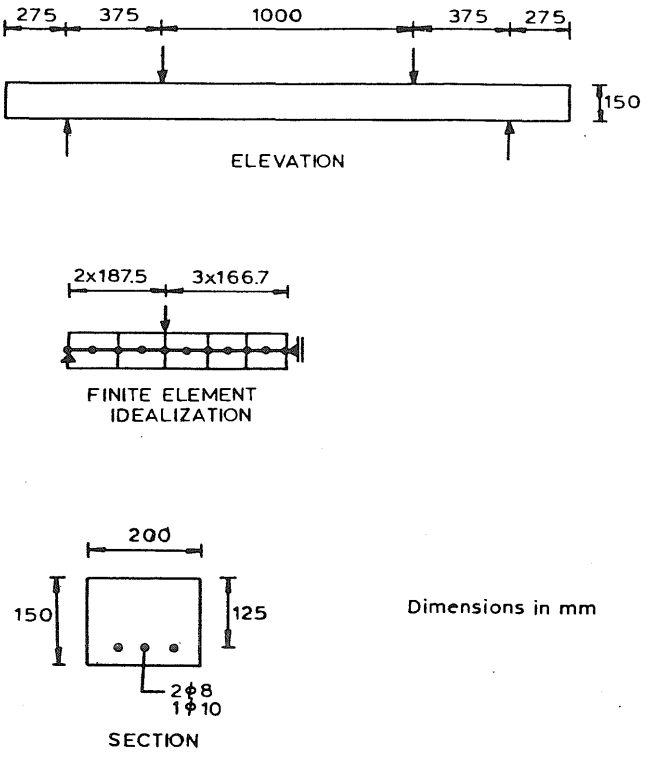

Figure 4.28 Details of Delft Beam.

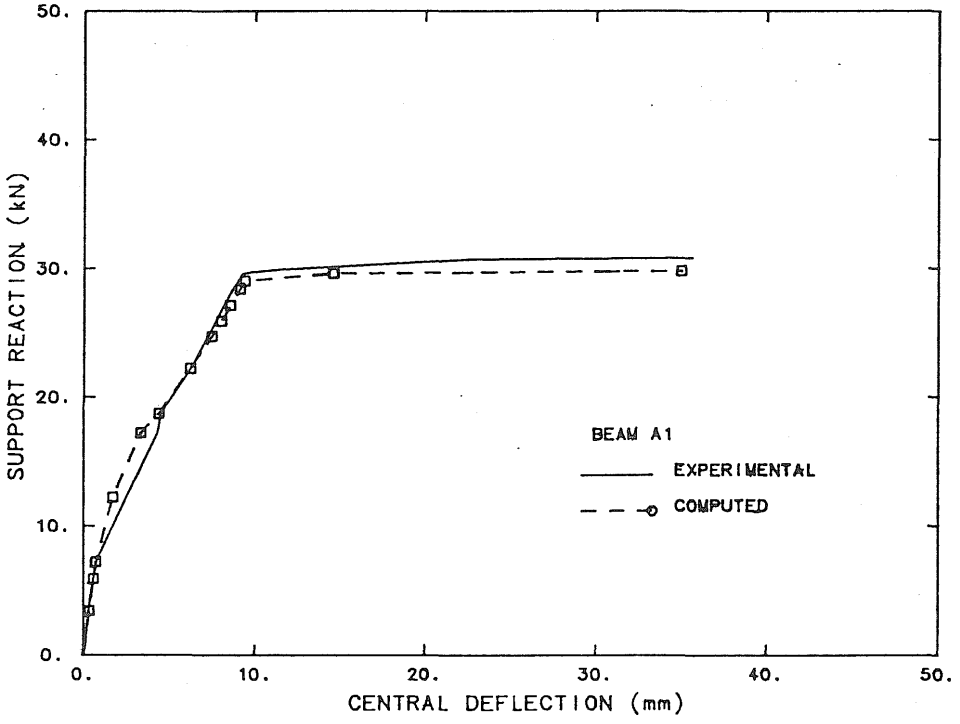

Figure 4.29 Load-Central Displacement Curves for Delft Beam.

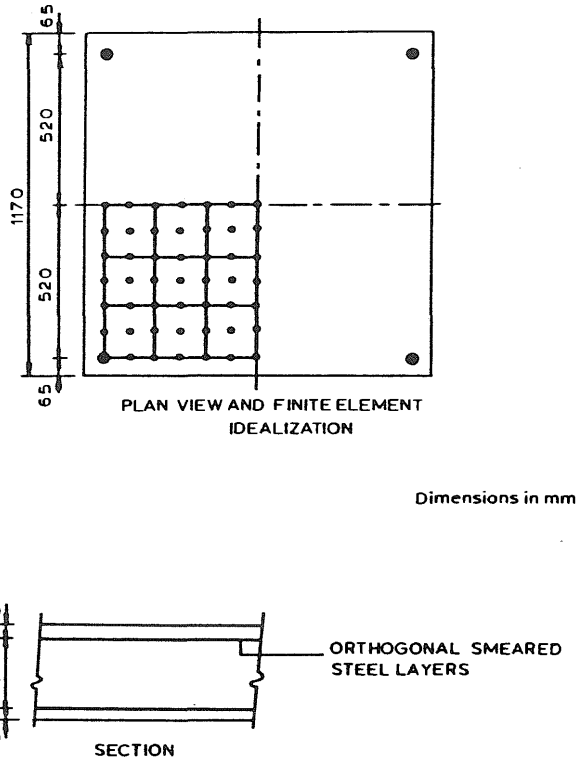

Figure 4.30 Details of Duddeck's Slabs.

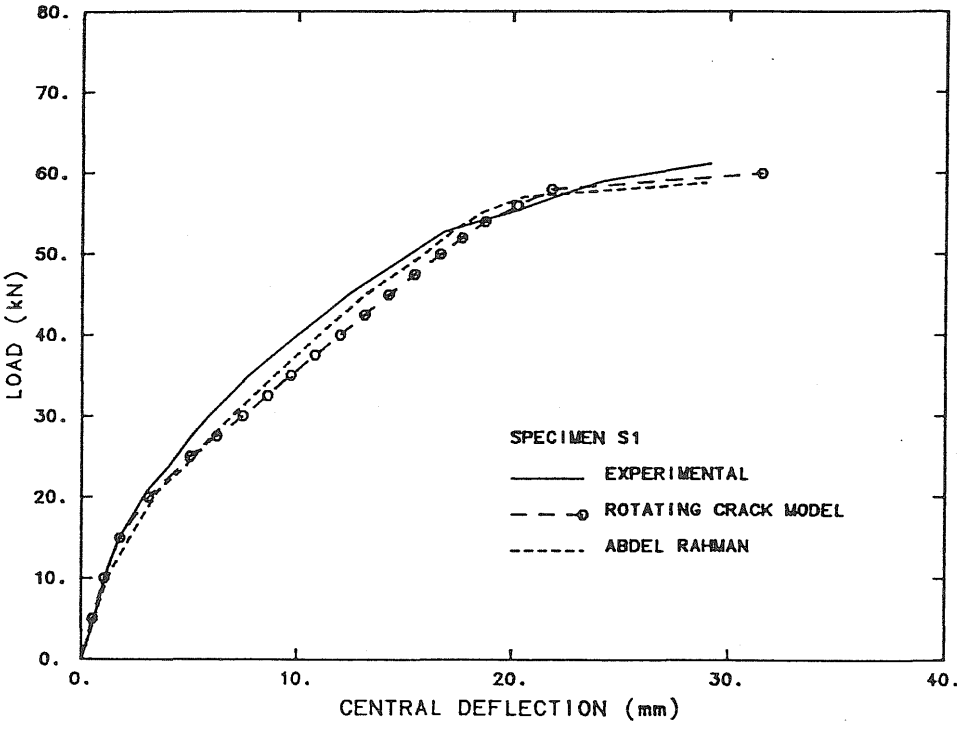

Figure 4.31 Load-Displacement Curves for Slab S1.

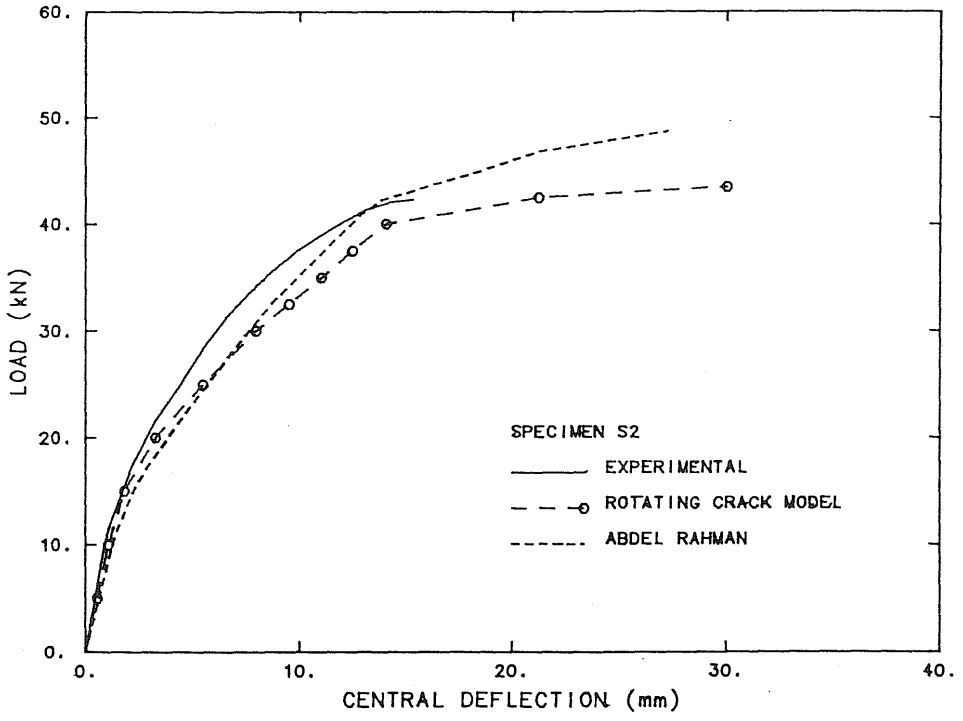

Figure 4.32 Load-Displacement Curves for Slab S2.

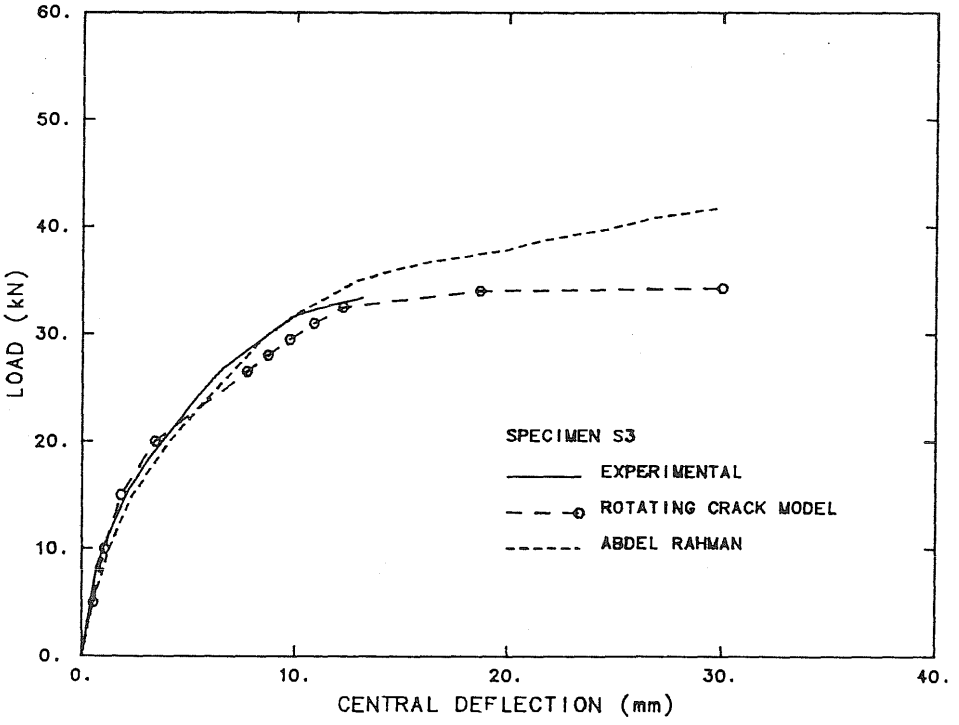

Figure 4.33 Load Displacement Curves for Slab S3.

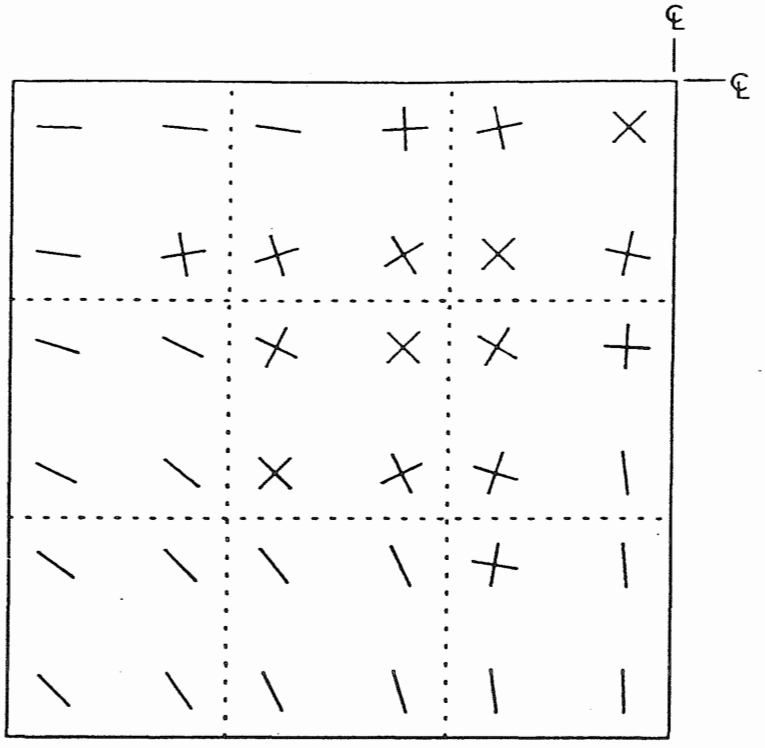

Crack pattern for bottom layer.

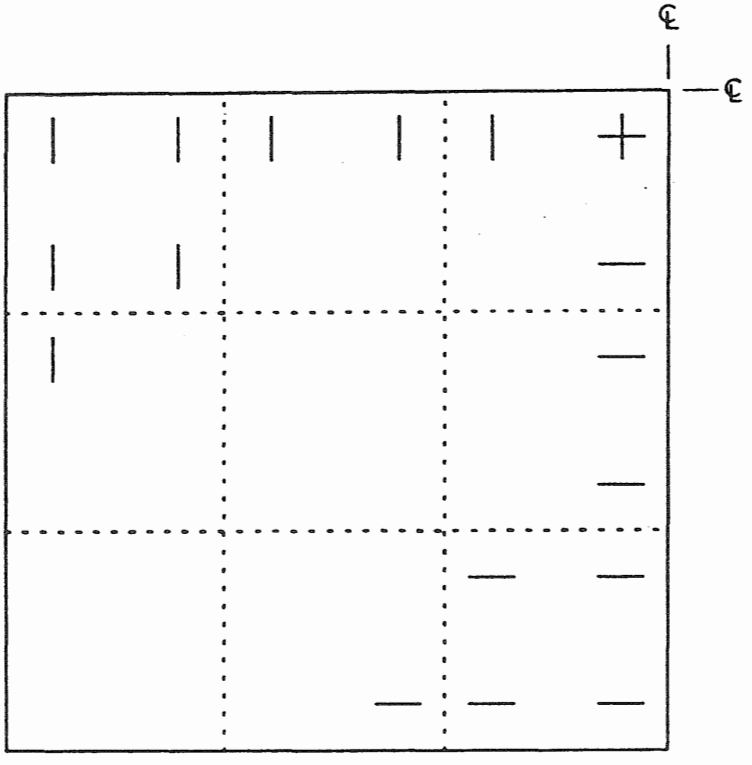

Yielded reinforcement in bottom layer.

Figure 4.34 Crack Pattern and Yielded Reinforcement for Slab S1.

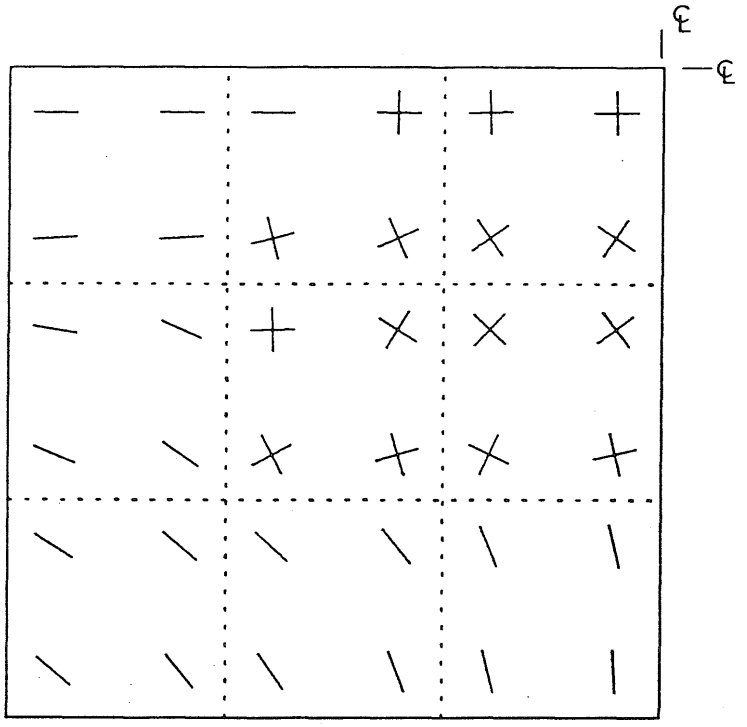

Crack pattern for bottom layer.

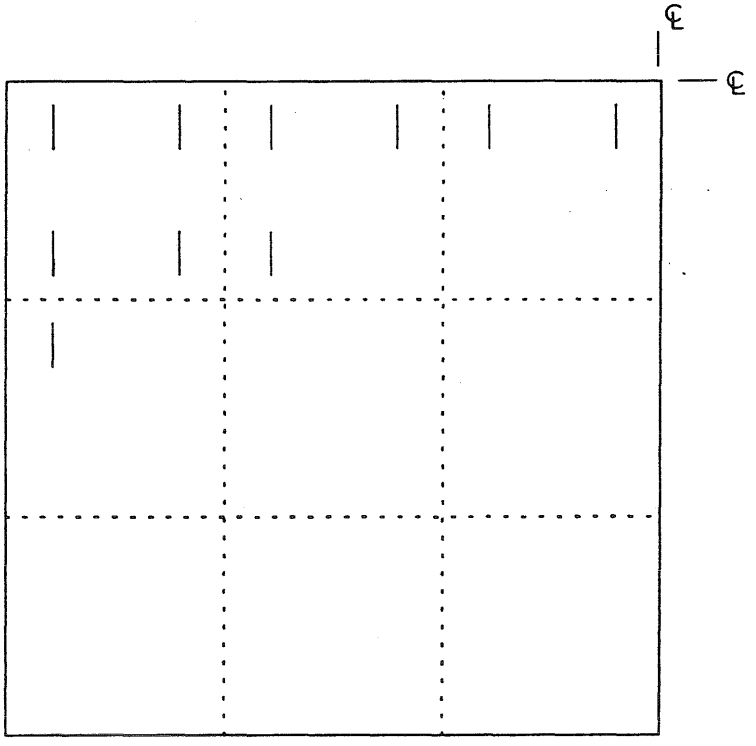

Yielded reinforcement in bottom layer.

Figure 4.35 Crack Pattern and Yielded Reinforcement for Slab S2.

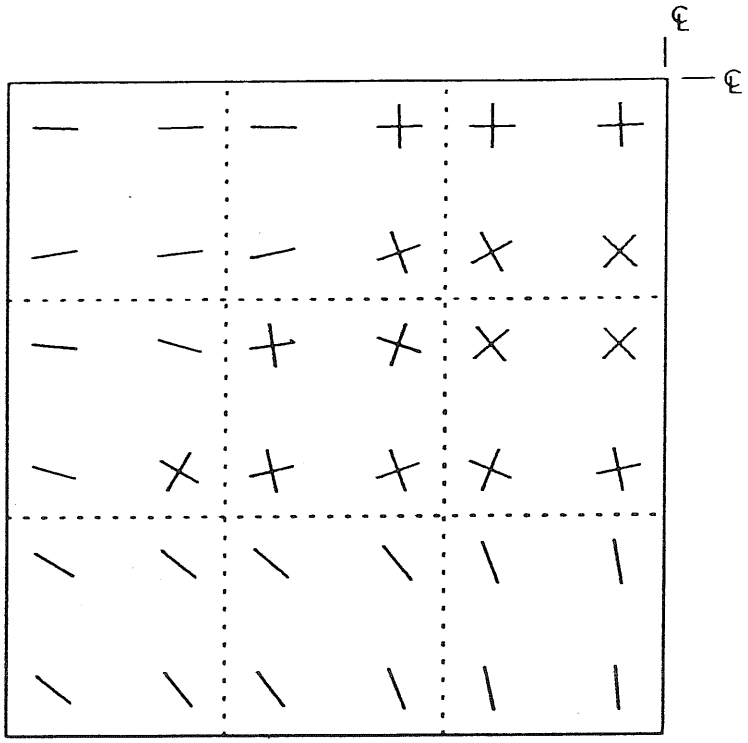

Crack pattern for bottom layer.

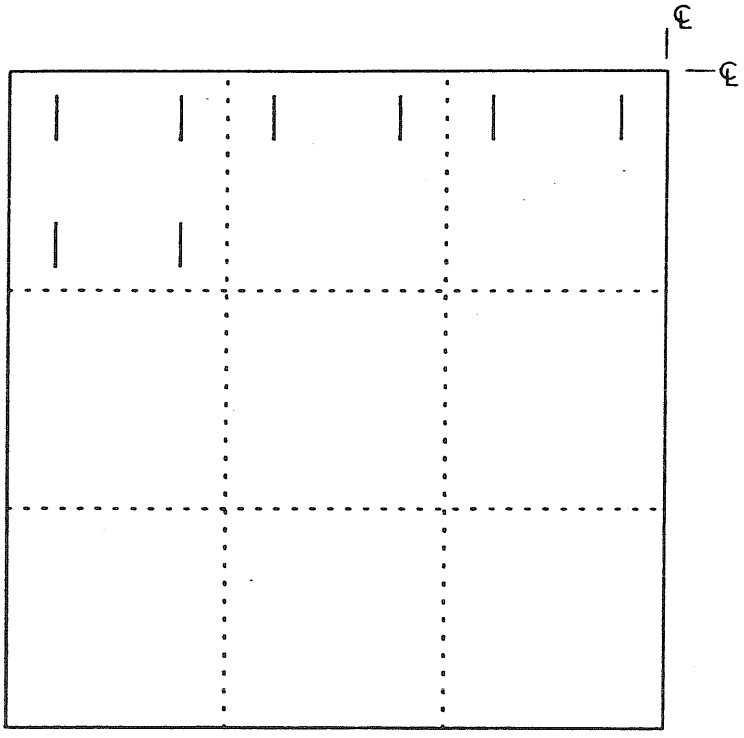

Yielded reinforcement in bottom layer.

Figure 4.36 Crack Pattern and Yielded Reinforcement for Slab S3.

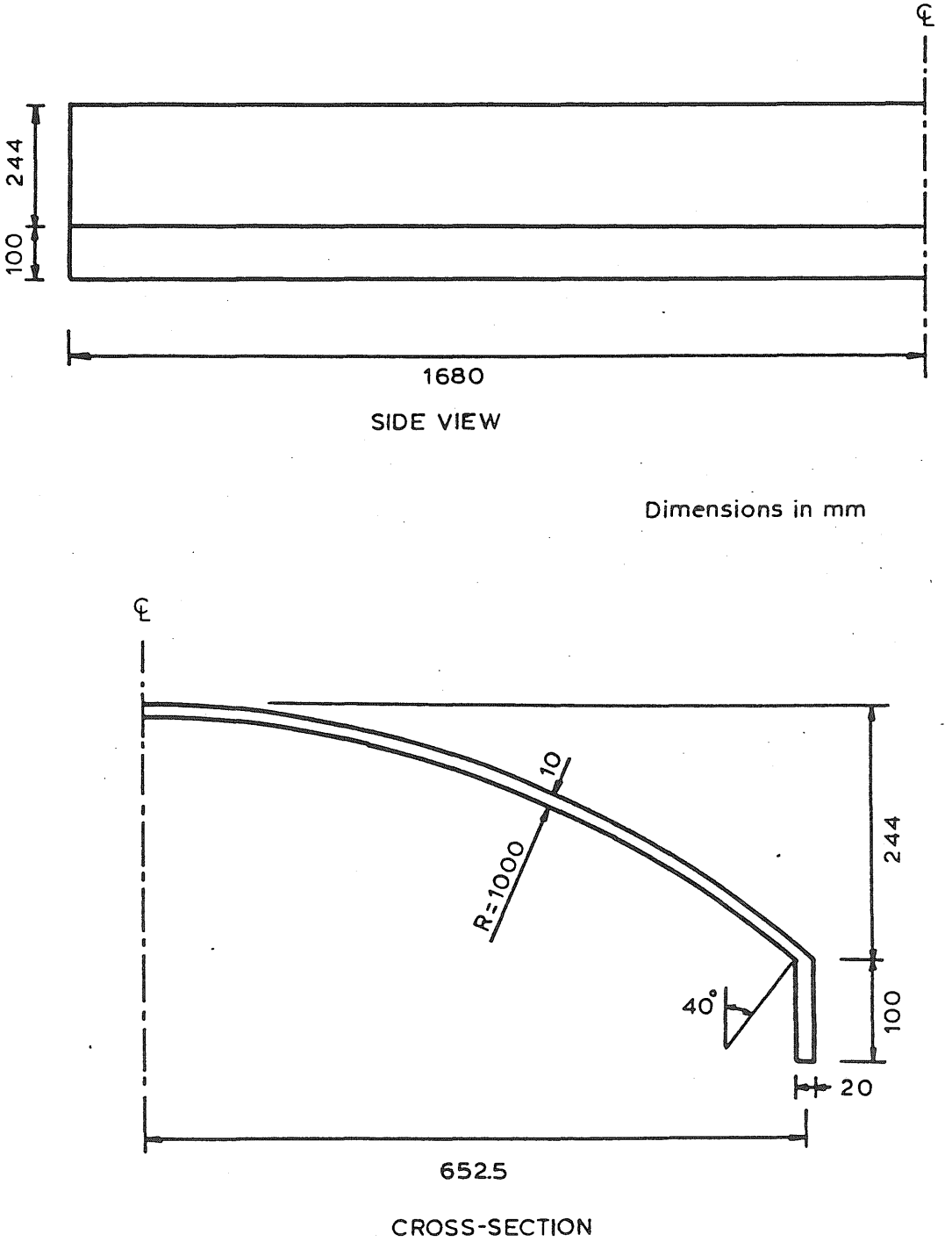

Figure 4.37 Details of Bouma's Cylindrical Shell.

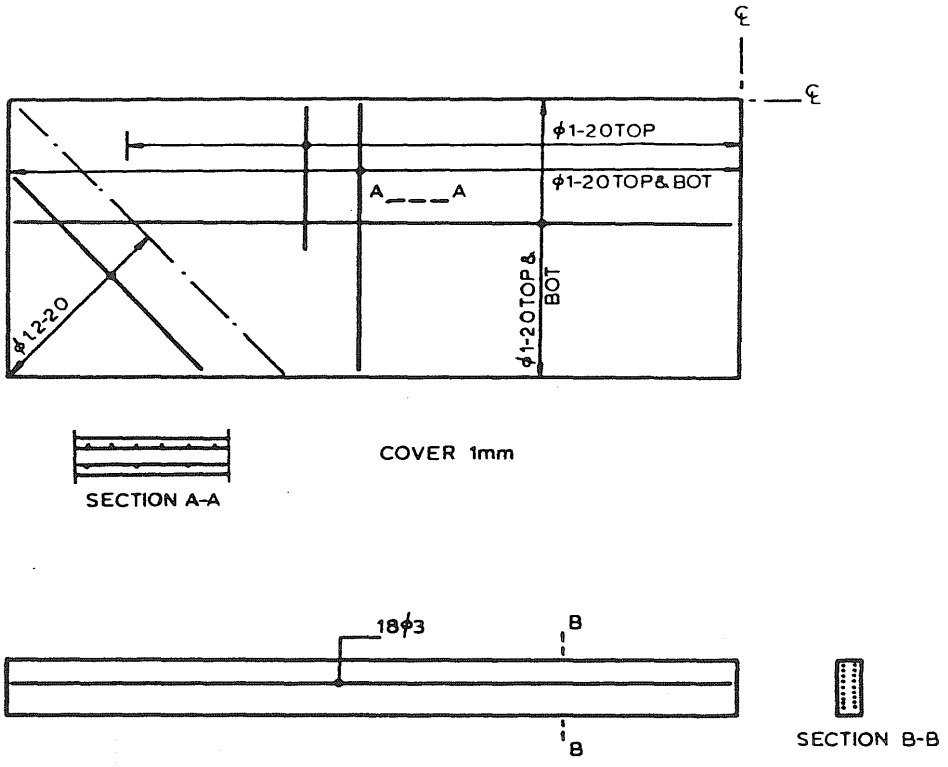

Figure 4.38 Reinforcement Details for Bouma's Shell.

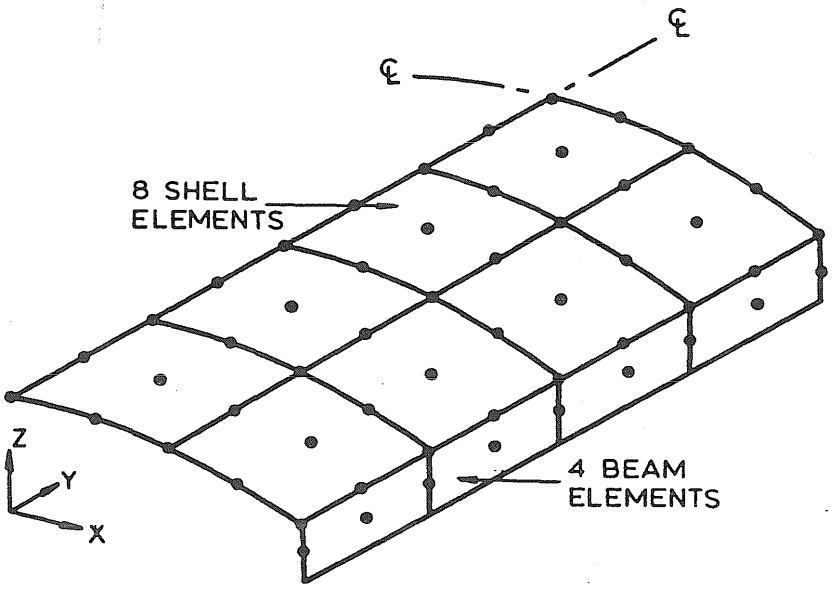

Figure 4.39 Finite Element Mesh for Cylindrical Shell.

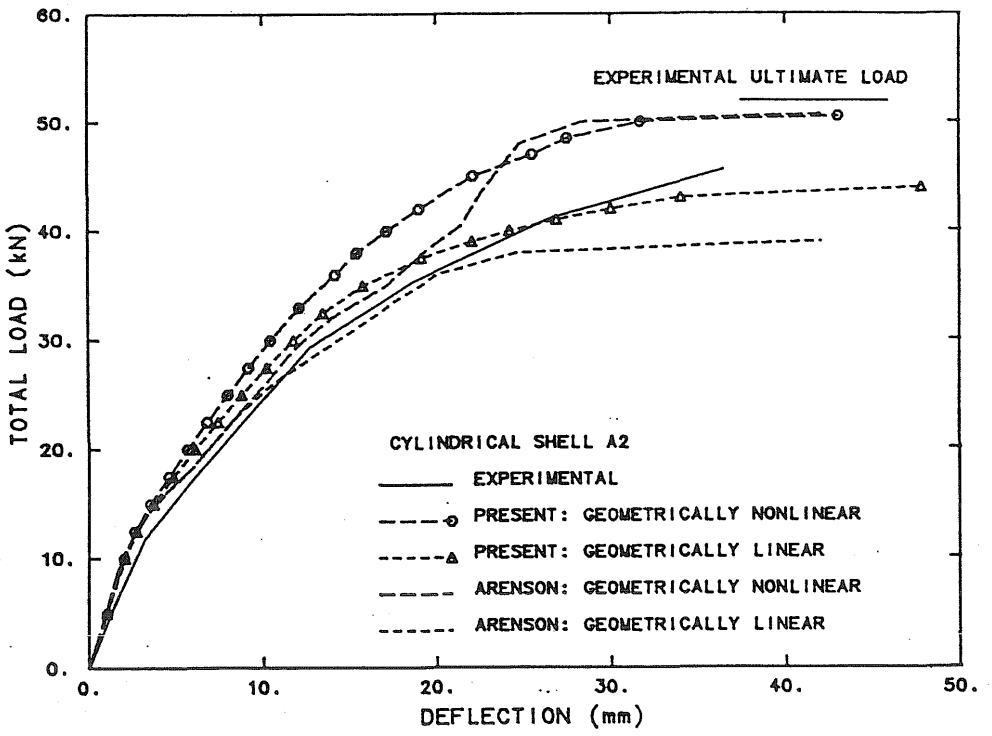

Figure 4.40 Load-Displacement Curves for Cylindrical Shell.

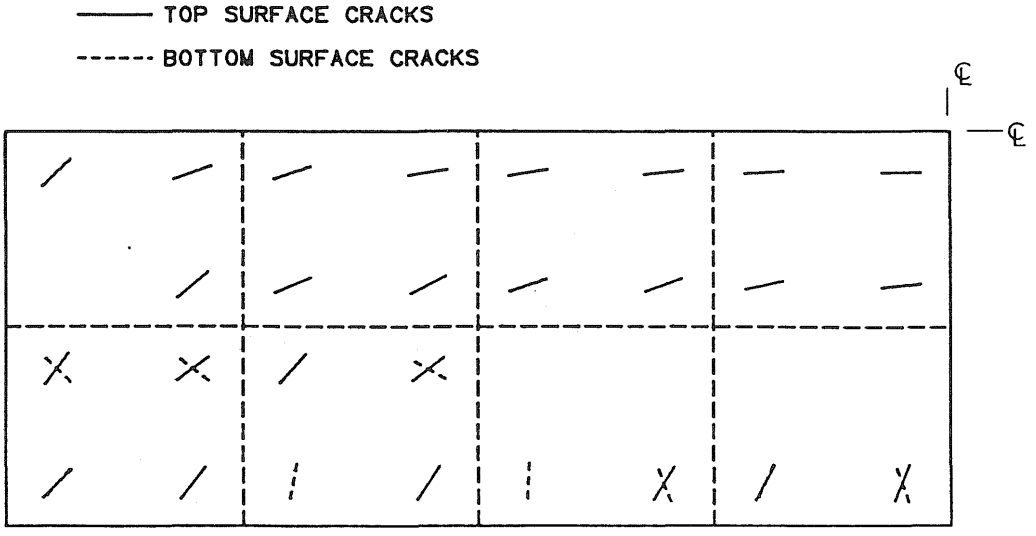

Figure 4.41 Crack Pattern for Cylindrical Shell.

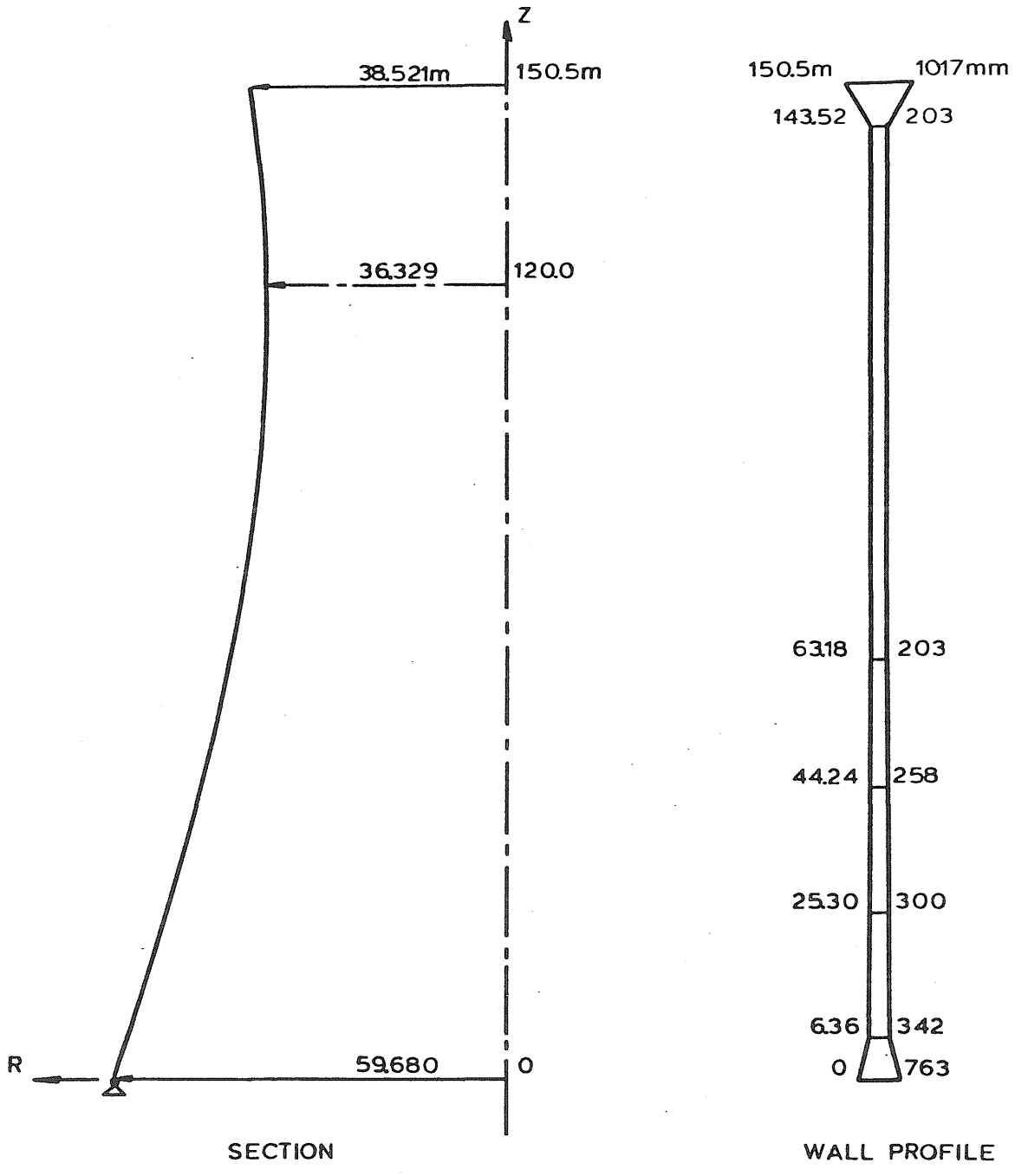

Figure 5.1 Geometry of Cooling Tower.

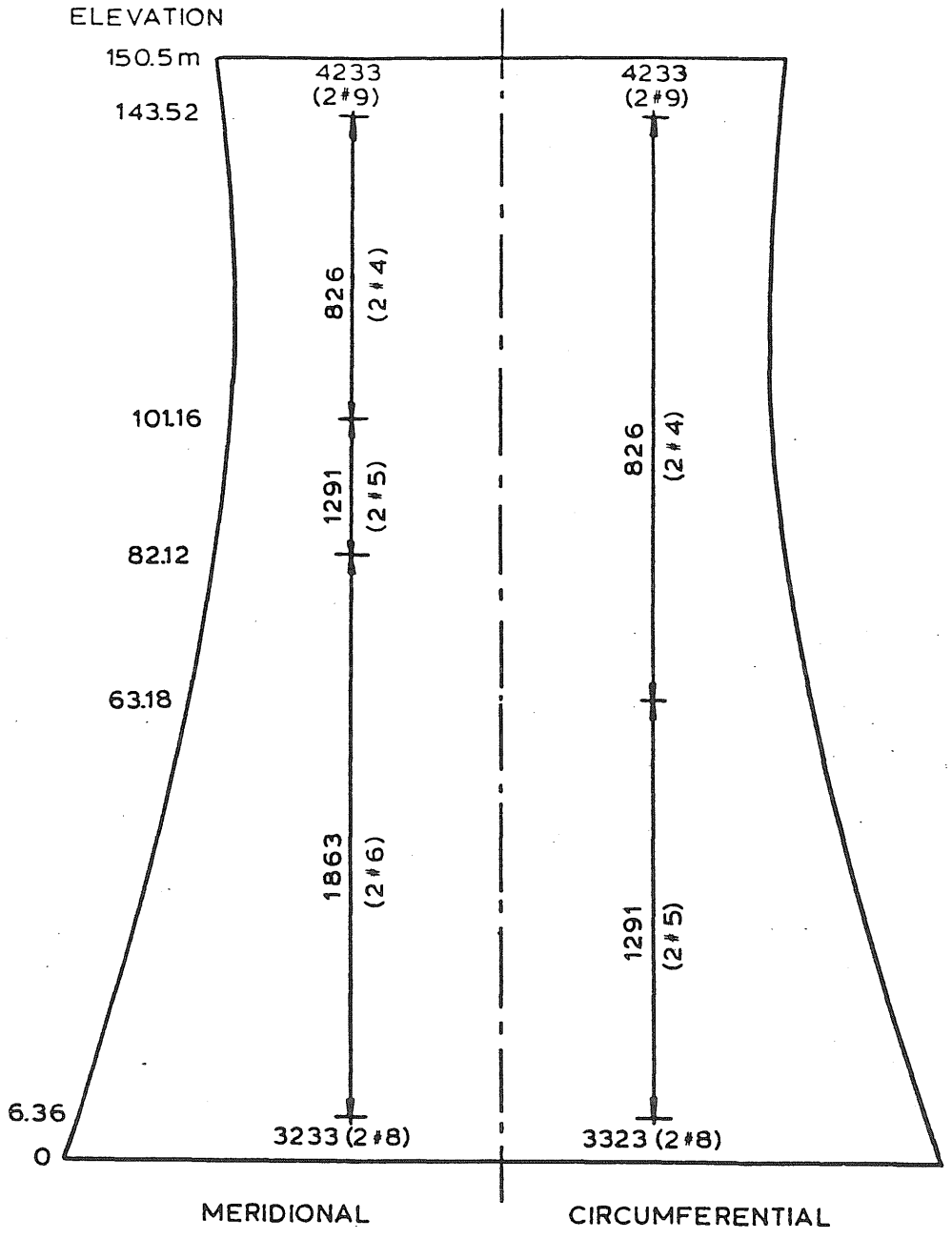

KEY: $\frac{1291}{(2\#5)}$ 1291 mm^2/m $2\#5/ft$

Notes: 1) Cover to meridional reinforcement (outer layer) 40 mm.
2) Reinforcement distributed equally in two layers.

Figure 5.2 Reinforcement Quantities for Cooling Tower.

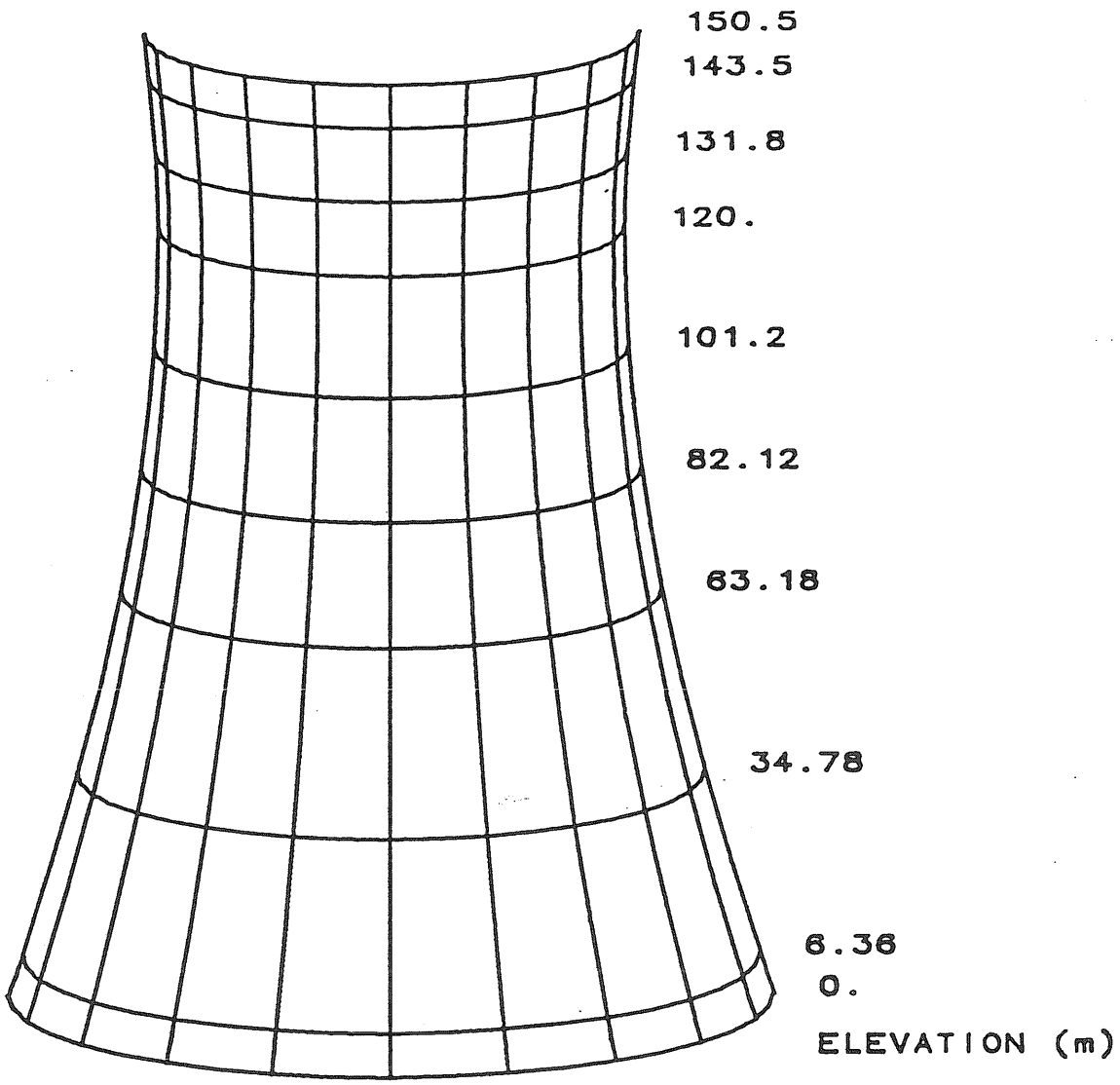

Figure 5.3 Finite Element Mesh for Cooling Tower.

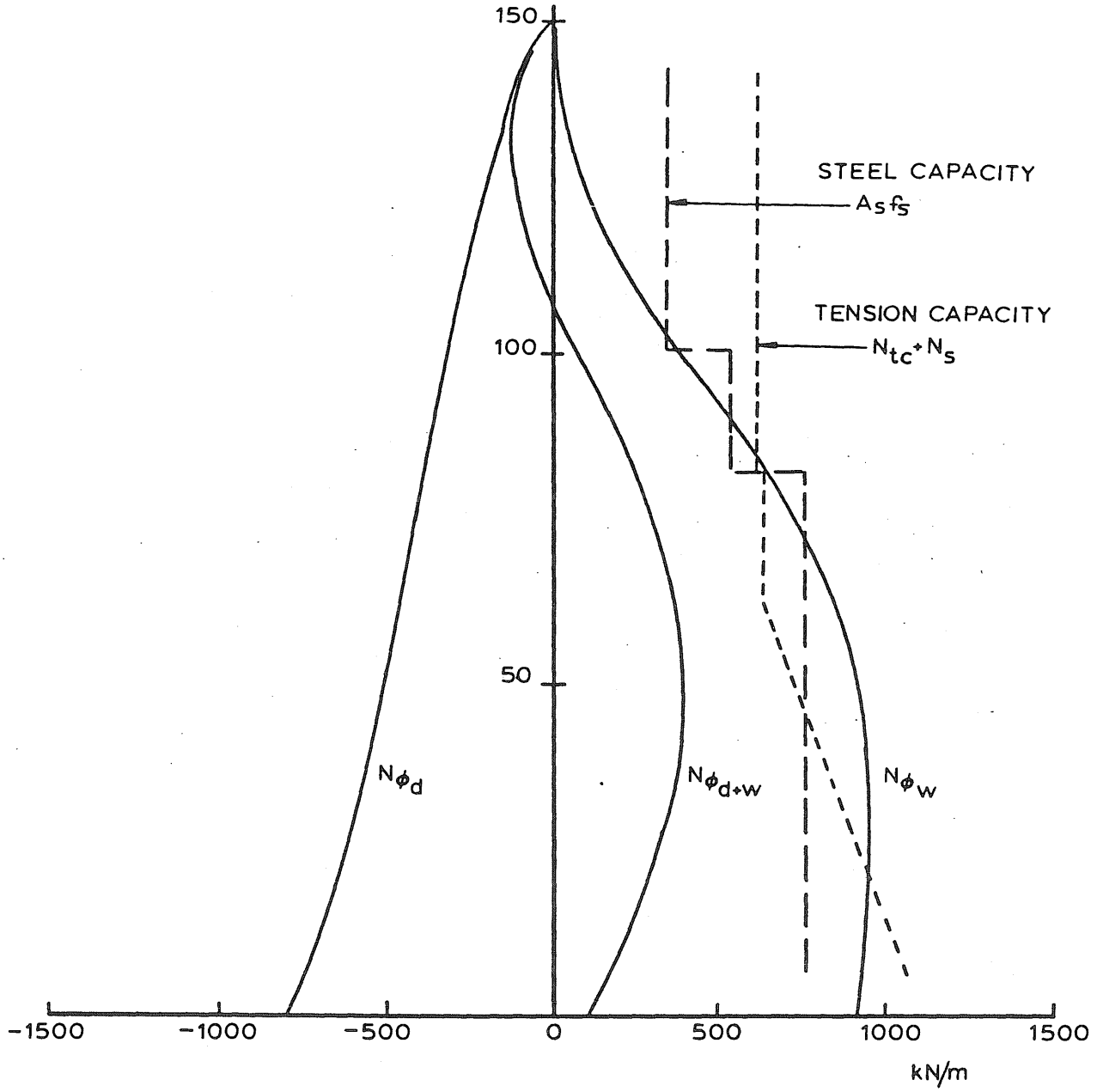

Figure 5.4 Meridional Forces and Design Strengths.

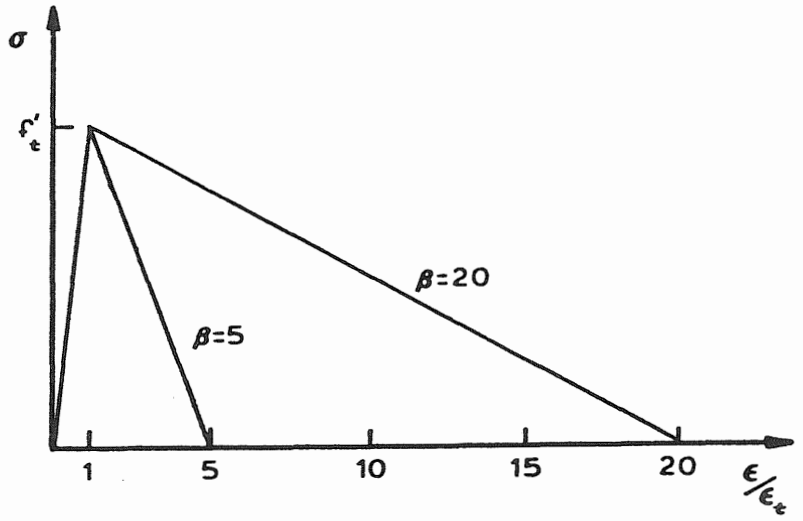

Figure 5.5 Tension Stiffening Models for Cooling Tower.

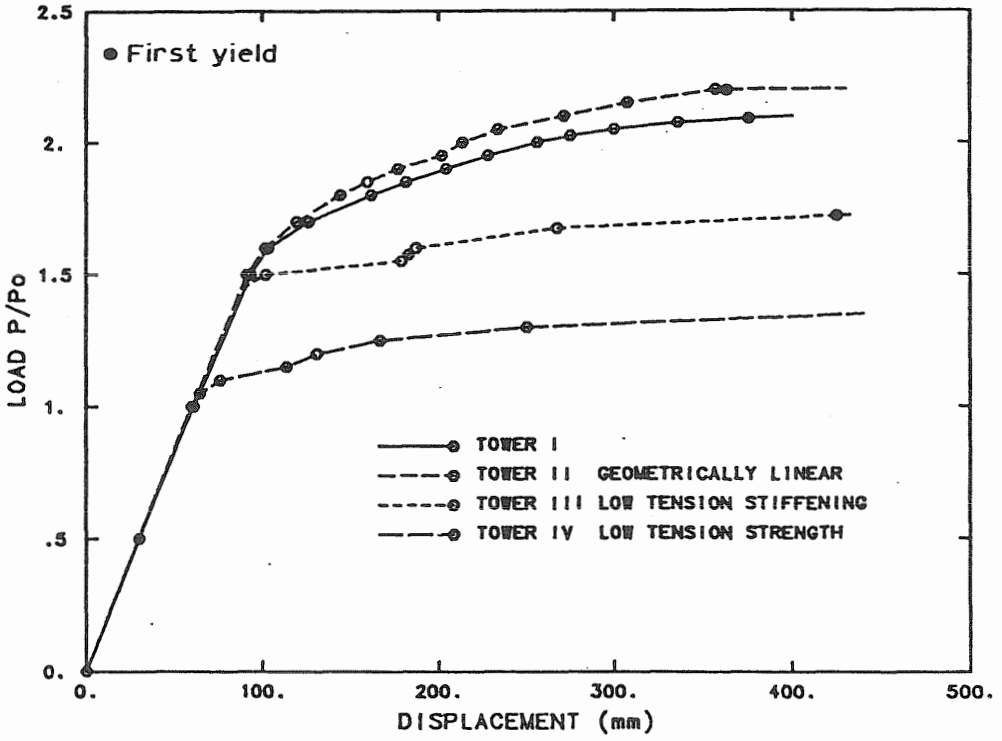

Figure 5.6 Load Displacement Curves for Cooling Tower.

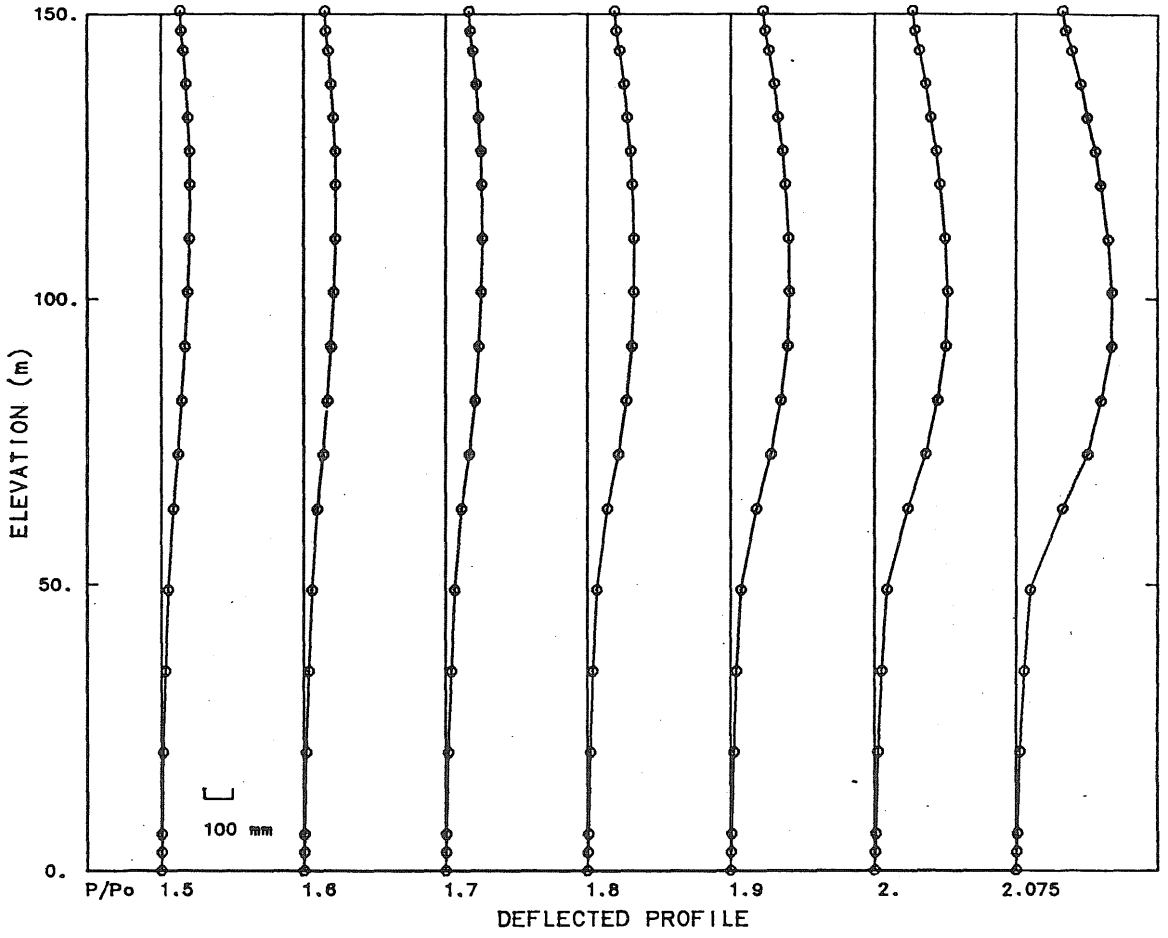

Figure 5.7 Deflected Profile of Windward Meridion for Tower I.

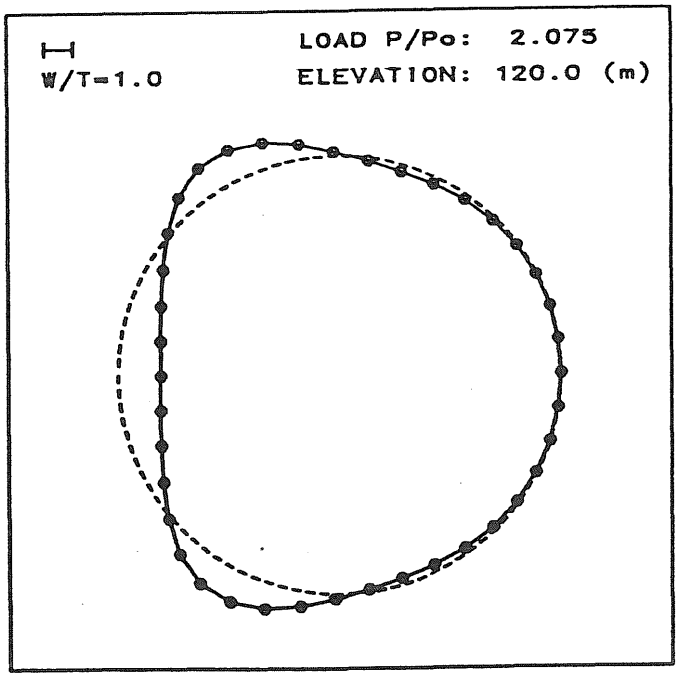

Figure 5.8 Radial Displacement at Throat for Tower I.

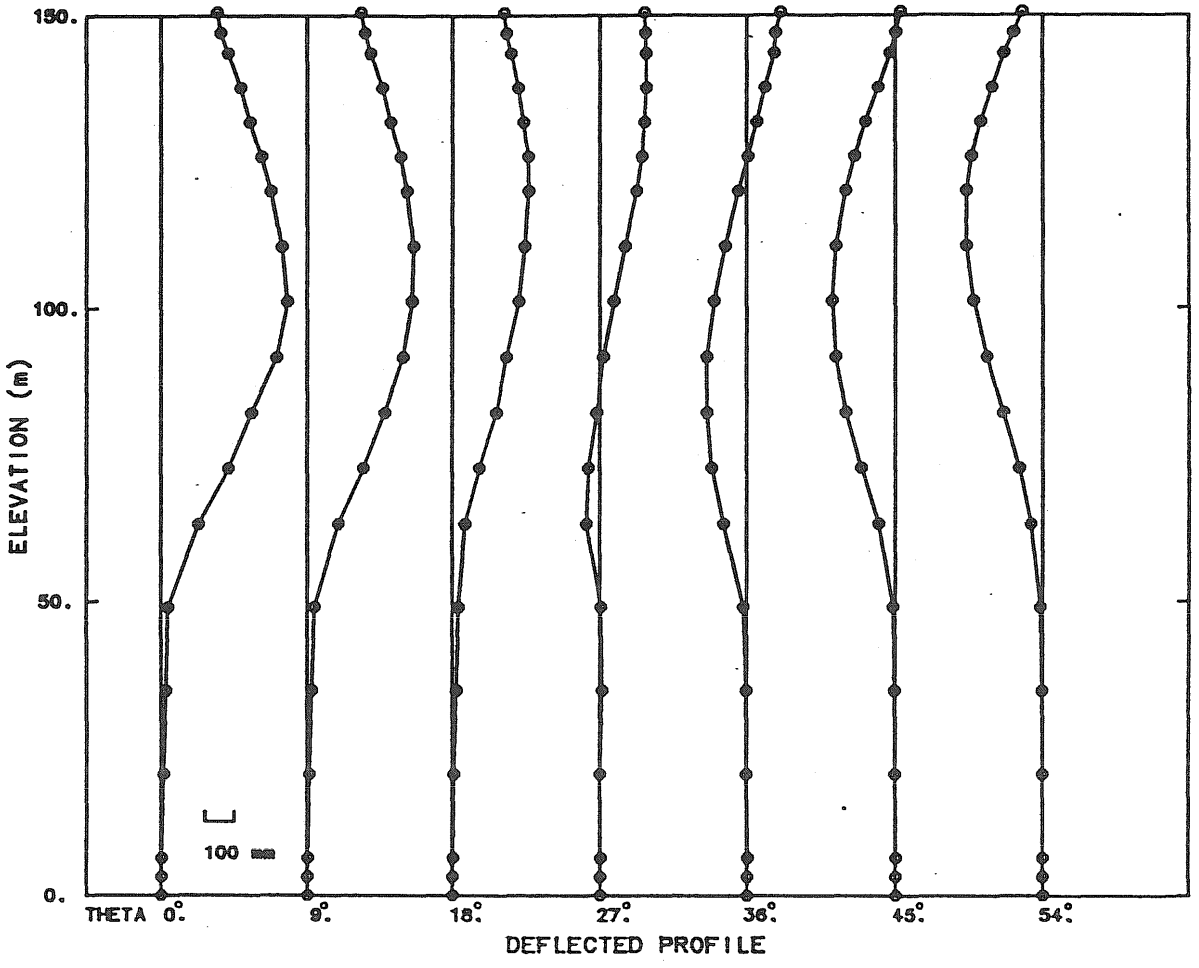

Figure 5.9 Deflected Meridional Profiles for Tower I.

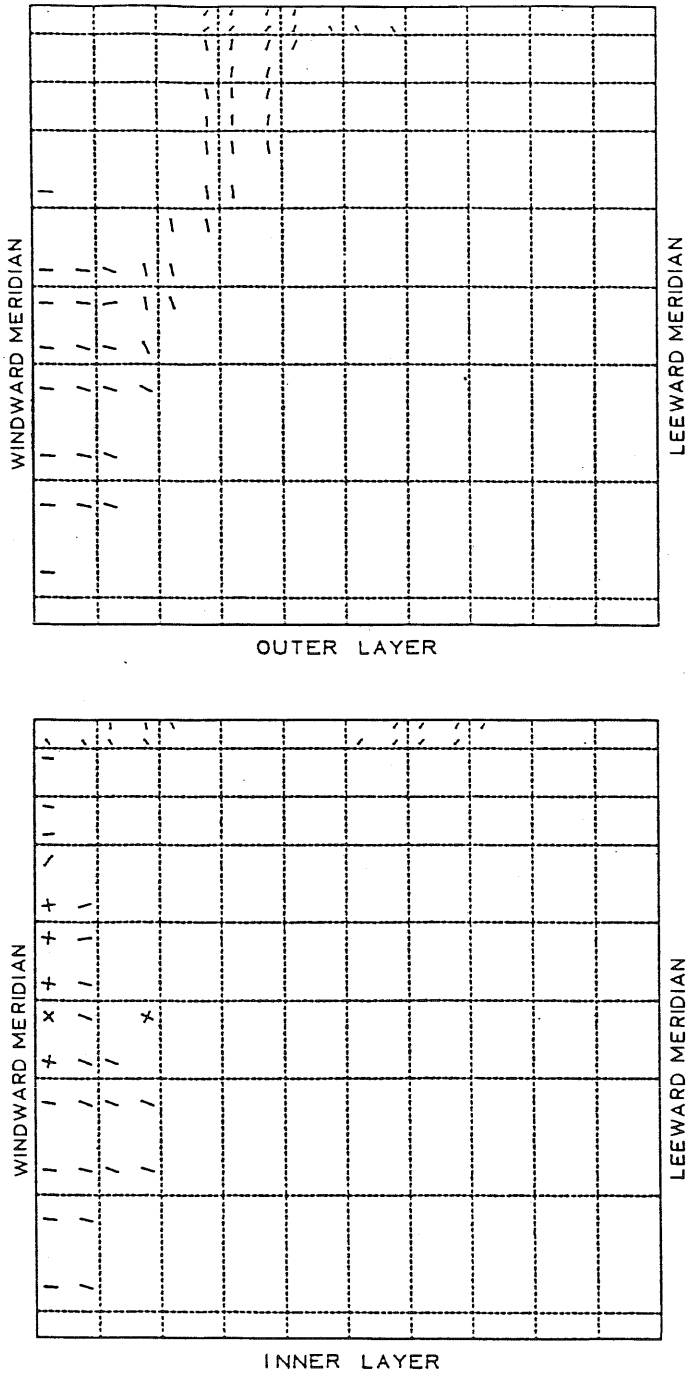

Figure 5.10 Crack Pattern for Tower I.

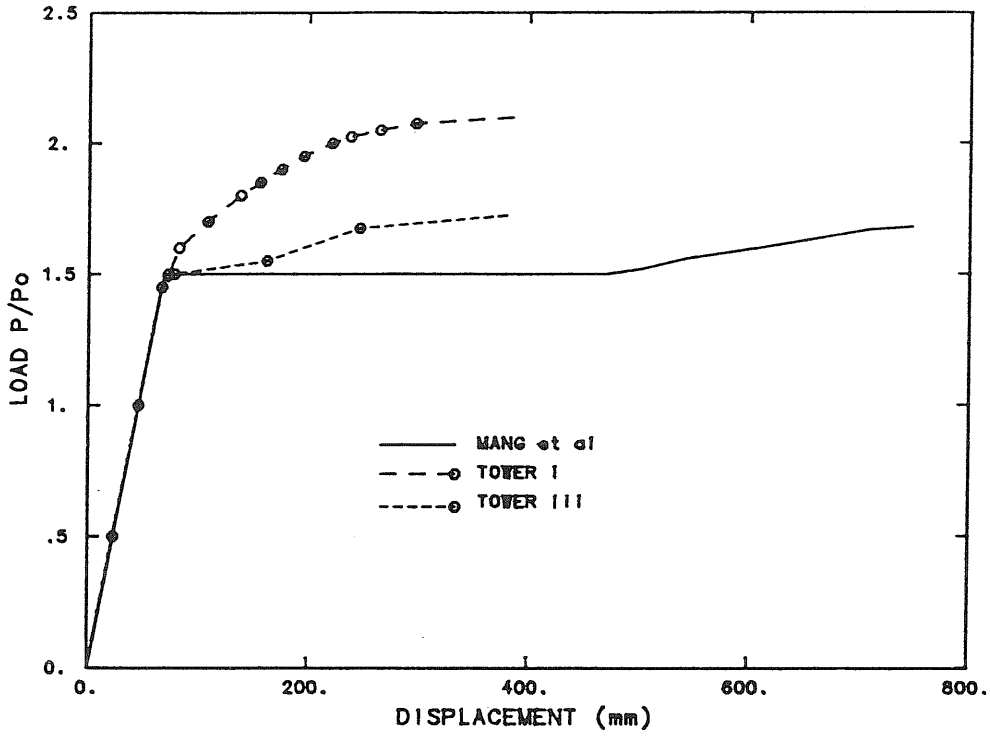

Figure 5.11 Comparison of Predicted Displacements with Mang et al.

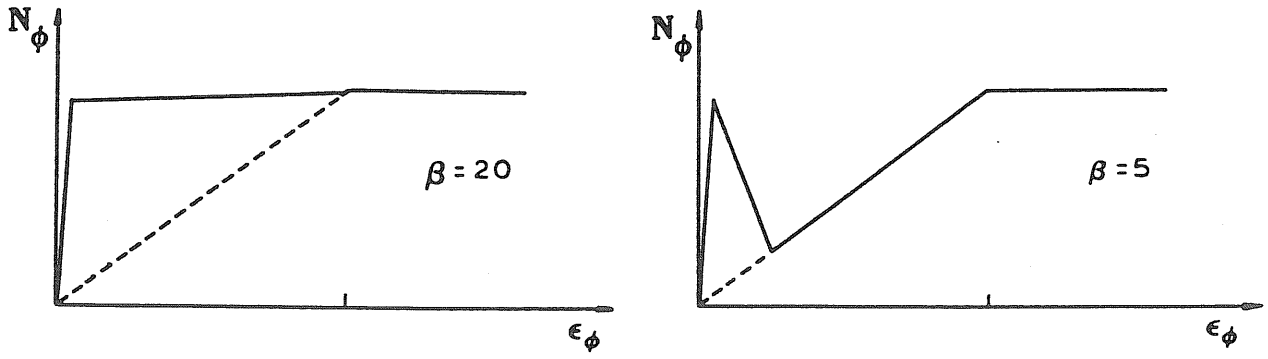

Figure 5.12 Uniaxial Force-Strain Curves for Towers I & III.

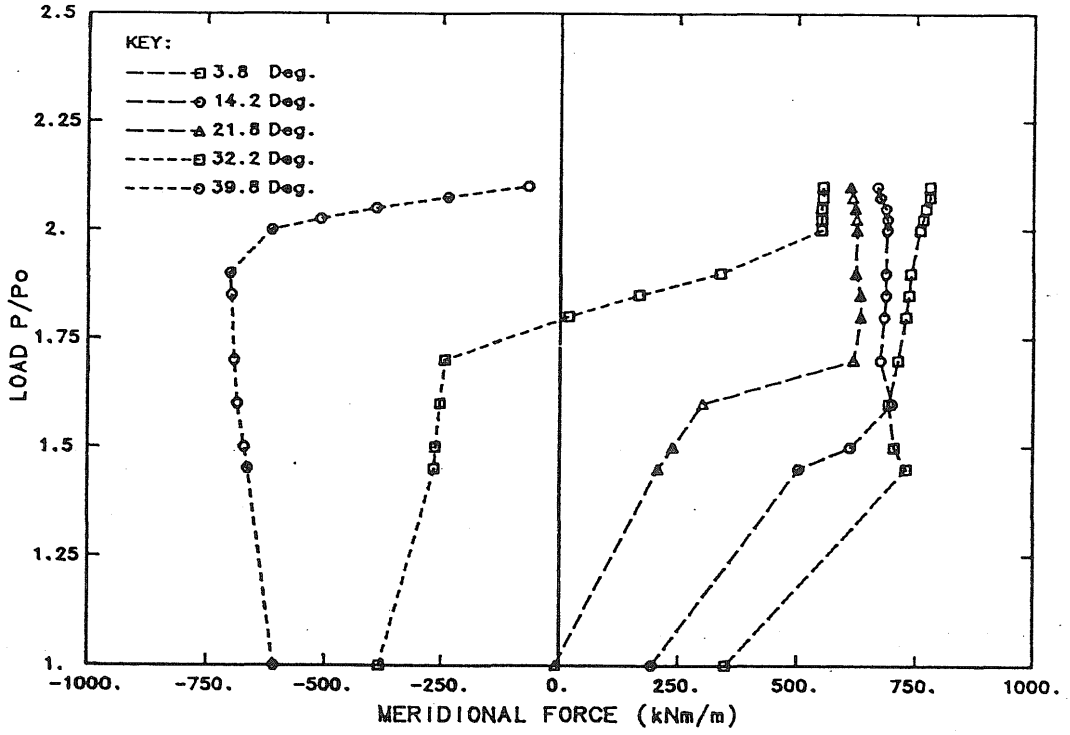

Figure 5.13 Meridional Force Distribution for Tower I.

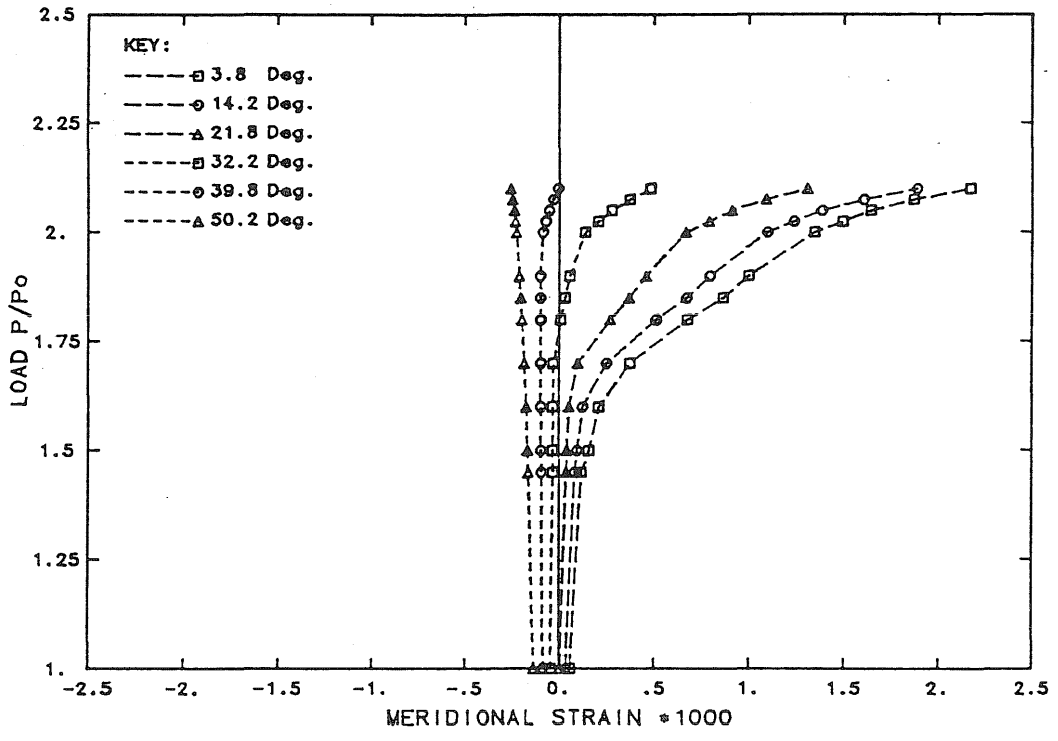

Figure 5.14 Meridional Strain Distribution for Tower I.

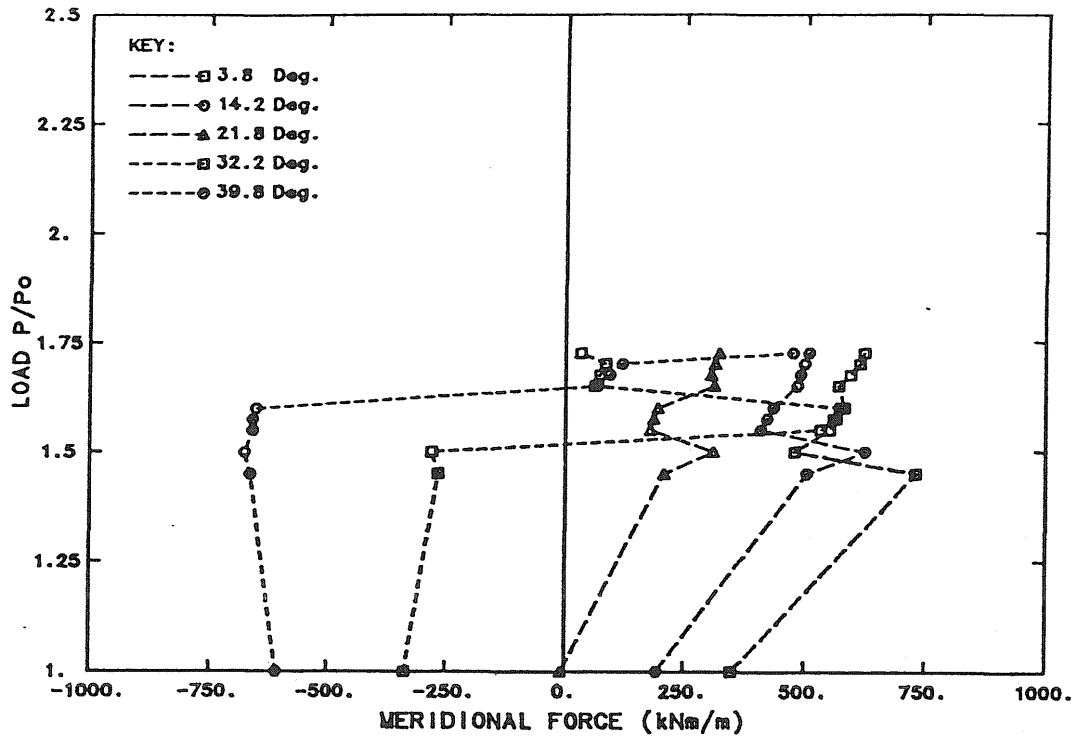

Figure 5.15 Meridional Force Distribution for Tower III.

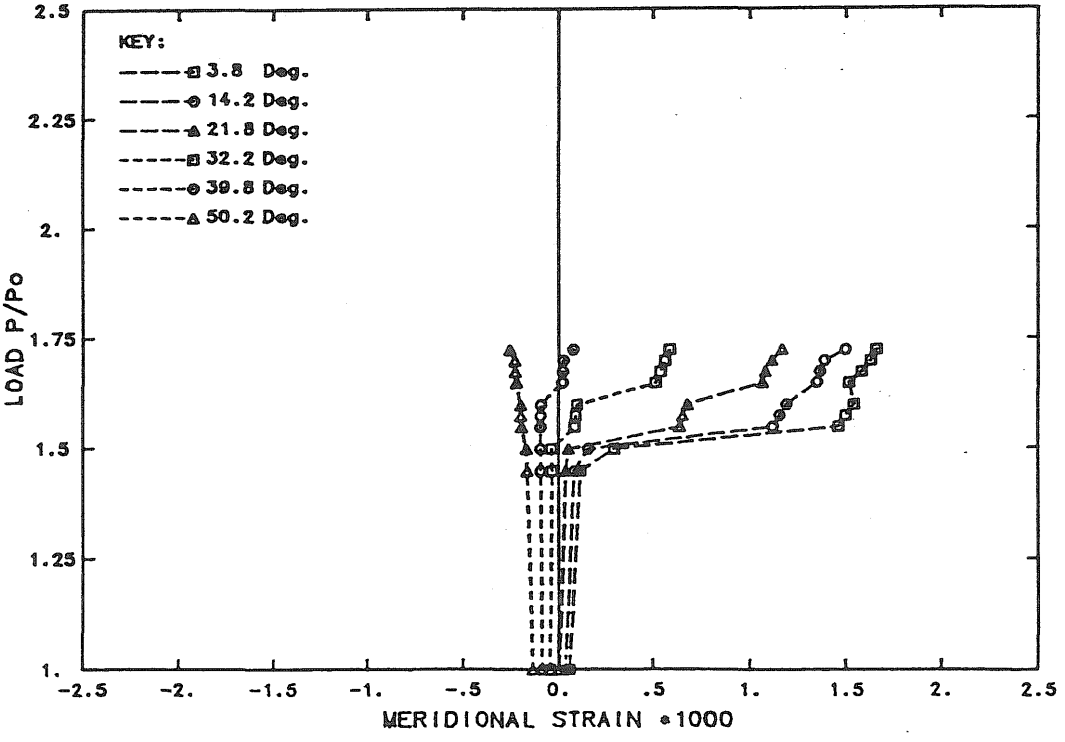

Figure 5.16 Meridional Strain Distribution for Tower III.

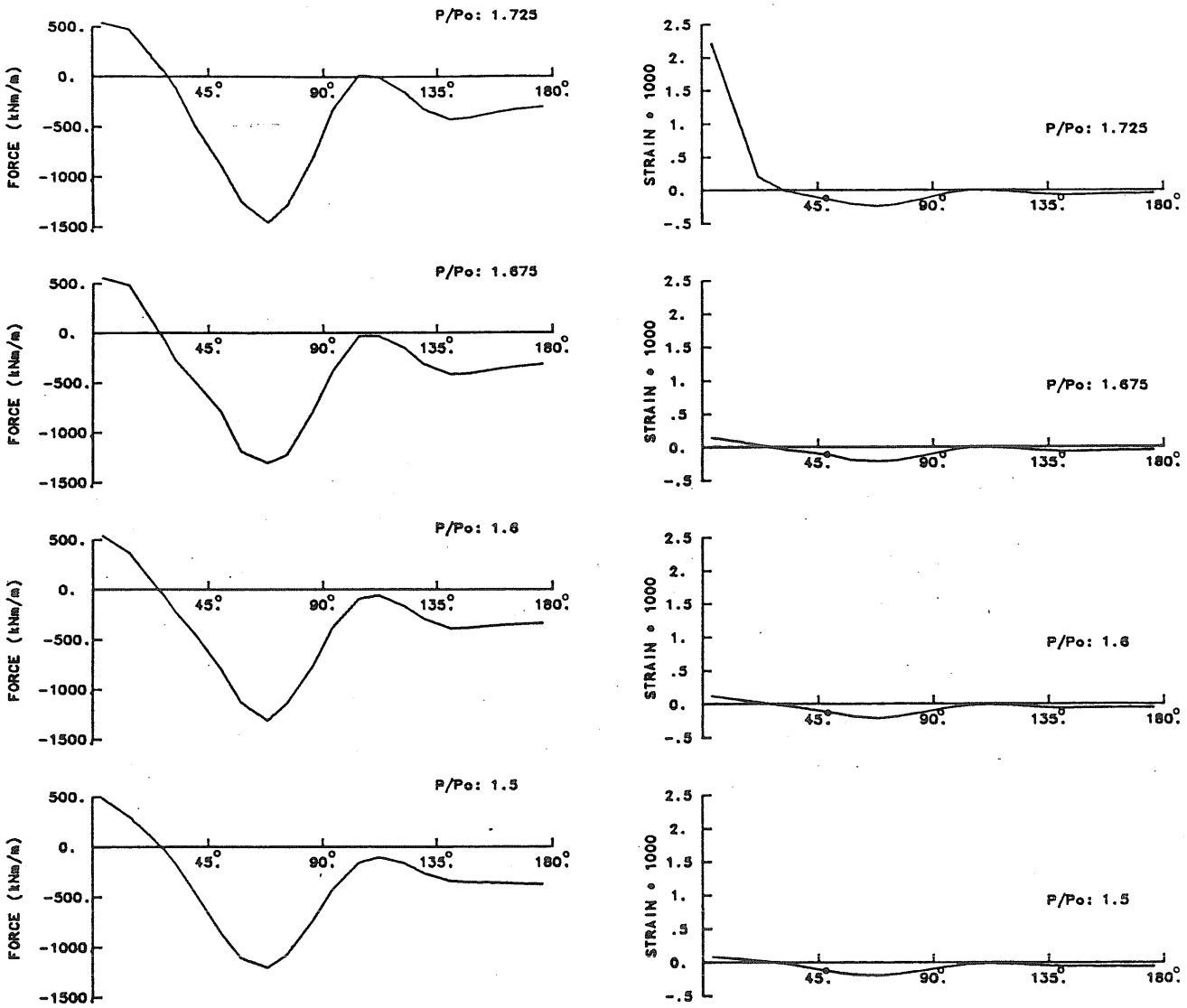

Figure 5.17 Circumferential Distribution of Meridional Force and Meridional Strain for Tower III.

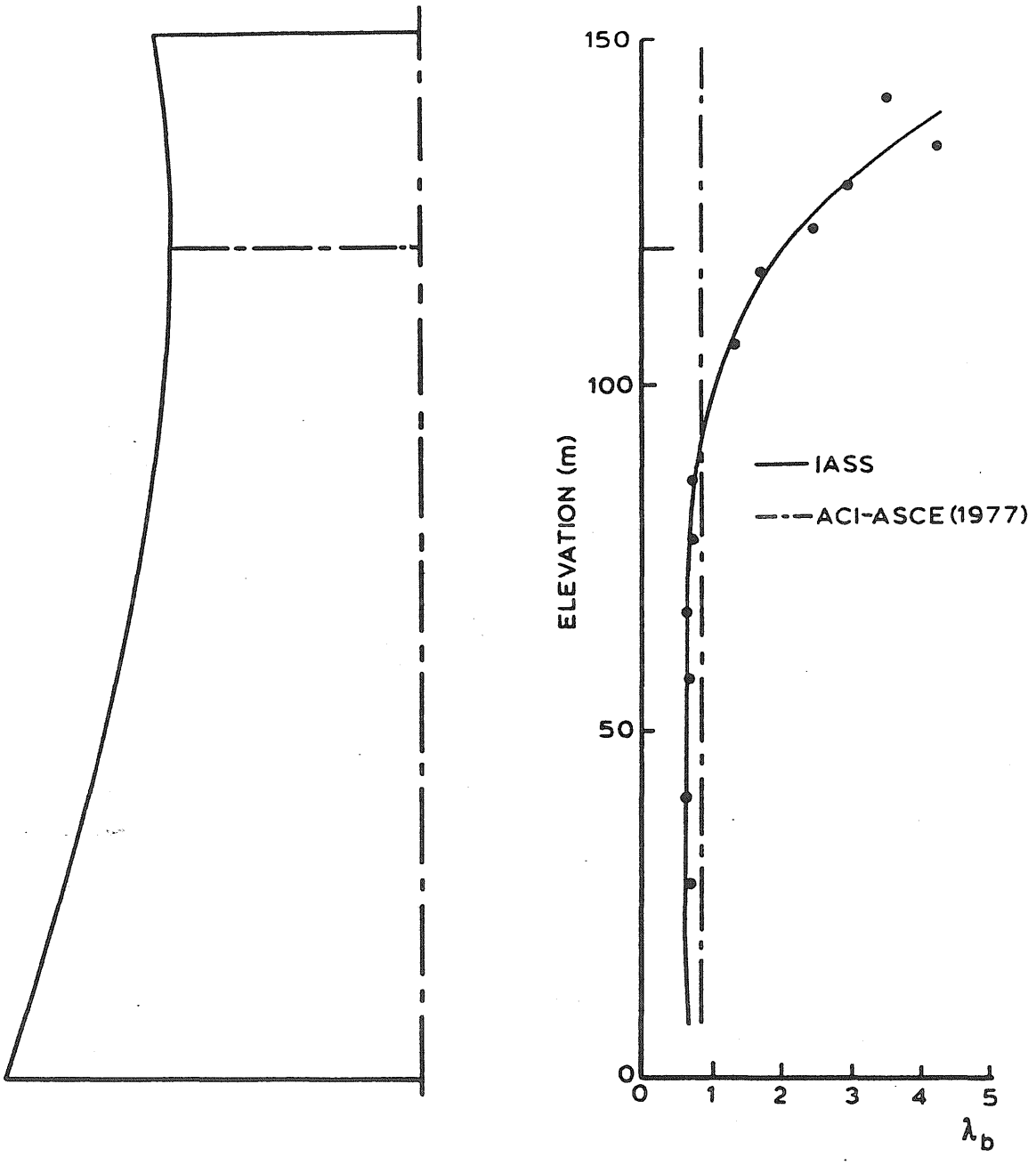

Figure 5.18 Factor of Safety Against Elastic Buckling.

APPENDIX A

DEGENERATED SHELL THEORY

A1 INTRODUCTION

The strain displacement expressions for the degenerated shell elements are written in terms of conventional shell theory notation. This is not done so as to arrive at an alternative formulation for degenerated elements, but rather to evaluate the underlying degenerated shell theory against existing classical shell theories. As a result the degenerated element can be judged against so called 'consistent' shell theories, such as the Koiter (1959) - Sanders (1963) theories, and the implications of the degenerated thin shell assumption can be investigated. In particular the question of rigid body rotations is addressed.

The term degenerated shell theory used above may in some cases be misleading, as all classical shell theories are in fact obtained by degenerating the equations of equilibrium to a two dimensional continuum. As will be shown below the 'degenerated thin shell' finite element proceedure results in equations very similar to those which can be obtained in classical thin shell theories, although a different (and computationally more convenient) starting proceedure is used. This is in fact to be expected, as many of the assumptions used in the degenerated proceedure are identical to those employed in Reissner's classical shell theory (Reissner, 1941). Reissner's theory, however, does not include shear deformations.

A2 PRELIMINARIES

The degenerated shell theory is examined by transforming the global cartesian quantities to an orthogonal curvilinear coordinate system which describes the midsurface of the shell. The equations are developed below for the particular case of an orthogonal curvilinear coordinate system $(\alpha_1,\alpha_2,\alpha_3)$, and assumes that the shell normal ($\underline{n}$) is strictly normal to the midsurface of the shell. These results can however be generalized to a non-orthogonal coordinate system, and to elements where the shell normal is not strictly normal to the midsurface.

The geometry of the shell, $\underline{x}$, is described in curvilinear coordinates as

$$x_i = x_i^o + \alpha_3 n_i \tag{A1}$$

The components of the displacement vector, $\underline{v}$, with respect to a corresponding local orthogonal coordinate system are denoted as

$$v_i = v_i^o + \alpha_3 \Delta v_i \tag{A2}$$

The following definitions will be required:

1) Base vectors

$$\begin{aligned} \underline{a}_i &= \frac{\partial \underline{x}}{\partial \alpha_i}\Big|_{\alpha_3=0} \\ &= \frac{\partial \underline{x}^o}{\partial \alpha_i} \quad i=1,2 \\ &= \underline{n} \quad i=3 \end{aligned} \tag{A3}$$

2) Unit direction vectors

$$\underline{e}_i = \underline{a}_i / A_i \tag{A4}$$

where A_i is the metric coefficient of the middle surface.

3) Jacobian

$$\underline{J} = [\frac{\partial x_j}{\partial \alpha_i}]$$

$$= \underline{J}^o + \alpha_3 \underline{R} \tag{A5}$$

where $\underline{J}^o$ is the Jacobian associated with the mid-surface of the shell and is obtained as

$$\underline{J}^o = \{ \underline{a}_1 \quad \underline{a}_2 \quad \underline{a}_3 \}^T \tag{A6}$$

and $\underline{R}$ is a matrix describing the curvature of the mid-surface

$$\underline{R} = [-\underline{a}_1/R_1 \quad -\underline{a}_2/R_2 \quad \underline{0}]^T \tag{A7}$$

In Eq. A7, R_i is the (principal) curvature of the shell in the i'th curvilinear coordinate direction.

4) Inverse of the Jacobian

A linear approximation to the inverse of the Jacobian is obtained as

$$\underline{J}^{-1} = \underline{J}^{o\,-1} + \alpha_3 \underline{B} \tag{A8}$$

For an orthogonal curvilinear system the following are obtained.

$$\underline{J}^{o\,-1} = \{ \underline{e}_1/A_1 \quad \underline{e}_2/A_2 \quad \underline{e}_3 \} \tag{A9}$$

$$\underline{B} = \{ \underline{e}_1/A_1R_1 \quad \underline{e}_2/A_2R_2 \quad \underline{0} \} \tag{A10}$$

A3 STRAIN DISPLACEMENT RELATIONS

The strain displacement relations investigated are derived specifically for thin shell applications by either neglecting the variation of the Jacobian through the shell thickness, or by retaining a first order expansion for the Jacobian. The former approach is identical to Love's first approximation (Reissner, 1941).

In the global cartesian coordinate system the Green's strain tensor is obtained in terms of the cartesian components of the displacement vector, $\underline{u}$, as

$$2\varepsilon_{ij} = u_{i,j} + u_{j,i} + u_{k,i}\, u_{k,j} \tag{A11}$$

Transforming from global cartesian to the curvilinear coordinate system using Eqs. A2, and A8 yields

$$2\varepsilon_{\alpha\beta} = e_{\alpha\beta} + \alpha_3 \kappa_{\alpha\beta} \tag{A12}$$

where,

$$2A_\alpha A_\beta e_{\alpha\beta} = \underline{a}_\alpha \cdot \underline{v}^o_{,\beta} + \underline{a}_\beta \cdot \underline{v}^o_{,\alpha} + \underline{v}^o_{,\alpha} \cdot \underline{v}^o_{,\beta} \tag{A13}$$

$$2A_\alpha A_\beta \kappa^{\ell}_{\alpha\beta} = \underline{a}_\alpha \cdot \Delta\underline{v}_{,\beta} + \underline{a}_\beta \cdot \Delta\underline{v}_{,\alpha} + (1/R_\alpha + 1/R_\beta)\, A_\alpha A_\beta e^{\ell}_{\alpha\beta} + (1/R_\alpha - 1/R_\beta)\, A_\alpha A_\beta \phi_{\alpha\beta} \tag{A14}$$

and $\phi_{\alpha\beta}$ is the inplane rotation of the normal

$$2A_\alpha A_\beta \phi_{\alpha\beta} = \underline{a}_\beta \cdot \underline{v}^o_{,\alpha} - \underline{a}_\alpha \cdot \underline{v}^o_{,\beta} \tag{A15}$$

In Eqs. A13 and A14, the superscript 'ℓ' denotes the linearized component, and '$,\alpha$' denotes the vector derivative in the curvilinear coordinate system.

These equations will now be discussed with reference to existing classical shell theories. Linearizing the inplane and curvature expressions

yields strains which are similar to the Koiter-Sanders consistent linear strain expressions, (or Reissner's expressions which are not based on Love's first approximation), with the exception of the terms in $e^{\ell}_{\alpha\beta}/R_{\alpha}$ which are discarded in the K-S theories. Neglecting the first order expansion in the derivation of the strain expressions results in the terms in $e^{\ell}_{\alpha\beta}/R_{\alpha}$ and $\phi_{\alpha\beta}$ being lost. This results in shell theories similar to those given by, for example, Reissner (1941), which are based on Love's first approximate. As noted by Koiter (1959), while the terms in $e^{\ell}_{\alpha\beta}/R_{\alpha}$ in the curvature expression are always small, the normal rotation contribution may in some instances not be small during inextensional deformation of the midsurface. Degenerated thin shell elements based on this formulation would therefore not be expected to perform satisfactory in certain applications (for example the right helicoidal shell (Reissner, 1941)), but in general this formulation gives results which are nearly as accurate as those obtained by including the expansion of the Jacobian, and hence $\phi_{\alpha\beta}$ (Sanders, 1963).

The linearized extensional strain resultant discussed above satisfies small (infinitesimal) rigid body rotation requirements. However, only the linearized curvature expression which includes the expansion of the Jacobian satisfies small rigid body rotation requirements.

The nonlinear strain relations can also be compared with the K-S and additional theories. The K-S theories for moderate rotations use a linear curvature tensor, which has been discussed above. The nonlinear contribution to the extensional strains used in the K-S expressions can be written as

$$2e^{n\ell}_{\alpha\beta} = \phi_{\alpha}\phi_{\beta} + \phi^{2}_{\alpha\beta} \tag{A16}$$

where

$$A_\alpha \phi_\alpha = \underline{e}_3 \cdot \underline{v}^o_{,\alpha} \tag{A17}$$

It is seen that that the degenerated element formulation does not contain the normal rotation contribution $\phi_{\alpha\beta}$. The derivatives of the inplane displacements are discarded in the K-S theory as they are small. It is difficult to asses the importance of the contribution of $\phi_{\alpha\beta}$ to the extensional strain as there is no information available in the literature. However as satisfactory results are obtained with classical shell theories, such as Donnell-Mushtari-Vlassov (Sanders, 1963), which do not contain this term, it appears that in most instances this contribution is not significant.

The nonlinear extensional strain expression (Eq. A13) satisfies rigid body rotations for arbitrary large rotations. Retaining the first order expansion of the Jacobian, both the linearized and the nonlinear curvature expression satisfy arbitrary large rigid body rotations.

A nonlinear curvature expression for the case in which the first order expansion is neglected can be obtained from Eq. A14 by deleting all terms in $1/R_\alpha$. However it is contended that this is not a consistent definition of curvature. A consistent definition can be obtained by rewriting Green's strain tensor in terms of the displacement gradients $u_{i,j}$ and the deformation Jacobian $g_{ij} = u_{j,i} + \delta_{ij}$, as follows

$$2\varepsilon_{ij} = \frac{1}{2}(u_{i,j} + u_{j,i}) + \frac{1}{2}(u_{k,i}g_{jk} + u_{k,j}g_{ik}) \tag{A18}$$

As the variation of the Jacobian through the thickness has been neglected, it follows that the variation in the deformation Jacobian should also be neglected. This results in

$$2\varepsilon_{ij} = \frac{1}{2}(u_{i,j} + u_{j,i}) + \frac{1}{2}(u_{k,i}g^{o}_{jk} + u_{k,j}g^{o}_{ik}) \qquad \text{(A19)}$$

It can be seen that the nonlinear contribution to the curvature tensor differs from that which can be obtained directly from Eq. A11 by a factor of $\frac{1}{2}$.

The curvature expression defined by Eq. A19 has the additional advantage that it yields no strain under arbitrary large rotations in curved beam and arch type problems. However in general shell applications, rigid body rotation requirements are not satisfied.

APPENDIX B

CONSTITUTIVE RELATIONS FOR CONCRETE

The biaxial stress-strain relation for concrete used in this investigation is based on an extension to Liu's biaxial orthotropic material model (Liu, et al., 1972). The material properties are described in terms of total strains, in the principal stress directions. It should be noted that this model predicts that the principal stress and principal strain directions coincide, which is not true for concrete in general. However this does not appear to limit the usefulness of this model (ASCE, 1981). This model is limited to structural applications such as beams, panels and thin shells where the stress is predominantly biaxial. Limited unloading capabilities have been included.

B1 BIAXIAL STRESS-STRAIN CURVES

Liu, et al. (1972), modeled concrete as an orthotropic material under biaxial loading. For biaxial compression they proposed a constitutive relationship of the form

$$\sigma_i = \frac{E_o \varepsilon_i}{(1-\nu\alpha_i)} \cdot [1 + (\frac{1}{1-\nu\alpha_i}\frac{E_o}{E_{s_i}} - 2)q_i + q_i^2]^{-1} \qquad \text{(B1)}$$

where σ_i and ε_i are the stress and strain in the i'th principal stress direction; E_o and E_{s_i} are the initial tangent modulus under uniaxial stress and the second modulus at maximum stress (= $\sigma_{ic} / \sigma_{ic}$); σ_{ic} and ε_{ic} are the maximum biaxial compressive stress and corresponding strain; α_i is the stress ratio σ_j/σ_i; q_i is the strain ratio $\varepsilon_i/\varepsilon_{ic}$ and ν is Poissons ratio.

For uniaxial stress (α_2=0) Eq. B1 reduces to the stress-strain relationship proposed by Saenz (1964). Equation B1 has also been used by Darwin and Pecknold (1974), by introducing the concept of equivalent uniaxial strain and removing the Poisson effect from the biaxial strain but retaining the effects of microcrack confinement.

Equation B1 has been used in the present investigation, together with a constant Poissons ratio of 0.2.

The tension region of the stress-strain curve is given by

$$\sigma_i = \frac{E_o \, \varepsilon_i}{1-\nu\alpha_i} \tag{B2}$$

Expressions for the maximum principal stress and corresponding strain are given in Section B2 below.

In Figs. B1 to B4 a comparison is made using Eqs. B1 and B2 and the experimental results of Nelissen (1972) and Kupfer and Gerstle (1973). In general good agreement is obtained with the experimental results.

B2 FAILURE ENVELOPE

The failure envelope for concrete under biaxial stresses is based on the biaxial strength envelope of Kupfer and Gerstle, as shown in Fig. B5. This envelope is divided into several regions depending on the ratio of maximum to minimum principal stress α_2, and the stress state. The values of maximum principal stress the corresponding principal strain are obtained as (Darwin and Pecknold, 1974; Rajagopal, 1976):

1. $1 > \alpha_2 > 0$ Biaxial Compression

$$\sigma_{2c} = \frac{1 + 3.65\alpha_2}{(1+\alpha_2)^2} f'_c \tag{B3a}$$

$$\sigma_{1c} = \alpha_2 \sigma_{2c} \tag{B3b}$$

$$\varepsilon_{2c} = \varepsilon_{cu}(1-\nu\alpha_2)(3p_2-2) \tag{B3c}$$

$$\varepsilon_{1c} = \varepsilon_{cu}(1-\nu\alpha_1)(-1.6p_1^3+2.25p_1^2+0.35p_1) \tag{B3d}$$

where $p_i = \sigma_{ic}/f'_c$

Failure is assumed to occur due to yielding and crushing of the concrete.

2. $0 > \alpha_2 > -0.17$ Biaxial Tension Compression

$$\sigma_{2c} = \frac{1 + 3.28\alpha_2}{(1+\alpha_2)^2} f'_c \tag{B4a}$$

$$\sigma_{1t} = \alpha_2 \sigma_{2c} \tag{B4b}$$

$$\varepsilon_{2c} = \varepsilon_{cu}(1-\nu\alpha_2)(4.42-8.38p_2+7.54p_2^2-2.58p_2^3) \tag{B4c}$$

$$\varepsilon_{1t} = \frac{\sigma_{1t}(1-\nu\alpha_1)}{E_o} \tag{B4d}$$

Failure is assumed to occur by yielding and crushing of the concrete in the compression direction.

3. $-0.17 > \alpha_2 > -\infty$ Biaxial Tension Compression

$$\sigma_{2c} = 0.65 f'_c \tag{B5a}$$

$$\sigma_{1t} = f_t \tag{B5b}$$

$$\varepsilon_{2c} = \varepsilon_{cu}(1-\nu\alpha_2)(4.42-8.38p_2+7.54p_2^2-2.58p_2^3) \tag{B5c}$$

$$\varepsilon_{1t} = \frac{\sigma_{1t}(1-\nu\alpha_1)}{E_o} \tag{B5d}$$

Failure in this zone is assumed to be due to cracking in the tension direction.

4. $\infty > \alpha_2 > 1$ Biaxial Tension

$$\sigma_{it} = f_t \tag{B6a}$$

$$\varepsilon_{it} = \frac{\sigma_{it}(1-\nu\alpha_i)}{E_o} \tag{B6b}$$

Failure is by cracking in the principal stress direction.

B3 CONSTITUTIVE MODEL

Under a biaxial state of stress, the concrete is assumed to behave as an orthotropic material in the two principal stress directions. Differentiating Eq. B1 with respect to the principal strain ε_i, and rearranging yields

$$\frac{d\sigma_i}{d\varepsilon_i} = \frac{E_o}{1-\nu\alpha_i} \cdot \frac{1 - q_i^2}{(1 + (\frac{1}{1-\nu\alpha_i}\frac{E_o}{E_{s_i}} - 2)q_i + q_i^2)}$$

$$= \frac{E_i}{1-\nu\alpha_i} \tag{B7}$$

where E_i is the slope of the 'uniaxial stress-strain curve' in the i'th

principal stress direction. This modulus can be considered as the tangent modulus of the material in the direction of the current principal stresses. Considering these as the directions of orthotropy for the concrete the incremental tangent stiffness matrix in the existing material axes is given by (Darwin and Pecknold, 1974)

$$\Delta\underline{\sigma} = \frac{1}{1-\nu^2}\begin{bmatrix} E_1 & \nu\sqrt{E_1E_2} & 0 \\ \nu\sqrt{E_1E_2} & E_2 & 0 \\ 0 & 0 & \frac{1}{4}(E_1+E_2-2\nu\sqrt{E_1E_2}) \end{bmatrix} \Delta\underline{\epsilon} \qquad \text{(B8)}$$

The use of E_1 and E_2 defined by Eq. B7 in Eq. B8 is not strictly correct, but this lack of consistancy is not serious since small errors introduced in the stresses will be corrected at each load step based on the total strains.

The value of Poissons ratio used in this study is assumed to be independent of the stress level used, although at a stress level higher than $0.8f'_c$ significant increase in Poissons value is known to occur. Poissons ratio for concrete has been taken to be 0.20 in this study.

B4 CRACKING AND TENSION STIFFENING

A maximum principal stress criteria is used to determine concrete failure in tension. When one of the principal stresses exceeds the uniaxial tensile strength of the concrete, a crack is assumed to form perpendicular to the direction of that stress.

The constitutive relation for the cracked concrete is then obtained by setting the tangent modulus in the direction of the offending principal stress, say E_1, to zero in Eq. B8.

$$\Delta\underline{\sigma} = \begin{bmatrix} 0 & 0 & 0 \\ 0 & E_2 & 0 \\ 0 & 0 & \beta_s E_2 \end{bmatrix} \Delta\underline{\varepsilon} \qquad \text{(B9)}$$

where β_s is a shear retention factor, which accounts for the effective shear modulus along the crack due to dowel action, friction and aggregate interlock. Studies have shown that the solution is insensitive to the value of β_s used (Hand, et al., 1972; Gerstle, 1981), and a constant value of 0.25 has been adopted in this investigation.

The formation of a second tension crack is restricted to form orthogonal to the first crack. The constitutive relation for doubly cracked concrete is then given by the null matrix

$$\Delta\underline{\sigma} = [\ 0\ ]\,\Delta\underline{\varepsilon} \qquad \text{(B10)}$$

Two forms of tension stiffening have been incorporated into the present study, namely a gradual unloading of the concrete stress-strain curve in tension (Lin, 1973) as shown in Fig. B6, and tension stiffening applied to the reinforcement (Gilbert and Warner, 1978) shown in Fig. B7. To prevent possible numerical instabilities when using the first form, the tangent modulus of the concrete is set to zero once a crack has formed, and the stresses are released in a stepwise fashion.

B5 STRAIN SOFTENING BEYOND THE MAXIMUM COMPRESSIVE STRENGTH

Concrete is a strain softening material and deteriorates with increasing strain beyond the maximum compressive level. Experiments indicate that the ultimate strain is generally 1.2 to 1.3 times the strain corresponding to the peak compressive strength in the major compressive

direction. The stress corresponding to the ultimate strain varies between 0.8 and 0.9 times the peak compressive stress. Both these paramaters are variables in the present study, but typically values of 1.25 and 0.8 respectively have been used. The strain softening curve is assumed to be linear between the peak compressive stress and the stress at the ultimate strain. See Fig. B8.

To prevent numerical instabilities, once yielding has occurred the tangent moduli are set to zero, and the unbalanced stresses are released in a stepwise fashion.

This formulation adopted here implies an 'unconstrained' flow-rule for the unloading part once yielding has begun, and subsequent unloading takes place along a path determined by the current unloaded stress corresponding to the current total strain. Lin (1973) has shown that in reinforced concrete applications there is little difference between an unconstrained flow rule and a normality flow rule.

B6 UNLOADING AND RELOADING

Limited unloading and reloading copabilities have been incorporated in the present model, as shown in Figs. B6 and B8. Unloading and reloading in compression is assumed to occur parallel to the initial tangent modulus, taking into account the Poisson effect.

This model is not suitable for modeling hysteretic behavior as observed in dynamic applications, but is satisfactory to model unloading of the concrete as would occur during an instability of the structure.

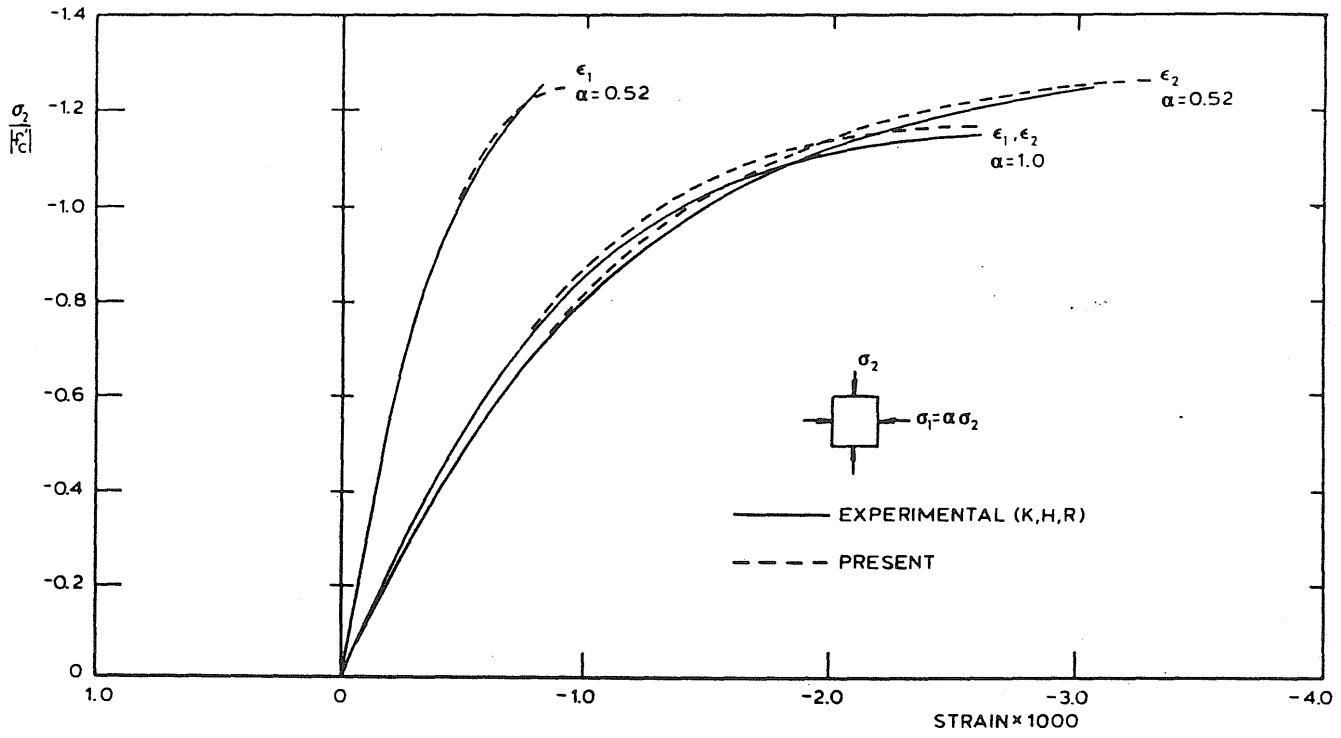

Figure B1 Comparison of Present Model with Biaxial Compression Tests, $\alpha = 1.0$ & 0.52

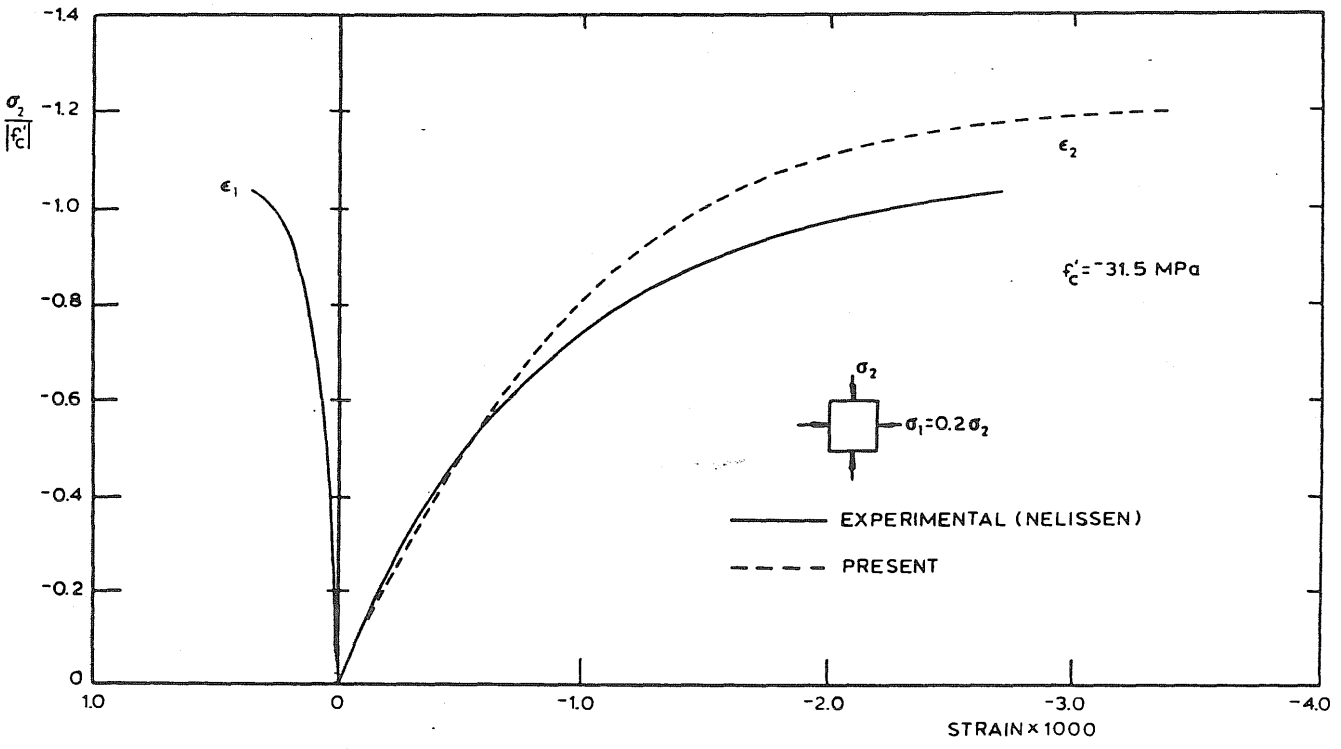

Figure B2 Comparison of Present Model with Biaxial Compression Test, $\alpha = 0.2$.

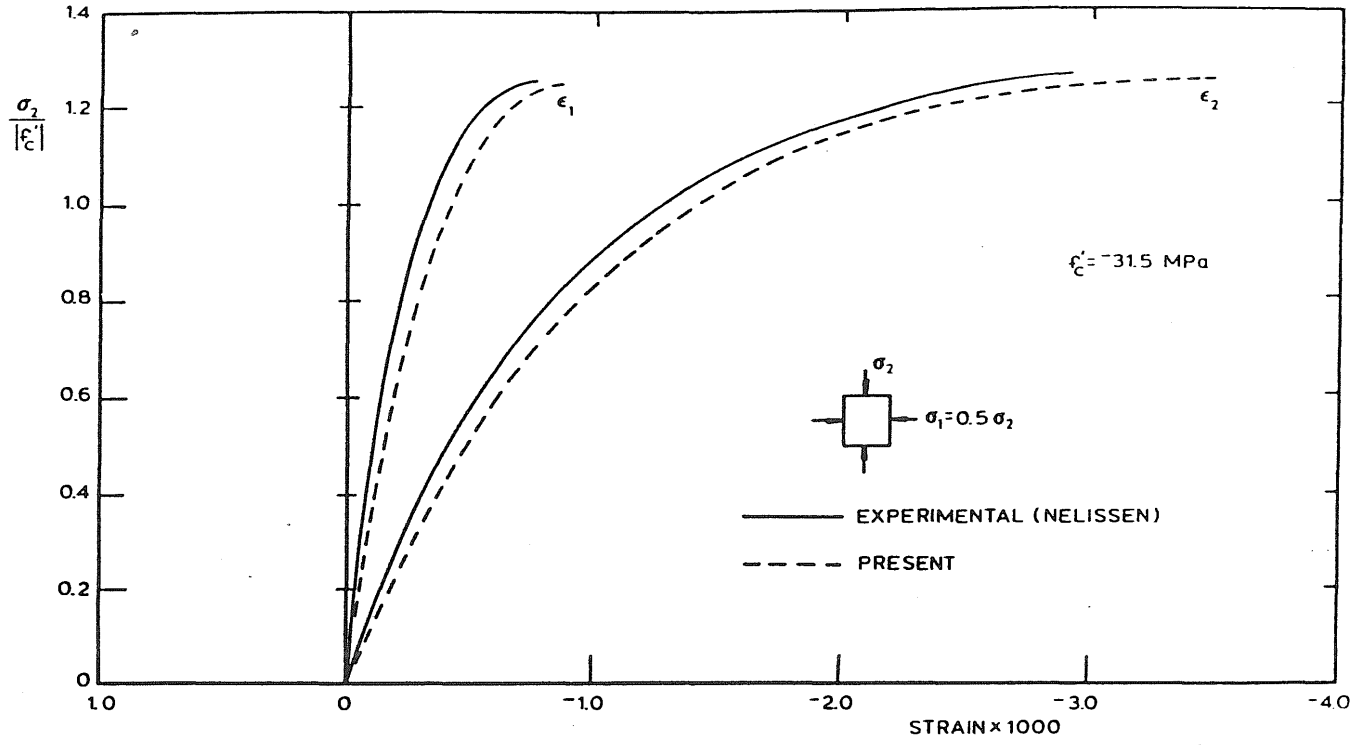

Figure B3 Comparison of Present Model with Biaxial Compression Test, $\alpha = 0.5$.

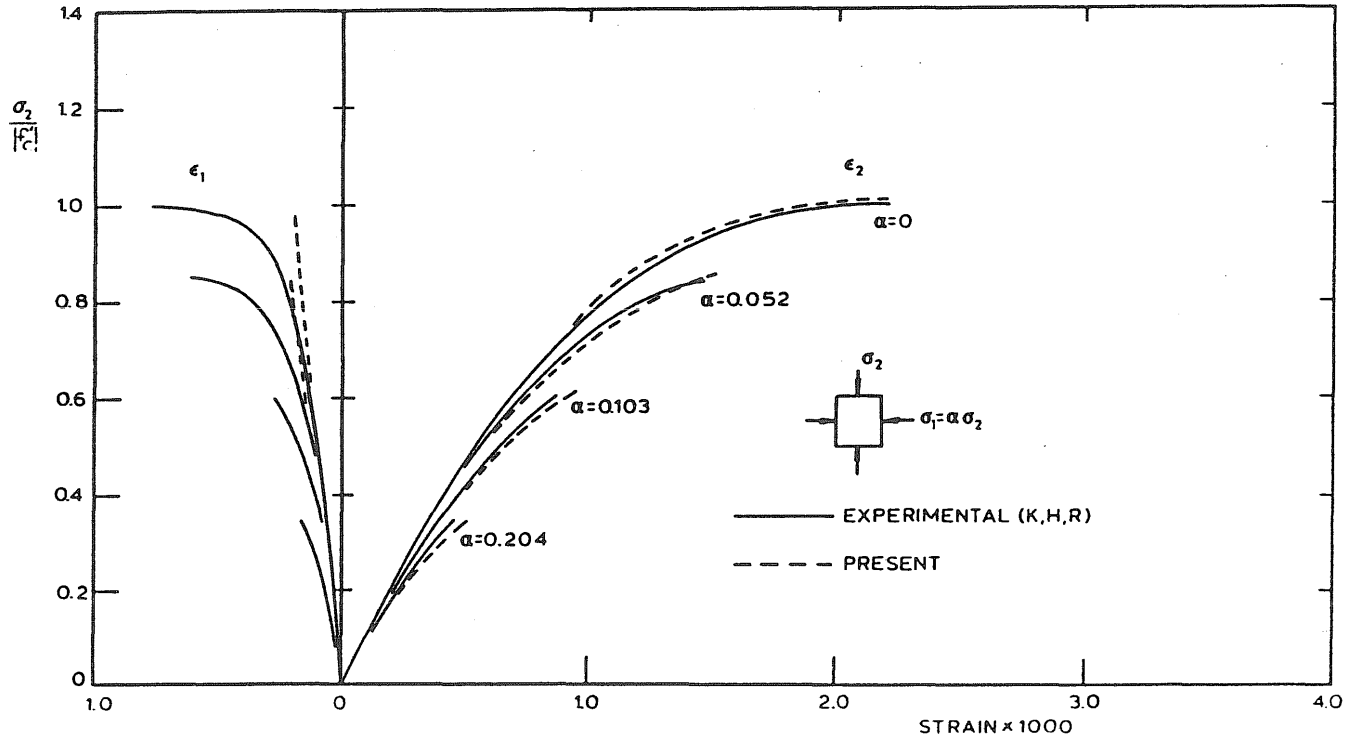

Figure B4 Comparison of Present Model with Tension-Compression and Uniaxial Compression Tests.

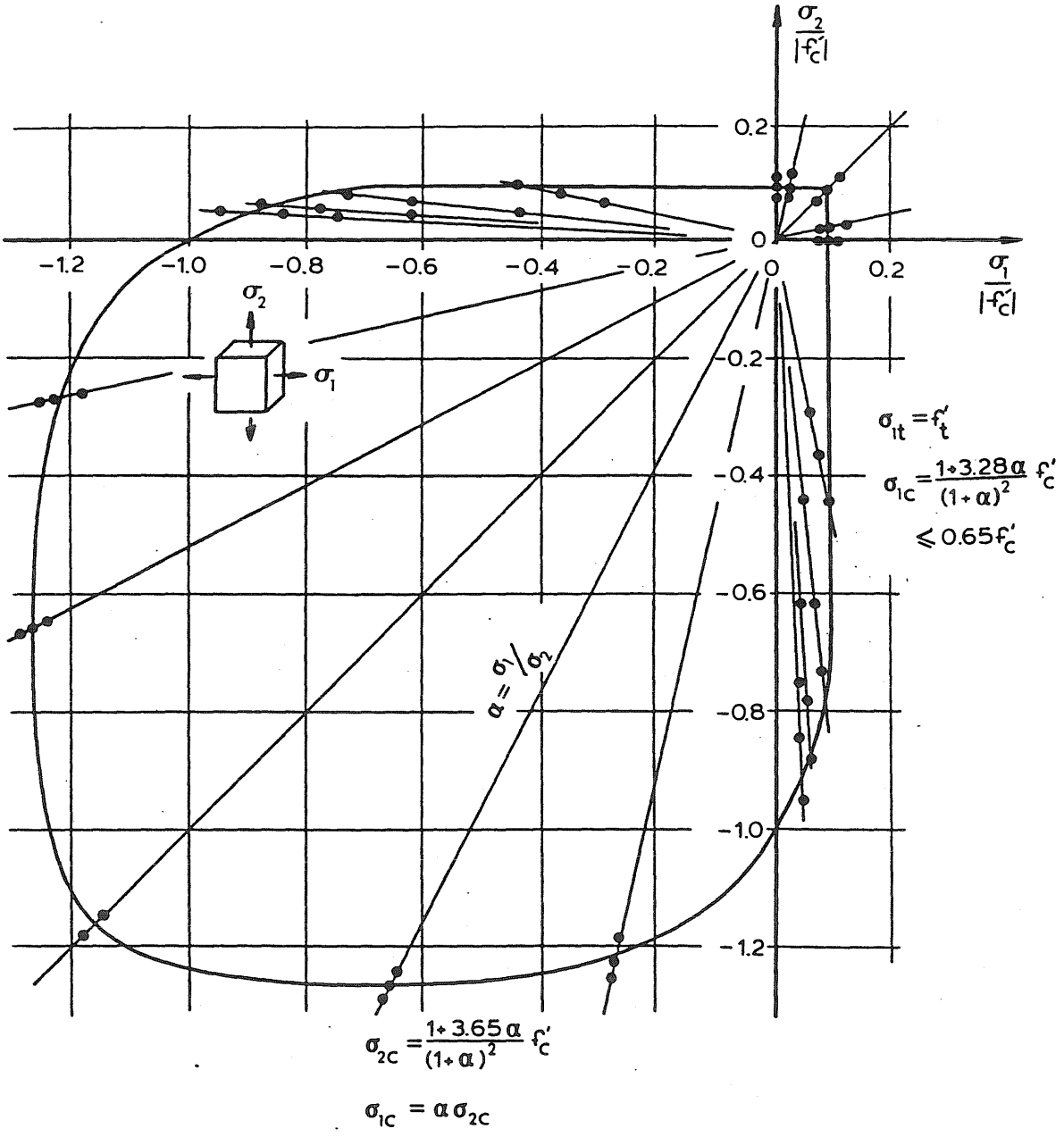

Figure B5 Biaxial Failure Envelope.

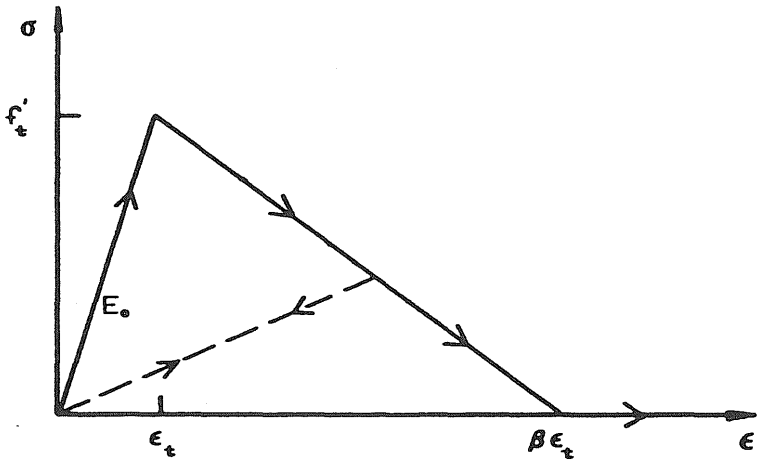

Figure B6 Concrete Tension Stiffening Model.

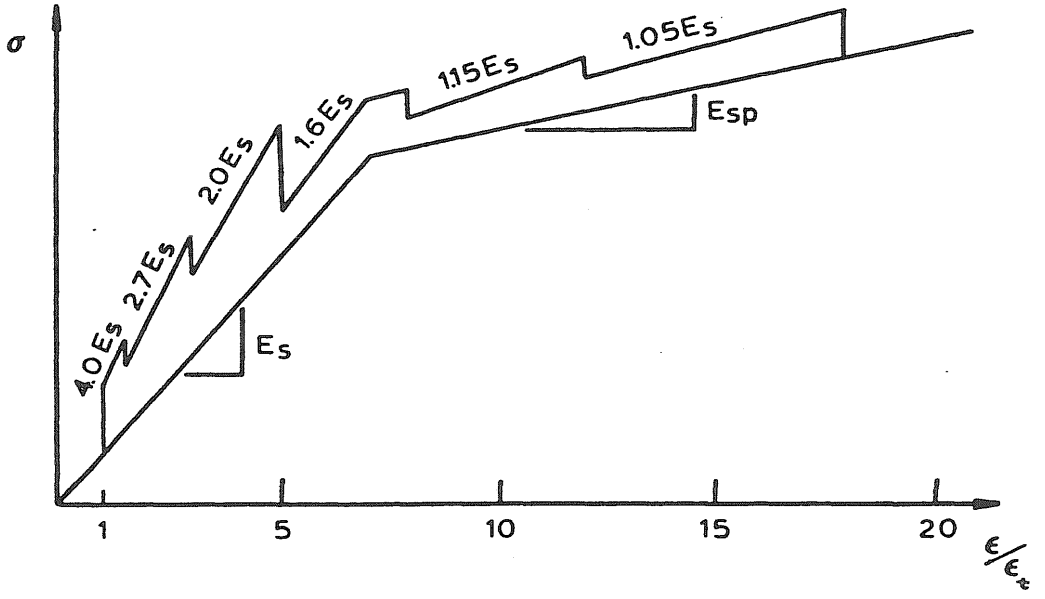

Figure B7 Reinforcement Tension Stiffening Model.

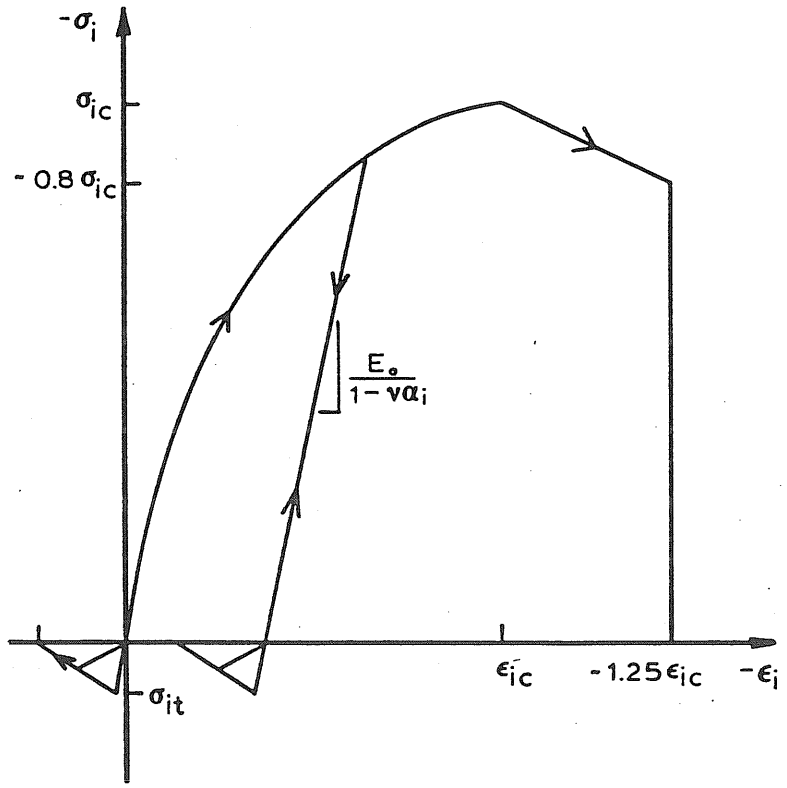

Figure B8 Uniaxial Stress-Strain Curve for Concrete.

APPENDIX C

USER INSTRUCTIONS FOR DEGENERATED SHELL AND BEAM ELEMENTS, AND REINFORCED CONCRETE MATERIAL MODELS

C1 ISOPARAMETRIC SHELL ELEMENTS

C1.1 General

The development of degenerated shell elements and their use in geometric and material nonlinear analysis can be found in Ramm, et al. (1977, 1981), Hughes and Liu (1981), Parisch (1981) and Surana (1981). The degenerated shell elements described here are restricted to thin to moderately thick shell applications, as they are formulated using explicit integration through the thickness of the shell. Both geometric nonlinearities and material nonlinearities (currently the material model RCSHELL) are supported by these elements. Three versions are available namely the 9-node quadratic Lagrangian element (QLSHELL), the 8-node quadratic Serindipity element (QSSHELL) and the bilinear 4-node element (BLSHELL).

C1.2 Element geometry

The geometry of the element is defined by specifying the coordinates of the midsurface nodes and additional geometric points on the shell normal, as shown in Fig. C1. This normal does not have to be strictly normal to the midsurface of the shell. The additional geometry points may be either on the top surface of the shell (=+1, the default option) or can be specified as being on the lower surface by including BOTTOM as an element property. The geometry of the element is interpolated from the midsurface nodes and

geometry points.

The node numbering system used for the 4-, 8- and 9-node elements are included in Fig. C1.

C1.3 Geometric nonlinear options

Two geometric nonlinear formulations are available, namely a small rotation and a moderate rotation formulation. The small rotation formulation utilizes a linear curvature tensor and a vectorial definition of rotations (ie. infinitesimal rotations or engineering definition). This formulation is similar to that used in most geometrically nonlinear finite elements. The moderate rotation formulation employs a nonlinear curvature tensor and a strict non-vectorial definition of rotations. For most practical applications the small rotation formulation is satisfactory.

The small rotation formulation is the default option, while the moderate rotation option can be specified (for a geometric nonlinear element) by including LARGE ROTATION as a element property.

C1.4 Nodal degrees of freedom

For geometric linear or geometric nonlinear analysis using the small rotation option, the nodal degrees of freedom apparant to the user are the three cartesian displacements of the midsurface of the shell, and the three 'rotations' of the normal at each node. For the moderate rotation option the nodal degrees of freedom are the cartesian midsurface displacements and the normalized relative displacement of the top of the shell. These nodal degrees of freedom are shown in Fig. C2, with reference to a local cartesian coordinate system.

The nodal degrees of freedom adopted for the moderate rotation formulation are identified in FINITE as UZZ, VZZ and WZZ (or THETAX, THETAY and THETAZ), but DO NOT correspond to the usual definition of rotations. This formulation must be used with caution, and in particular this option should not be used when this element is combined with any other element in the FINITE element library.

C1.5 Stress and strain resultants

Stress and strain resultants are calculated at each integration point. At present these values are not interpolated to the node points. Eight stress-strain pairs are given, namely the inplane membrane resultants

Nxx , Exx Nyy , Eyy Nxy , Eyy

the transverse shear resultants

Qx , GAMx Qy , GAMy

and the flexural resultants

Mxx , Kxx Myy , Kyy Mxy , Kxy

These stress-strain resultants are referred to a local cartesian coordinate system at each integration point, as shown in Fig. C3. The strain point numbering is shown in Fig. C4.

For geometric nonlinear analysis the stress resultants correspond to the 2´nd Piola Kirchoff definition, and the strain resultants to the Green´s strain definition.

C1.6 Element loads

The degenerate shell elements described here support two types of loads, namely

C1.6.1 Type BODY: A constant body force/unit volume. The loading is described by specifying the load direction (X, Y or Z) and the intensity value (W), for example

```
1 FORCE X BODY W 22.4
```

C1.6.2 Type DISTRIBUTED: A distributed force/unit area applied to one of the six faces of the element ,FACE1, FACE2, , , FACE6, shown in Fig. C5. The load may be either nonuniform by specifying the intensity values at each node (W1, W2, W3, , ,) or as a uniform load by specifying a single intensity value (W), for example

```
5 FORCE X DISTRIBUTED W1 1.0 W2 1.0 W3 2.0 W4 2.0,
W5 1.5 W6 1.5 W7 1.0 W8 2.0 W9 1.5 FACE6
```

or

```
5 FORCE X DISTRIBUTED W 1.5 FACE 6
```

A normal (pressure type) force can be specified by using the NORMAL option. The direction of the load is then strictly normal to the face to which it is applied.

```
7 DISTRIBUTED W 1.0 NORMAL FACE2
```

If a distributed load is applied to either face 5 or face 6, the element treats the load as being applied to the midsurface of the shell.

At present moments and temperature loads cannot be applied.

C1.7 Element properties

The available element properties for the degenerate thin shell elements are given in Table C1

C2 ISOPARAMETRIC ECCENTRIC SHELL STIFFENING ELEMENTS

C2.1 General

The eccentric shell stiffening elements are compatible with the degenerate shell elements QLSHELL, QSSHELL and BLSHELL. These elements can also be used as stand-alone elements. Two elements are available, namely a 3-node quadratic element QLBEAM and a 2-node linear element BLBEAM.

These elements support geometric nonlinearities and material nonlinearities (currently RCBEAM) In linear material applications the beam is essentially a Timoshenko beam (Bouberg and Jirousek, 1980; Jirousek, 1981) and includes biaxial bending and torsion. In nonlinear material applications, out of plane bending and torsion is lost.

C2.2 Element geometry

The geometry of the beam is defined by specifying the nodal coordinates of the reference axis of the beam (usually the mid-surface of the shell) together with the coordinates of an additional four axes. The node numbering and coordinate points required are shown in Fig. C6, where 'o' refers to the reference axis of the beam, 'e' is the joint axis along which displacement continuity is enforced, when using the beam as a shell stiffener in the default position, 'g' is the centroidal axis of the beam,

´g-i´ defines a principal axis of the beam, and ´s´ is the shear center. In material nonlinear applications the shear center is omited. The displacement of the beam is refered to the reference axis ´o´.

When the element is used as an eccentric shell stiffener, the default position of the beam with respect to the shell is on the same side as the geometry points defining the surface of the shell- as shown in Fig. C7. The beam can be placed on the opposite side, as in Fig. C7, by the OPPOSITE command. The coordinates of the axis ´e´ required are then the coordinates of the corresponding nodes defining the surface of the shell. The true joint axis of the beam is then interpolated by the beam element, using the shell normal.

A suitable configuration for the beam in a stand-alone application is illustrated in Fig. C8.

The geometric properties required for the elastic option are specified with reference to the local coordinate system shown in Fig. C9. These properties are assumed to be constant along the axis of the beam. The geometric properties required are the area´s of the beam, AREAX, AREAY and AREAZ, and the second moment of area´s with respect to the centroidal axis of the beam INERTX, INERTY and INERTZ.

In nonlinear material applications, the cross section of the beam is restricted to being rectangular in shape, but can vary along the axis of the beam. In this case the principal axis of the beam is defined by the vector ´g-i´, which must not coincide with the vector ´g-e´. The width of the beam at each node is given by B1, B2, B3, or simply B if the width of the beam is constant.

C2.3 Geometric and material nonlinearities

The geometric nonlinear formulation for the beam elements is based on a small rotation, linear curvature formulation. This is compatible with the small rotation option of the shell elements QLSHELL, QSSHELL and BLSHELL. This element should NOT be used when the LARGE ROTATION option has being included for the shell element.

Material nonlinearities are included by using a layered material model. The direction of the layers is parallel to the axis 'g-i' as shown in Fig. C9. When the element is defined as material nonlinear, the element property LAYER must be included.

C2.4 Stress and strain resultants

Stress and strain resultants are calculated at the integration points. Six stress-strain resultant pairs are given for the linear material option, and three for nonlinear material applications. These stress-strain resultants are shown in Fig. C10. The strain point numbering is sequential in the positive axis direction.

C2.5 Element loads

At present this element does not support any loads.

C2.6 Element properties

The available element properties are given in Table C2.

C3 BIAXIAL REINFORCED CONCRETE MATERIAL MODEL

C3.1 General

The reinforced concrete material model RCSHELL is a biaxial orthotropic model suitable for use with the shell elements QLSHELL, QSSHELL and BLSHELL. This model is limited to structural applications where the stress is predominately biaxial, such as beam, pannel and shell type problems. This model considers compression softening and cracking of the concrete, and includes tension stiffening. Reinforcement is modeled as being elastoplastic with optional strain hardening. Full bond is assumed between the steel and concrete. Limited unloading capabilities are included in the model.

C3.2 Constitutive model for concrete

The constitutive model used for plain concrete is a modified version of Liu's biaxial orthotropic model (Liu, et al., 1972). The failure criteria used is based on that proposed by Darwin and Pecknold (1974) and modified modified by Rajagopal (1976). Typical stress strain curves for plain concrete in biaxial compression obtained using this model are shown in Fig. C11. The failure envelope used is shown in Fig. C12.

The material properties required to specify this model are given in Table C3, and in Fig. C13 by considering the uniaxial behavior of concrete. A linear elastic-cracking model can be invoked by specifying LINEAR as an element property. All nonlinearities, except cracking, are then excluded.

The number of integration points used through the thickness of the element is specified by the element property NLYRC. Generally from 6 to 8 layers are satisfactory for flexural applications.

C3.3 Reinforcement

Reinforcement is included by superimposing the stress-strain behavior of the steel on top of the concrete. Reinforcement layers are smeared, and each individual bar is not modeled. Up to five layers of reinforcement can be specified (using the NLYRS element property). The properties of the reinforcement required are given in Table C3, and include the normalized distance from the midsurface of the beam to the i'th reinforcement layer, Zi, (Zi= 0.5 corresponds to the top and bottom surface of the shell), the the area of the i'th reinforcement layer, ASi, expressed as a percentage of the gross concrete area, the orientation of the i'th reinforcement layer, DIRi,with respect to the local x-axis of the shell at each integration point, and the yield stress of the i'th reinforcement layer, FYi. The quantities ASi and Zi must be specified for each layer if uniform over the element, or for each layer at each integration point if nonuniform properties are used, ie Zij, ASij.

For example

```
NLYRS 2 Z1 -.45 Z2 -.42 AS1 0.50 AS2 0.25,
        DIR1 0.  DIR2 90.  FY1 425 FY2 425.
```

specifies and element with two layers of reinforcement with uniform properties at each integration point, while

```
NLYRS 2 Z11 -.45 Z12 -.45 Z13 -.40 Z14 -.40,
        Z21 -.42 Z22 -.42 Z23 -.38 Z24 -.38,
        AS11 0.50 AS12 0.50 AS13 0.45 AS14 0.45,
        AS21 0.25 AS22 0.25 AS23 0.22 AS24 0.22,
        DIR1 0.  DIR2 90.  FY1 425.  FY2 220.
```

specifies two layers of reinforcement with different properties at the four integration points.

The reinforcement is modeled as ideal elasto-plastic, with optional strain hardening.

C3.4 Cracking and tension stiffening

Cracking of the concrete can be modeled using either a 'rotating crack' model (Gupta and Habibollah, 1982) in which it is assumed that the direction of the crack is normal to the current principal strain direction, or using a 'fixed crack' model (Hand, et al., (1972); Darwin and Pecknold, (1974)) in which the direction of the crack is fixed once it has formed. The default option is the 'rotating crack' model, while 'fixed' cracks' can be invoked by specifying NOROT as an element property. The formation of secondary cracks is restricted to being orthogonal to the primary crack.

Unloading and closing of cracks is allowed, but once a crack has closed no history of this event is kept by the material model. The concrete is then treated as a previously intact material. If a crack closes a warning message is printed by the material identifying the element, integration point and layer.

Two forms of tension stiffening are available, namely tension stiffening applied either to the concrete (Lin, 1973) or lumped to the steel reinforcement (Gilbert and Warner, 1978)- see Fig. C14. The default option is no tension stiffening, while the first form is invoked by specifying TENSC and the latter by TENSS. Both forms can be used simultaneously.

C3.5 Output

A history of events at each cracked integration point can be obtained by specifying TRACE as an element property. The form of the output is

CONCRETE DATA:

LAYER: i

STATE: n.ij

DIRCN: xx

where n=0 denotes intact concrete, n=1 denotes the formation of one crack, n=2 denotes two (orthogonal) cracks; for n=1 or 2 i=1 (j=1) denotes that the crackwidth of the first (second) crack is increasing, i=0 (j=0) denotes that the crack width is decreasing, ie unloading. The definition of the direction is shown in Fig. C15.

and

REINFORCEMENT DATA:

LAYER: i

STATE: j

The reinforcement state is defined as '0' if no yielding has occurred and +1 or -1 if the plastic strain is positive or negative respectively.

The state of the concrete and steel corresponds to the state existing at the end of the last iteration for the previous load step. For this reason some fluctuations in loading or unloading of the cracks may be observed.

C4 UNIAXIAL REINFORCED CONCRETE MATERIAL MODEL

C4.1 General

The reinforced concrete material model RCBEAM is a specialization of the more general model RCSHELL to uniaxial conditions. This model is

compatible with the degenerate beam elements QLBEAM and BLBEAM. The model considers compression softening and cracking of the concrete, and includes tension stiffening. Reinforcement is modeled as ideal elastoplastic, with strain hardening.

C4.2 Material properties

The material properties required to describe this material model are given in Table C4. They are identical to the material model RCSHELL with the exception that reinforcement data at each strain point must be the same. A maximum of five reinforcement layers can be specified. Further details can be obtained by refering to the biaxial material model RCSHELL.

C4.3 Output

A history of events at each cracked integration point can be obtained by specifying TRACE as an element property. The form of the output is the same as RCSHELL, except that the crack direction is no longer applicable.

Table C1 Element Properties for Shell Elements QLSHELL, QSSHELL and BLSHELL.

Physical Quantity	Keyword	Default Value
Young's Modulus	E	1.0
Poisson's Ratio	NU	0.3
Integration Rule (NxN)	NINT	2
Coordinate Points Defining Normal are on Bottom of Shell	BOTTOM	FALSE
No Artificial Normal Spring	NOSPRINGS	FALSE
Normal Spring Stiffness Multiplier	KSPRINGS	0.001
Moderate Rotation Option	LARGE ROTATION	FALSE

Table C2 Element Properties for Beam Elements QLBEAM and BLBEAM.

Physical Quantity	Keyword	Default Value
Young's Modulus	E	1.0
Poisson's Ratio	NU	0.3
Integration Rule	NINT	2
Beam Element is Placed on Opposite Side of Shell Normal	OPPOSITE	FALSE
Cross Section Area	AREAX	1.0
Y-axis Shear Area	AREAY	0.833
Z-Axis Shear Area	AREAZ	0.833
Torsional Moment of Inertia	INERTX	0.100
Y-Axis Moment of Inertia	INERTY	0.0833
Z-Axis Moment of Inertia	INERTZ	0.0833
Width of Beam at Node	B or B1,B2,B3	1.0
Material Nonlinearity Specified	LAYER	FALSE

Table C3 Material Properties for Material Model RCSHELL.

Physical Quantity	Keyword	Default Value
Concrete Initial Tangent Modulus	ECONC	1.
Concrete Cylinder Strength	FCYL	1.
Concrete Tensile Strength	FT	1.
Strain at Maximum Concrete Stress	STRNCY	.002
Ultimate Stress Factor	FCU	0.8
Ultimate Strain Factor	ECU	1.25
Linear Elastic Option	LINEAR	FALSE
Fixed Crack Direction Option	NOROT	FALSE
Concrete Tension Stiffening	TENSC	FALSE
Concrete Tension Stiffening Factor	STRNTS	20.
Number of Concrete Layers	NLYRC	1
Reinforcement Tangent Modulus	ESTEEL	1.
Reinforcement Plasitc Modulus	ESTEELP	1.
Reinforcement Tension Stiffening	TENSS	FALSE
Number of Reinforcement Layers	NLYRS	0
Depth of Reinft. Layer i	Zi or Zij	0.
Area of Reinft. for Layer i (%)	ASi or ASij	0.
Direction or Reinft. Layer i	DIRi	0.
Yield Stress of Reinforcement	FYi	1.
Output Material History	TRACE	FALSE

Table C4 Material Properties for Material Model RCBEAM.

Physical Quantity	Keyword	Default Value
Concrete Initial Tangent Modulus	ECONC	1.
Concrete Cylinder Strength	FCYL	1.
Concrete Tensile Strength	FT	1.
Strain at Maximum Concrete Stress	STRNCY	.002
Ultimate Stress Factor	FCU	0.8
Ultimate Strain Factor	ECU	1.25
Linear Elastic Option	LINEAR	FALSE
Concrete Tension Stiffening	TENSC	FALSE
Concrete Tension Stiffening Factor	STRNTS	20.
Number of Concrete Layers	NLYRC	1
Reinforcement Tangent Modulus	ESTEEL	1.
Reinforcement Plasitc Modulus	ESTEELP	1.
Reinforcement Tension Stiffening	TENSS	FALSE
Number of Reinforcement Layers	NLYRS	0
Depth of Reinft. Layer i	Zi	0.
Area of Reinft. for Layer i (%)	ASi	0.
Yield Stress of Reinforcement	FYi	1.
Output Material History	TRACE	FALSE

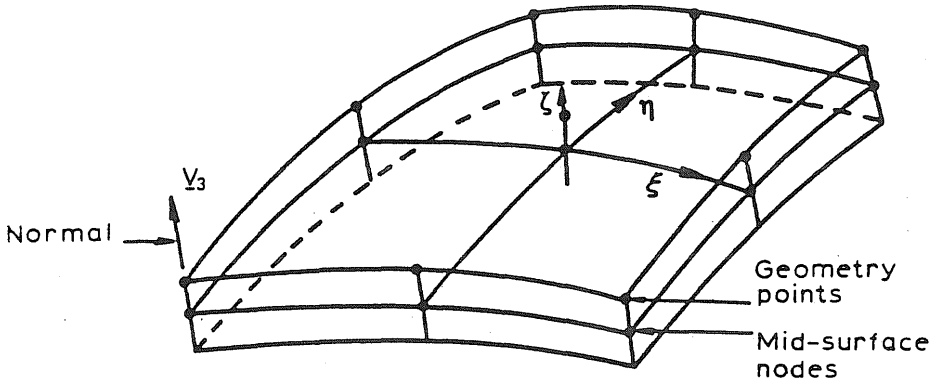

SHELL GEOMETRY

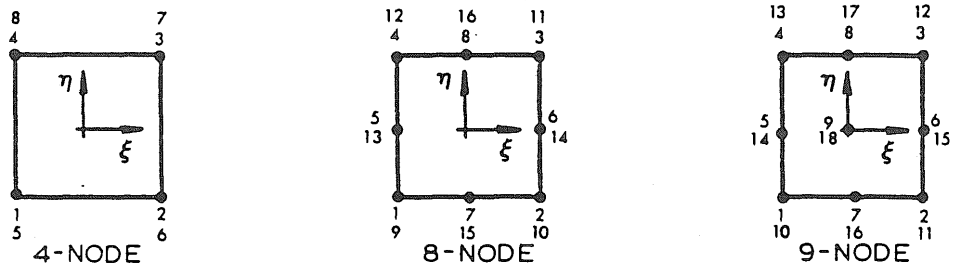

COORDINATE POINT NUMBERING

Figure C1 Geometry of Degenerated Shell Element.

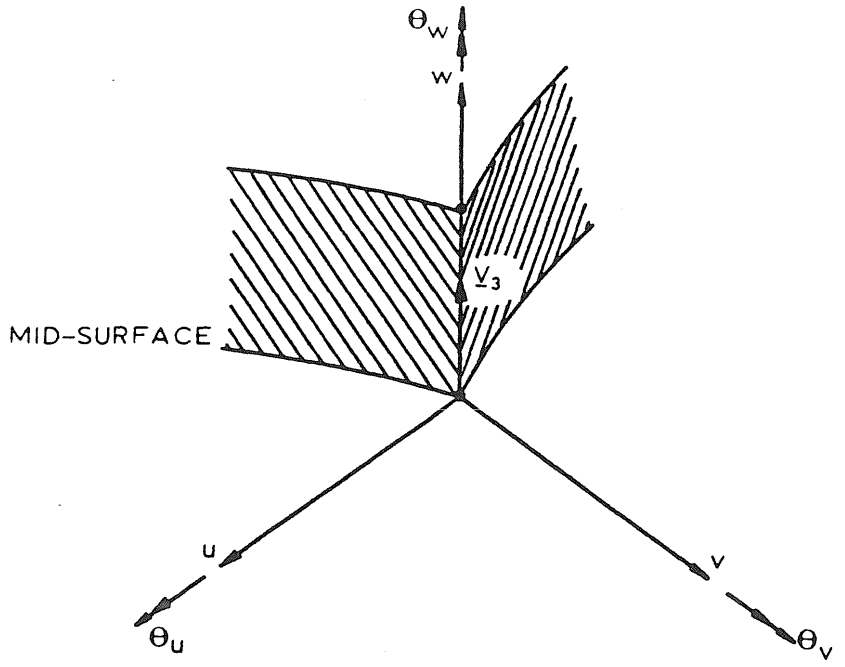

SMALL ROTATION FORMULATION

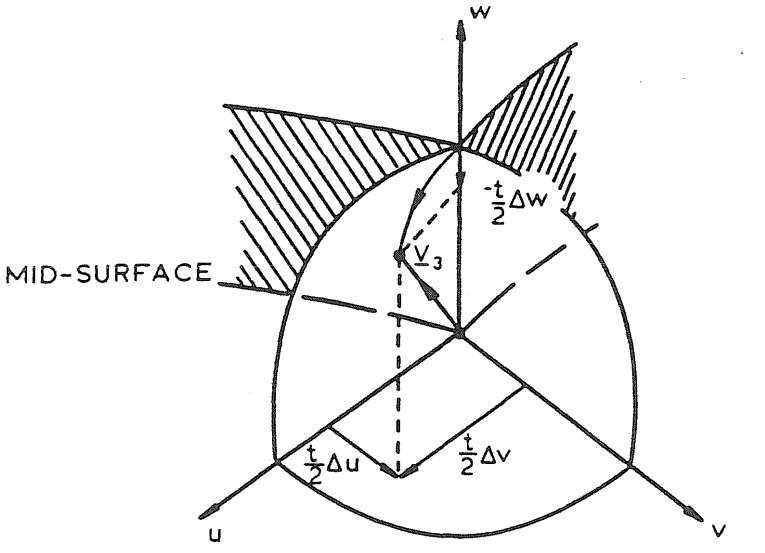

MODERATE ROTATION FORMULATION

Figure C2 Nodal Degrees of Freedom for Shell Element.

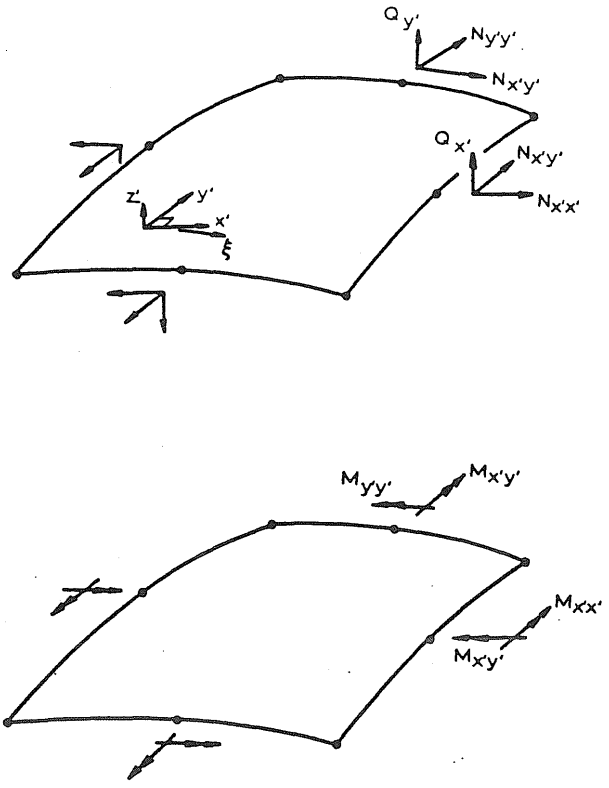

Figure C3 Stress Resultants for Shell Element.

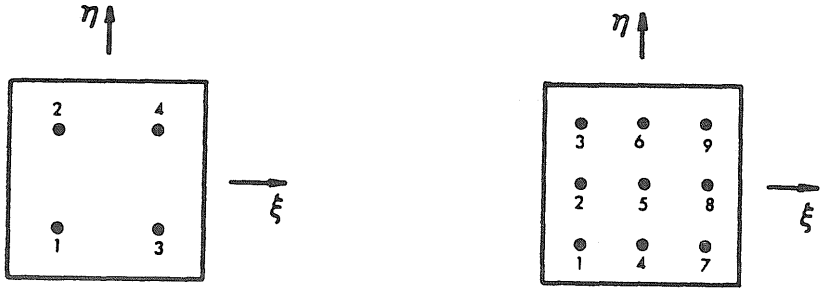

Figure C4 Strain Point Numbering of Shell Element.

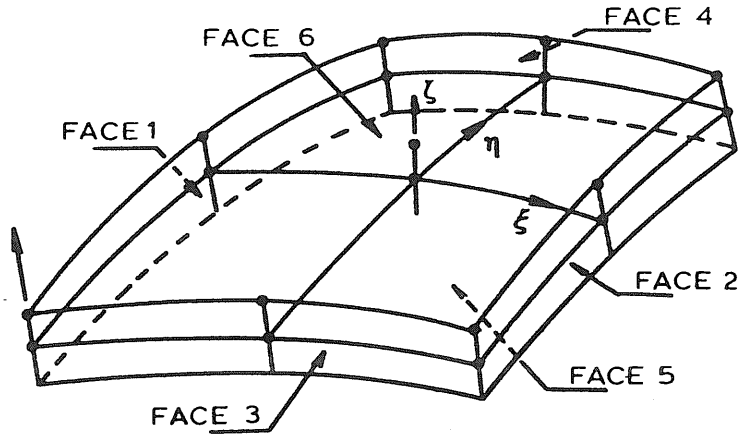

Figure C5 Face Numbers for Shell Element.

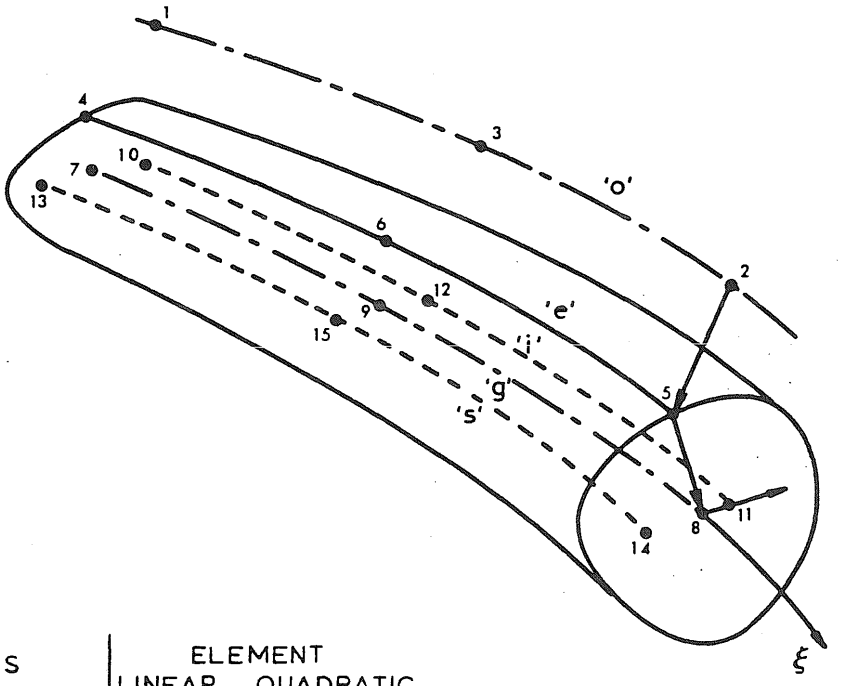

AXIS	ELEMENT LINEAR	ELEMENT QUADRATIC
'o' Reference	1-2	1-2-3
'e' Joint	3-4	4-5-6
'g' Centroidal	5-6	7-8-9
'i' Principal	7-8	10-11-12
's' Shear center	9-10	13-14-15

Figure C6 Geometry of Beam Element.

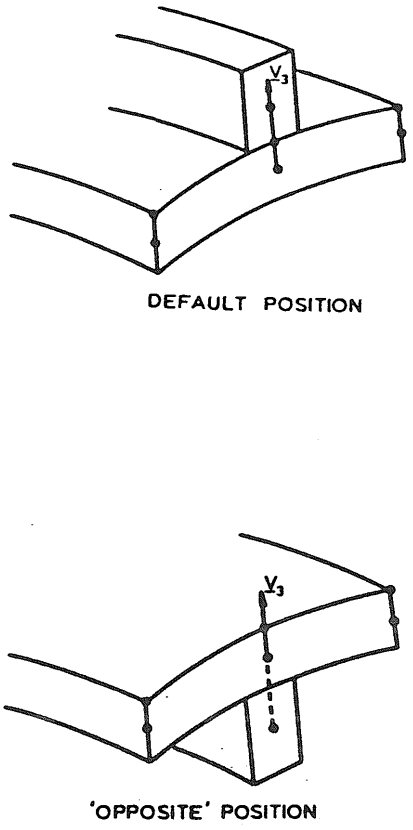

Figure C7 Positioning of Beam Element as a Shell Stiffener.

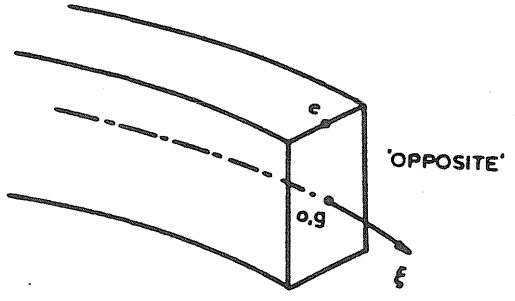

Figure C8 Stand-Alone Configuration for Beam Element.

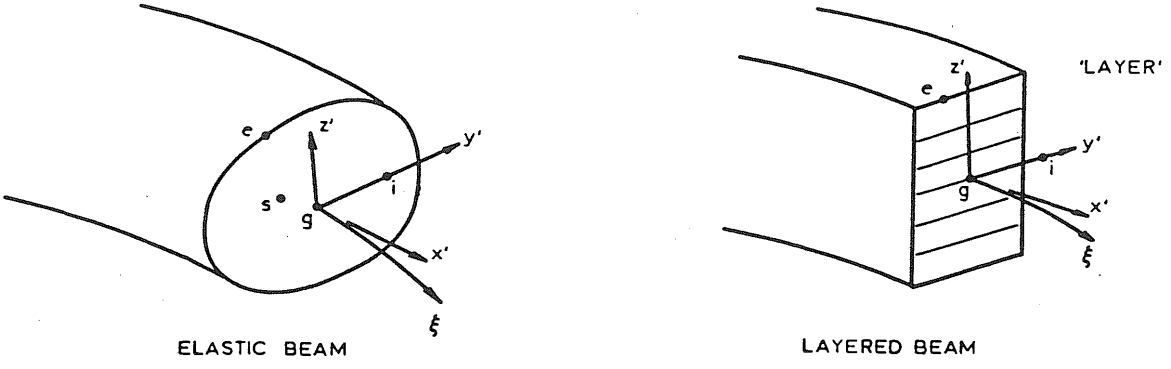

Figure C9 Local Coordinate Frame for Beam Element.

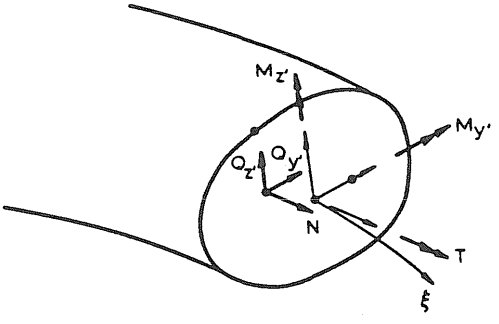

Figure C10 Stress Resultants for Beam Element.

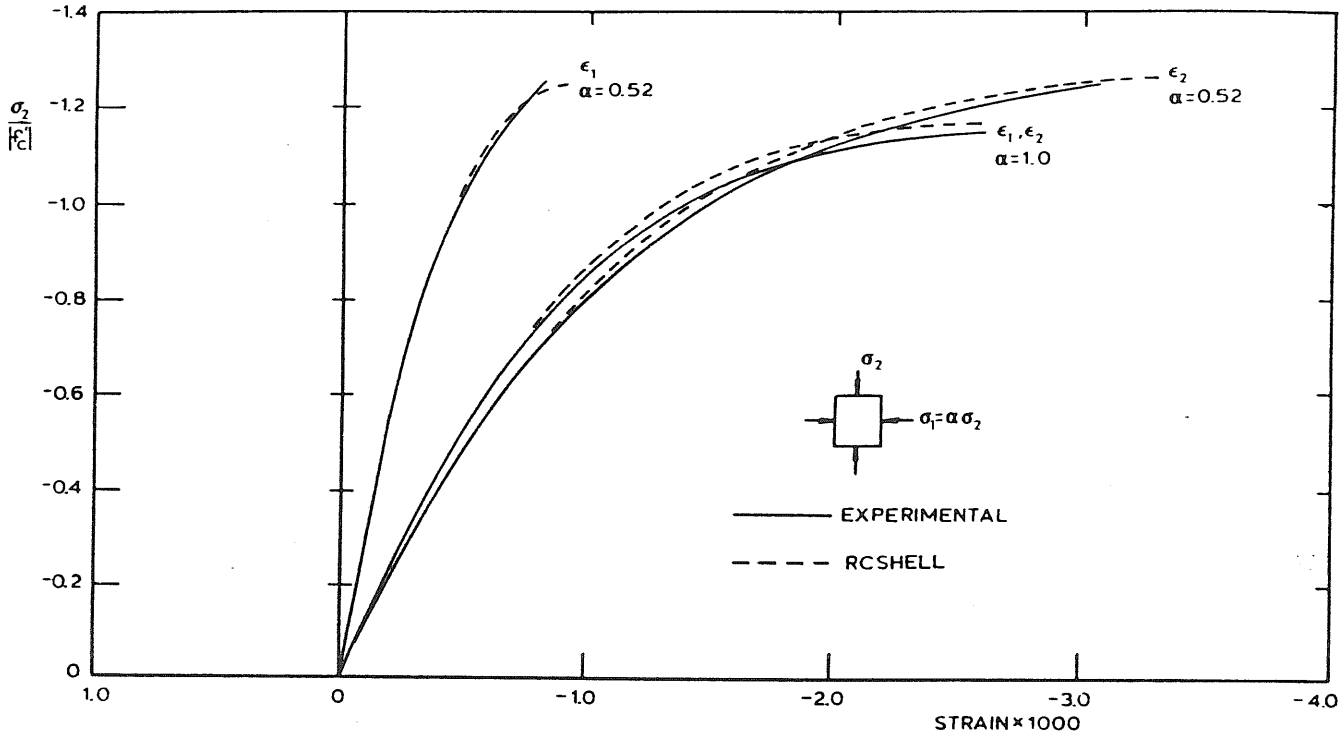

Figure C11 Biaxial Compression Curves Obtained with Model RCSHELL.

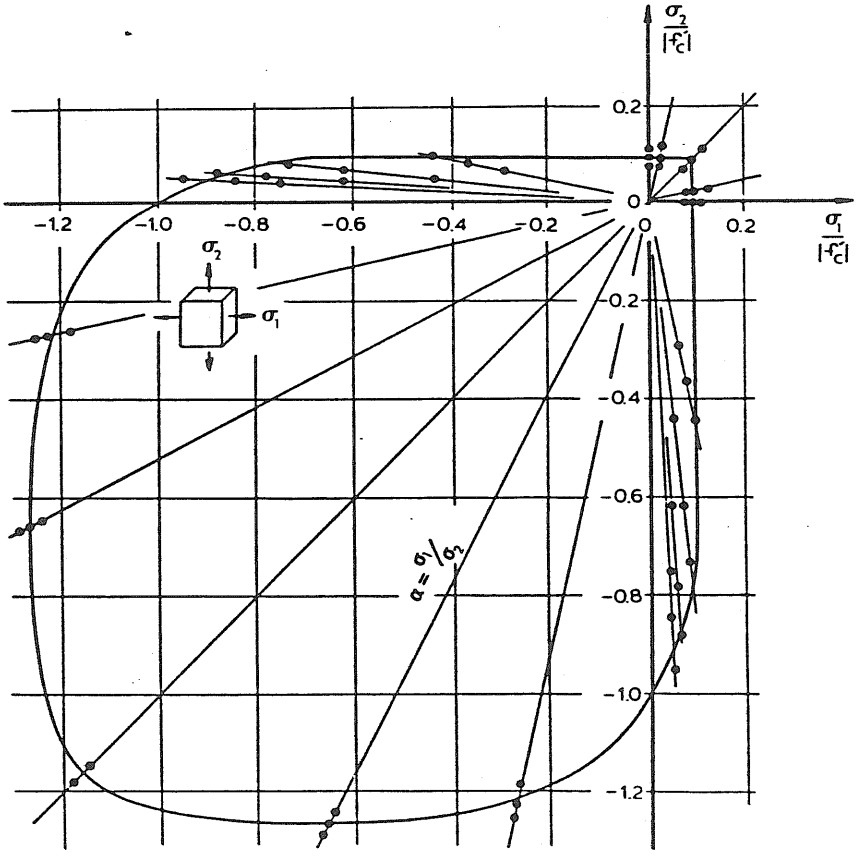

Figure C12 Biaxial Failure Envelope for RCSHELL.

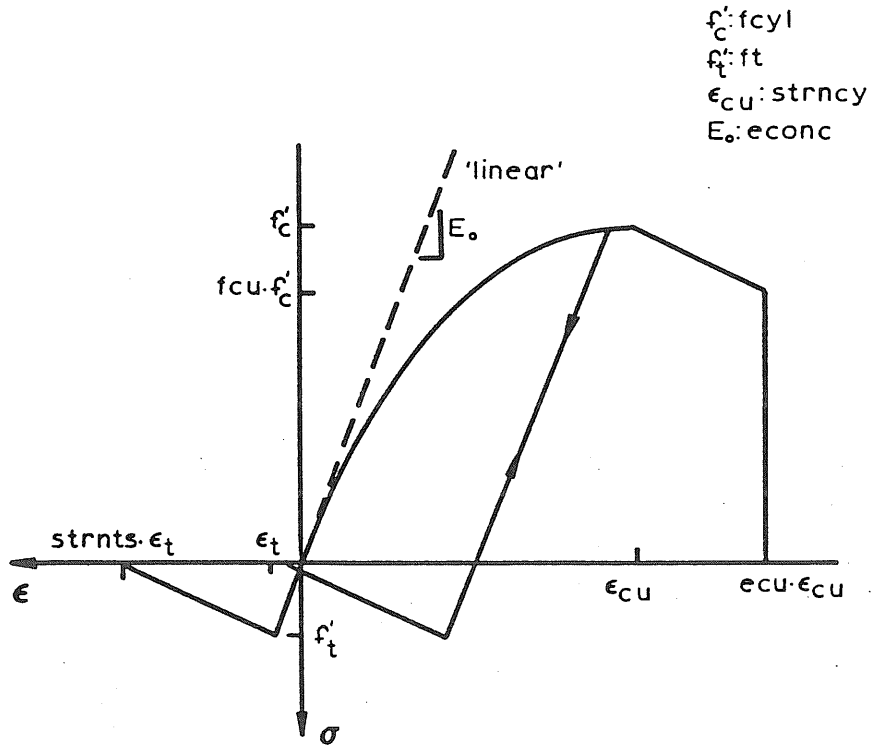

Figure C13 Uniaxial Stress-Strain Curve and Material Properties for RCSHELL.

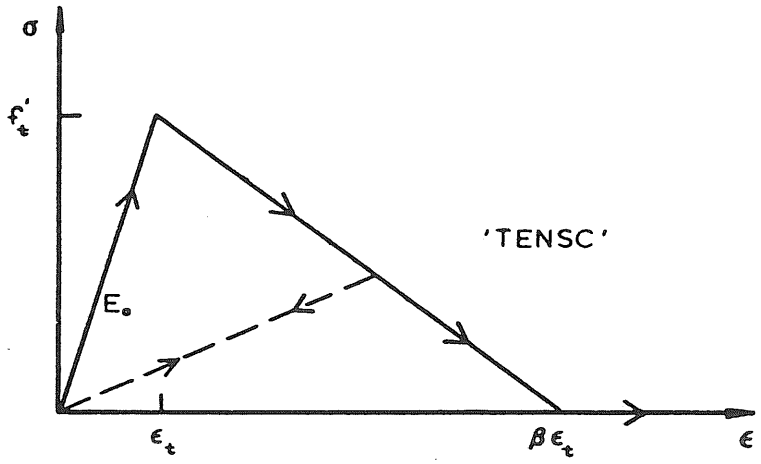

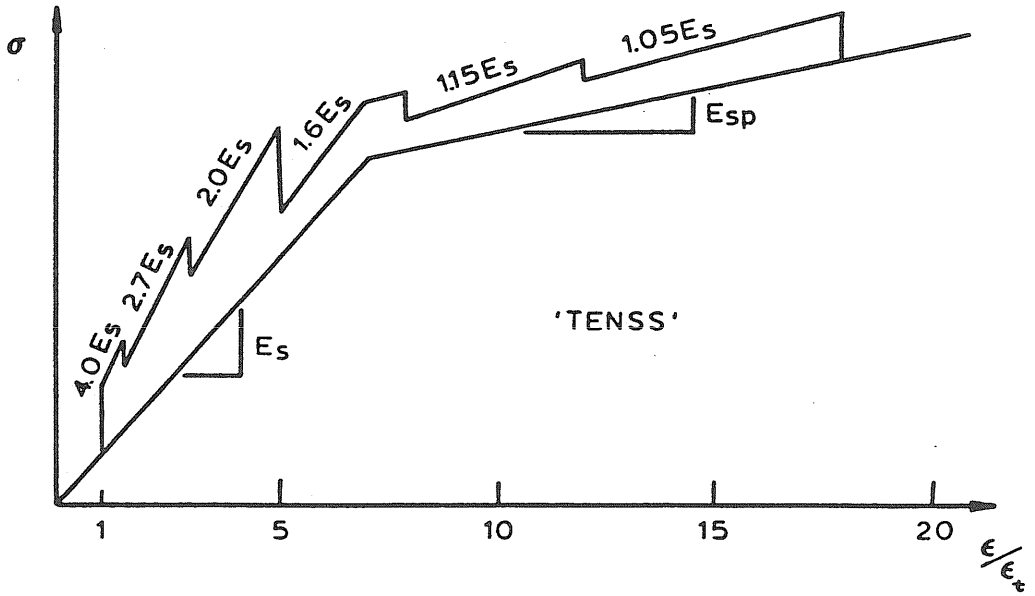

Figure C14 Tension Stiffening Models used by RCSHELL.

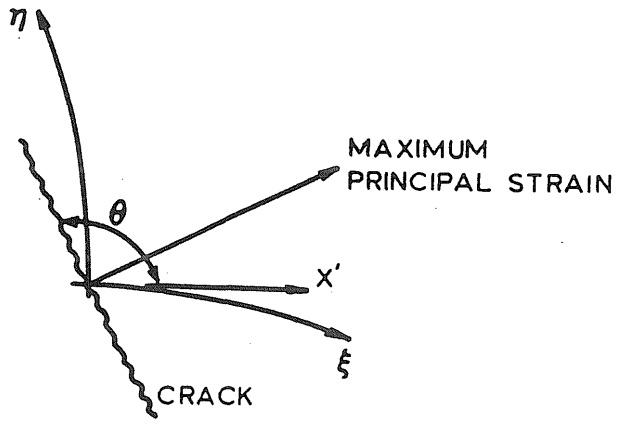

Figure C15 Orientation of Crack.

REFERENCES

1. Abdel Rahman, H. H., "Computational Models for the Nonlinear Analysis of Reinforced Concrete Flexural Slab Systems", Ph.D. Thesis, Univ. College of Swansea, 1982.

2. Abel, J. F. and Gould, P. L., "Buckling of Concrete Cooling Tower Shells", in "Concrete Shell Buckling", ed. E. P. Popov and S. J. Medwadowski, Amer. Conc. Inst. Publication SP-67, Detroit, 1981, pp. 135-160.

3. Abel, J. F., Billington, D. P., Nagy, D. A. and Witta-Dworkin, C., "Buckling of Cooling Towers", J. Struct. Div., ASCE, Vol. 108, No. ST10, Oct. 1982, pp. 2162-2174.

4. ACI-ASCE Committee 334, "Reinforced Concrete Cooling Tower Shells-Practice and Commentary", J. Amer. Conc. Inst., Vol. 74, Jan. 1977, pp. 21-31.3

5. ACI-ASCE Committee 334, "Reinforced Concrete Cooling Towers - Practice and Commentary (Proposed Text)" Dec. 1982.

6. Ahmad S, Irons, B. M., and Zienkiewicz O. C., "Analysis of Thick and Thin Shell Structures by Curved Finite Elements", Int. J. Num. Meth. Eng., Vol. 2, 1970, pp. 419-451.

7. Arenson, A., "Analysis of Reinforced Concrete Shells Considering Material and Geometric Nonlinearities", Report No. 79-1, Div. of Struct. Mech., Univ. of Trondheim, Norway, July 1979.

8. Argyris, J. H. and Scharpf, D. W., "The SHEBA Family of Shell Elements for the Matrix Dislacement Method. Part II: Large Displacements", J. Roy. Aeron. Soc., Vol. 73, 1969, pp. 423-426.

9. ASCE Task Committee on Concrete and Masonary Structures, "State of the Art Report on Finite Element Analysis of Reinforced Concrete", ASCE, 1981.

10. Backlund, J., "On Isoparametric Elements", Int. J. Num. Meth. Eng., Vol. 12, 1978, pp. 731-732.

11. Bathe, K. J., Ramm, E. and Wilson, E. L., "Finite Element Formulations for Large Deformation Dynamic Analysis", Int. J. Num. Meth. Eng., Vol. 9, 1975, pp. 353-386.

12. Bathe, K. J. and Bolourchi, S., "A Geometric and Material Non-Linear Plate and Shell Element", Comp. and Struct., Vol. 11, 1980, pp. 23-48.

13. Batoz, J. L., Chattopadhyay, A. and Dhatt, G., "Finite Element Large Deflection Analysis of Shallow Shells", Int. J. Num. Meth. Eng., Vol. 10, 1976, pp. 39-58.

14. Batoz, J. L., "Curved Finite Elements and Shell Theories with Particular Reference to the Buckling of a Circular Arch", Int. J. Num. Eng., Vol. 14, 1979, pp. 774-779.

15. Bazant, Z. P., Discussion of Session 2, Part 1, Final Report, IABSE Colloquium on Advanced Mechanics of Reinforced Concrete, Delft, 1981, pp 481-491.

16. Bergan, P. G. and Clough, R. W., "Large Deflection Analysis of Plates and Shallow Shells Using the Finite Element Method", Int. J. Num. Meth. Eng., Vol. 5, 1973, pp. 543-556.

17. Bouberg, A. and Jirousek, J., "A Family of Special-Purpose Elements for Analysis of Ribbed and Reinforced Shells", Comp. and Struct., Vol. 12, 1980, pp. 253-264.

18. Bouma, A. L., van Riel, A. C., van Koten, H. and Beranek, W. J., "Investigations on Models of Eleven Cylindrical Shells Made of Reinforced and Prestressed Concrete", Symp. of Shell Research, Delft, 1961.

19. Braestrup, M. W. and Nielsen, M. P., "Plastic Design Methods of Analysis and Design", in "Handbook of Structural Concrete", ed. F. K. Kong, et al, McGraw-Hill, 1983.

20. Brebbia, C. and Connor, R. W., "Geometrically Nonlinear Finite Element Analysis", ASCE, J. Eng. Mech. Div., Vol. 95, 1969, pp. 463-483.

21. Brendel, B. and Ramm, E., "Linear and Nonlinear Stability Analysis of Cylindrical Shells", Comp. and Struct., Vol. 12, 1980, pp. 549-558.

22. Brush, D. O. and Almroth, B. O., "Buckling of Bars, Plates, and Shells", McGraw Hill 1975.

23. BSI (British Standards Institution) BS4485: Part 4, "Specification for Water Cooling Towers - Structural Design", London, 1975.

24. Cardenas, A. and Sozen, M. A., "Strength and Behavior of Isotropically and Nonisotropically Reinforced Concrete Slabs Subjected to Combinations of Flexural and Torsional Moments", Civil Engineering Studies, SRS No. 336, Univ. of Illinois, Urbana, Illinois, May 1968.

25. CEGB (Central Electricity Generating Board), "Report of the Committee of Enquiry into the Collapse of Cooling Towers at Ferrybridge, Monday 1, November 1965", Central Electricity Generating Board, London, Aug. 1966.

26. Cervenka, V., "Inelastic Finite Element Analysis of Reinforced Concrete Panels Under In-Plane Loads", Ph.D. Thesis, Univ. of Colorado at Boulder, Colorado, 1970.

27. Chan, A. S. L. and Firmin, A., "The Analysis of Cooling Towers by the Matrix Finite Element Method, Patr II: Large Displacements", The Aero. J. Royal Aero. Soc., Vol. 74, No. 12, Dec. 1970, pp. 971-982.

28. Chan, E. C., "Nonlinear Geometric, Material and Time Dependent Analysis of Reinforced Concrete Shells with Edge Beams", Ph.D. Thesis, UC-SESM 82-8, Univ. of California at Berkeley, California, Aug. 1982.

29. Chen, W. F., "Plasticity in Reinforced Concrete", McGraw-Hill, N.Y., 1981.

30. Cole, P. P., Abel, J. F., and Billington, D. P., "Buckling of Cooling- Tower Shells: State of the Art", J. Struct. Div., ASCE, Vol. 101, No. ST6, June 1975, pp. 1185-1203.

31. Cole, P. P., Abel, J. F., and Billington, D. P., "Buckling of Cooling- Tower Shells: Bifurcation Results", J. Struct. Div., ASCE, Vol. 101, No. ST6, June 1975, pp. 1205-1222.

32. Cook, W. A., "The Effect of Geometric Shape on Two-Dimensional Elements", Proc. 6'th Int. Seminar on Computational Aspects of the Finite Element Method, ed J. F. Gloudeman, Paris, 1981.

33. Cook, W. A. and Zhao-Hua, F., "Control of Spurious Modes in the Nine-Node Quadrilateral Element", Int. J. Num. Meth. Eng., Vol. 18, 1982, pp. 1576-1580.

34. Cope, R. J. and Rao, P. V., "Non-linear Finite Element Analysis of Concrete Slab Structures", Proc. Instn., Civil Engrs., Vol. 63, 1977, pp. 159-179.

35. Cope, R. J., Rao, P. V., Clark, L. A. and Norris, P., "Modelling of Reinforced Concrete Behaviour for Finite Element Analysis of Bridge Slabs", in "Numerical Methods for Non-linear Problems", Vol. 1, Pineridge Press, Swansea, 1980, pp. 457-470.

36. Cope, R. J. and Rao, P. V., "Non-linear Finite Element Strategies for Bridge Decks", IABSE Colloquium on Advanced Mechanics of Reinforced Concrete, Delft, Final Report, June 1981, pp. 273-288.

37. Darwin, D. and Pecknold, D. A., "Inelastic Model for Cyclic Biaxial Loading for Reinforced Concrete", Civil Engineering Studies, SRS 409, Univ. of Illinois, Urbana, Illinois, July 1974.

38. Der, T. J. and Fidler, R., "A Model Study of the Buckling of Hyperbolic Shells", Proc. Instn. Civil Engrs., Vol. 41, Sept. 1968, pp. 105-118.

39. Duchon, N. B., "Analysis of Reinforced Concrete Membrane Subjected to Tension and Shear", ACI Journal, Vol. 69, No. 9, Sept. 1972, pp. 578-583.

40. Duddeck, H., Griebenow, G. and Schaper, G., "Material and Time Dependent Nonlinear Behaviour of Cracked Reinforced Concrete Slabs", in "Nonlinear Behaviour of Reinforced Concrete Spatial Structures", Vol. 1, Preliminary Report, IASS Symposium, Darmstadt, Ed. G. Mehlhorn, H. Ruhle and W. Zerna, Werner-Verlag, Dusseldorf, July 1978, pp. 101-113.

41. Dumitrescu, J. A, Croll, J. G. and Billington, D. P., "Cooling Towers on Flexible Foundations", J. Struct. Div., ASCE, Vol. 109, No. 10, Oct. 1983, pp. 2248-2264.

42. Eibl, J. and Kesting, K., "Numerical Investigation of Slender Reinforced Concrete Walls", in "Nonlinear Behaviour of Reinforced Concrete Spatial Structures", Vol. 1, Preliminary Report, IASS Symposium, Darmstadt, Ed. G. Mehlhorn, H. Ruhle and W. Zerna, Werner-Verlag, Dusseldorf, July 1978, pp. 293-300.

43. ENR (Engineering News Record), "U.K. Cooling Tower Collapses", Eng. News Record, Feb. 9, 1984, pp. 32.

44. Ewing, D. J. F., "The Buckling and Vibration of Cooling Tower Shells, Part II: Calculations", Lab. Report No. RD/L/R 1763, Central Electricity Research Labaratories, Leatherhead, England, Nov. 1971.

45. Floegl, H. and Mang, H. A., "Zum Einfluss der Verschiebungsabhangigkeit ungleichformigen hydrostatischen Druckes auf das Ausbeulen dunner Schalen allgemeiner Form´, Ing.- Archiv., Vol. 50, 1981, pp. 15-30.

46. Franklin, H. A., "Nonlinear Analysis of Reinforced Concrete Frames and Panels", Ph.D. Thesis, Univ. of California at Berkeley, California, 1970.

47. Gerstle, K. N., "Material Modelling of Reinforced Concrete", Introductory Report, IABSE Colloquium on Advanced Mechanics of Reinforced Concrete, Delft, 1981, pp. 41-61.

48. Gilbert, R. I. and Warner, R. F., "Tension Stiffening in Reinforced Concrete Slabs", J. Struct. Div., ASCE, Vol. 104, No. ST12, 1978, pp. 1885-1900.

49. Green, A. E. and Zerna, W., "Theoretical Elasticity", Oxford Univ. Press, 1954.

50. Gupta, A. K., "Membrane Reinforcement in Shells", J. Struct. Div., ASCE, Vol. 107, No. ST1, Jan. 1981, pp. 41-56.

51. Gupta, A. K. and Habibollah, A., "Changing Crack Direction in Reinforced Concrete Analysis", Report, Dept. Civil Eng., North Carolina State Univ., Rayleigh, North Carolina, Jan. 1982.

52. Hand, F. R., Pecknold, D. A. and Schnobrich, W. C., "A Layered

Finite Element Nonlinear Analysis of Reinforced Concrete Plates and Shells", Civil Engineering Studies, SRS 389, Univ. of Illinois, Urbana, Illinois, Aug. 1972.

53. Hayashi, K. and Gould, P. L., "Some Aspects of the Response of Wind-Loaded Reinforced Concrete Cooling Towers", Struct. Eng. Research Report No. 63, Dept. of Civil Eng., Washington Univ., 1982.

54. Hayashi, K. and Gould, P. L., "Cracking Load for a Wind-Loaded Reinforced Concrete Cooling Tower", J. Amer. Conc. Inst., Vol. 79, July 1983, pp. 318-325.

55. Hayman, B. and Chilver, A. H., "The Effect of Structural Degeneracy on the Stability of Cooling Towers", Colloq. on "Recommendations for the Structural Design of Hyperbolic or Other Similarly Shaped Cooling Towers", IASS, May 1971.

56. Hughes, T. J. R., Taylor, R. L. and Kanoknukulchai, W., "A Simple and Efficient Element for Plate Bending", Int. J. Num. Meth. Eng., Vol. 11, 1977, pp. 1529-143.

57. Hughes, T. J. R., Cowen, M. and Haroun, M., "Reduced and Selective Integration Schemes in the Finite Element Analysis of Plates", Nucl. Eng. Design, Vol. 46, 1978, pp. 203-222.

58. Hughes, T. J. R. and Liu, W. K., "Nonlinear Finite Element Analysis of Shells: Part I. Three-dimensional Shells", Comp. Meth. Appl. Mech. Eng., Vol. 26, No. 3, 1981, pp. 331-362.

59. Hughes, T. J. R. and Tezduyar, T. E., "Finite Elements Based on Mindlin Plate Theory with Particular Reference to the Four-Node Bilinear Isoparametric Element", ASME, J. Appl. Mech., Vol. 48, No. 3, 1981, pp. 587-596.

60. IASS Working Group No. 3, "Recommendations for the Design of Hyperbolic or Other Similarly Shaped Cooling Towers", Int. Assoc. for Shell and Spatial Structures, Brussels, Belgium, 1977.

61. ICI (Imperial Chemical Industries Ltd.), "Report of the Committee of Enquiry into the Collapse of the Cooling Tower at Ardeer Nylon Works, Ayrshire, on Thursday 27 September 1973", Imperial Chemical Industries Ltd., London 1974.

62. Ivanyi, G., "Modeling of Cracked Elastic State of Reinforced Concrete", IABSE Colloquium on Advanced Mechanics of Reinforced Concrete, Delft, Final Report, June 1981, pp. 315-325.

63. Jirousek, J., "A Family of Variable Section Curved Beam and Thick-Shell of Membrane-Stiffening Isoparametric Elements", Int. J. Num. Meth. Eng., Vol. 17, 1981, pp. 171-186.

64. Kabir, A. F., "Nonlinear Analysis of Reinforced Concrete Panels,

Slabs and Shells for Time Dependent Effects", Ph.D. Thesis, UC-SESM 76-6, Univ. of California, Dec. 1976.

65. Koiter, W. T., "A Consistent First Approximation in the General Theory of Thin Elastic Shells", in "Theory of Thin Elastic Shells", IUTAM, Delft, North-Holland Publishing Co., 1959, pp. 12-33.

66. Kundurpi, P. S., Samavedam, G. and Johns, D. J., "Stability of Cantilever Shells under Wind Loads", ASCE, J. Eng. Mech. Div., Vol. 101, No. EM5, Oct. 1975, pp. 517-530.

67. Kupfer, H. and Gerstle, K. N., "Behavior of Concrete under Biaxial Stresses", J. Eng. Mech. Div., ASCE, Vol. 99, No. EM4, Aug. 1973, pp. 852-866.

68. Langhaar, H. L., Boresi, A. P., Miller, R. E. and Brueging, J. J., "Stability of Hyperboloidal Cooling Towers", J. Eng. Mech. Div., ASCE, Vol. 96, No. EM5, Oct. 1970, pp. 753-789.

69. Larrabee, R. D., Billington, D. P. and Abel, J. F., "Thermal Loading of Thin-Shell Concrete Cooling Towers", J. Struct. Div., ASCE, Vol. 100, No. ST12, Dec. 1974, pp. 2367-2383.

70. Lin, C. S, "Nonlinear Analysis of Reinforced Concrete Slabs and Shells", Ph.D. Thesis, UC-SESM 73-7, Univ. of California at Berkeley, California, April 1973.

71. Liu, T. C. Y., Nilson, A. H. and Slate, F. O., "Biaxial Stress-Strain Relations for Concrete", J. Struct. Div., ASCE, Vol. 98, No. ST5, May 1972, pp. 1025-1034.

72. Lopez, L. A., "Finite: An Approach to Structural Mechanics Systems", Int. J. Num. Meth. Eng., Vol. 11, 1977, pp. 851-866.

73. MacNeal, R. H., "A Simple and Quadrilateral Shell Element", Comp. and Struct., Vol. 8, 1978, pp. 175-183.

74. Mang, H. A., Gallagher, R. H., Cedolin, L. and Schwinden, W. D., "Finite Element Instability Analysis of Hyperbolic Cooling Towers", in "Advances in Civil Engineering Through Engineering Mechanics", ASCE, New York, N.Y., 1977, pp. 246-249.

75. Mang, H. A. and Floegl, H., "Tension Stiffening Concept for Reinforced Concrete Surface Structures", IABSE Colloquium on Advanced Mechanics of Reinforced Concrete, Delft, Final Report, June 1981, pp. 351-369.

76. Mang, H. A., Floegl, H., Trappel, F. and Walter, H., "Wind-Loaded Reinforced-Concrete Cooling Towers: Buckling or Ultimate Load", Eng. Struct., Vol. 5, July 1983, pp. 163-180.

77. Mehl, M., "Uber das Tragverhalten von Naturzugkuhlturmen aus Stahlbeton", Doctoral Dissertation, Tech. Univ. of Vienna, Vienna, Austria, June 1982 (Quoted in Ref. 76).

78. Melhorn, G., "A Calculation for Reinforced Concrete Beams under Bending and Torsion using Three-Dimensional Finite Elements", IABSE Colloquium on Advanced Mechanics of Reinforced Concrete, Delft, Final Report, June 1981, pp. 591-601.

79. Mikkola, M. J. and Schnobrich, W. C., "Material Characteristics for Reinforced Concrete Shells Stressed Beyond the Elastic Range", Civil Engineering Studies, SRS 367, Univ. of Illinois, Urbana, Illinois, Aug. 1970.

80. Mushtari, K. and Galimov, K., "Nonlinear Theory of Elastic Shells", NASA TT-F62, 1962.

81. Mungan, I., "Buckling Stress States of Hyperboloidal Shells", J. Struct. Div., ASCE, Vol. 102, No. ST10, Oct. 1976, pp. 2005-2020.

82. Mungan, I., "Buckling Stresses of Stiffened Hyperboloidal Shells", J. Struct. Div., ASCE, Vol. 105, No. ST8, Aug. 1979, pp. 1589-1604.

83. "Natural Draught Cooling Towers- Ferrybridge and After", Proc. Conf., Instn. Civil Engrs, London, June 1967.

84. Nelissen, L., J., M., "Biaxial Testing of Normal Concrete", Heron, Netherlands, Vol. 18, No. 1, 1972.

85. Ngo, D. and Scordelis, A. C, "Finite Element Analysis of Reinforced Concrete Beams", J. Am. Conc. Inst., Vol. 64, No. 3, March 1967, pp. 152-163.

86. Owen, D. R. J. and Figueiras, J. A., "Anisotropic Elasto- Plastic Finite Element Analysis of Thick and Thin Plates and Shells", Int. J. Num. Meth. Eng, Vol. 19, 1983, pp. 541-566.

87. Parisch, H., "A Critical Survey of the Nine-Node Degenerated Shell Element with Special Emphasis on Thin Shell Application and Reduced Integration", Comp. Meth. Appl. Mech. Eng., Vol. 20, 1979, pp. 323-350.

88. Parisch, H., "Large Displacements of Shells Including Material Nonlinearities", Comp. Meth. Appl. Mech. Eng., Vol. 27, 1981, pp. 183-214.

89. Pawsey, S. E. and Clough, R. W., "Improved Numerical Integration of Thick Finite Elements", Int. J. Num. Meth. Eng., Vol. 3, 1971, pp. 545-586.

90. Pica, A. and Wood, R. D., "Postbuckling Behaviour of Plates and Shells using a Mindlin Shallow Shell Formulation", J. Comp. Struct., Vol. 12, 1980, pp. 759-768.

91. Rajagopal, K. R., "Nonlinear Analysis of Reinforced Concrete Beams, Beam-Columns and Slabs by Finite Elements", Ph.D. Thesis, Iowa State Univ., Ames, Iowa, 1976. (Quoted in Ref. 64).

92. Ramm, E., "A Plate/Shell Element for Large Deflections and Rotations", Ch. 10 in "Formulations and Computational Algorithms in Finite Element Analysis: U.S.-Germany Symposium", ed Bathe, K. J., Oden, J. T. and Wunderlich, W., MIT Press, 1977, pp. 264-293.

93. Ramm, E. and Sattele, J. M., "Elasto-Plastic Large Deformation Shell Analysis Using Degenerated Elements", in "Nonlinear Finite Element Analysis of Plates and Shells", ed Hughes, T. J. R., Pifko, A. and Jay, A., Proc. ASME Winter Annual Meeting, Washington, AMD-Vol. 48, 1981, pp. 265-282.

94. Ramm E. and Stegmuller, H., "The Displacement Finite Element Method in Nonlinear Buckling Analysis", in "Buckling of Shells", ed E. Ramm, Proc. State of the Art Colloq., Univ. Stuttgart, Germany, 1982, Springer-Verlag, pp. 201-235.

95. Rashid, Y. R., "Analysis of Prestressed Concrete Pressure Vessels", Nucl. Eng. Design, Vol. 7, No. 4, April 1968, pp. 334-344.

96. Reissner, E., "A New Derivation of the Equations for the Deformation of Elastic Shells", Amer. J. Math., Vol. 63, 1941, pp. 177-184.

97. Robinson, J. R. and Demorieux, J. M., "Essare de Traction-Compression sur Modeles d'ame de Pocitre en Beton Arme", Institute de Recherches Appliques du Beton Arme, Paris, June 1968 and May 1972. (Quoted in Ref. 111).

98. Rowe, R. E., "Making the Most of Models", Concrete International, Feb. 1981, pp. 7-12.

99. Saenz, L. P., Discussion of "Equation for the Stress-Strain Curve of Concrete", by Desayi and Krishnan, ACI Journal, Vol. 61, No. 9, September 1964, pp. 1229-1235.

100. Sageau, J. -F., "Wind-Tunnel Testing of Cooling Towers at the Electricity de France", informal presentation at Conf. for Design Against Wind Induced Failure, Bristol, England. Jan. 1984.

101. Sanders, E. L., "Nonlinear Theories for Thin Shells", Q. Appl. Math., Vol. 21, No. 1, 1963, pp. 21-36.

102. Schlaich, J. and Schafer, K., "Zur Druck-Querzug-Festigkeit des Stahlbetons", Beton-und Stahlbetonbau, Vol. 3, 1983, pp. 73-78.

103. Shield, R. T., "A Consistent Theory for Elastic Deformations with Small Strains", Theoretical and Applied Mechanics, TAM 459, Univ. of Illinois, Urbana, Ill., 1983.

104. Stallbohm, H., Mungan, I. and Gould, P. L., Discussion on "Buckling of Cooling-Tower Shells: Bifurcation Results", by Cole, P. P. et al, J. Struct. Div., ASCE, Vol. 102, No. ST1, Jan. 1976, pp. 303-304.

105. Stricklin, J. A., Ho. W. S., Richardson, E. Q. and Haisler, W. E., "On Isoparametric vs. Linear Strain Triangular Elements", Int. J. Num. Meth. Eng., Vol. 11, 1977, pp. 1041-1043.

106. Surana, K. S., "Geometrially Nonlinear Formulation for the Curved Shell Elements", Int. J. Num. Meth. Eng., Vol. 19, 1983, pp. 581-615.

107. Swartz, S. E., Chien, C. D., Hu, K. K. and Mozaffarian, H., "Tests on a Micro-Concrete Model of Hyperbolic Cooling Tower", Proc. 1982 Fall Meeting, Soc. for Exp. Stress Analysis, Brookfield Center, 1982, pp. 25-31.

108. Thomas, G. R. and Gallagher, R. H., "A Triangular Thin Shell Finite Element: Nonlinear Analysis", NASA CR 2483, 1975.

109. Timoshenko, S., "Strength of Materials, Part II", 2´nd Ed., Van Nostrand, New York, 1941.

110. Timoshenko, S. and Gere, J. M., "Theory of Elastic Stability", 2´nd Edition, McGraw-Hill, N.Y., 1961.

111. Vecchio, F. and Collins, M. P., "The Response of Reinforced Concrete to Inplane Shear and Normal Stresses", Publication No. 82-03, Univ. of Toronto, March 1982.

112. Veronda, D. R. and Weingarten, V. I., "Stability of Hyperboloidal Shells: An Experimental and Analytical Investigation", USCCE 009, School of Engineering, Univ. of Southern California, Los Angeles, California, Mar. 1973.

113. Walraven, J., "The Influence of Depth on the Shear Strength of Lightweight Concrete Beams Without Shear Reinforcement", Stevin Laboratory Report No. 5-78-4, Delft, 1982.

114. Yeh, C. H. and Shieh, W. Y. J., "Stability and Dynamic Analysis of Cooling Towers", J. Power Div., ASCE, Vol. 99, No. PO2, Nov. 1973, pp. 1005-1023.

115. Yuzugullu, O. and Schnobrich, W. C., "A Numerical Proceedure for the Determination of the Behavior of a Shear Wall Frame System", J. Amer. Conc. Inst., Vol. 70, No. 7, July 1973, pp. 474-479.

116. Zerna, W. and Mungan, I., "Construction and Design of Large Cooling Towers", J. Struct. Div., ASCE, Vol. 106, No. ST2, Feb. 1980, pp. 531-544.

117. Zerna, W. and Mungan, I., "Buckling Stresses of Shells Having Negative Gaussian Curvature", in "Buckling of Shells", ed E. Ramm, Proc. State of the Art Colloq., Univ. Stuttgart, Germany, 1982, Springer-Verlag, pp. 201-235.

118. Zienkiewicz, O. C., Taylor, R. L. and Too, J. M., "Reduced

Integration Techniques in General Analysis of Plates and Shells", Int. J. Num. Meth. Eng., Vol. 3, 1971, pp. 275-290.

119. Zintilis, G. M. and Croll, J. G. A., "Combined axial and Pressure Buckling of End Supported Shells of Revolution", Eng. Struct., Vol. 5, July 1983, pp. 199-206.